LANDSLIDE RISK ASSESSMENT
USING DIGITAL ELEVATION MODELS

by

Amanda McLean

Submitted in partial fulfillment of the requirements
for the degree of Master of Science

at

Dalhousie University
Halifax, Nova Scotia
March 2011

DALHOUSIE UNIVERSITY

DEPARTMENT OF ENGINEERING MATHEMATICS

The undersigned hereby certify that they have read and recommend to the Faculty of Graduate Studies for acceptance a thesis entitled "LANDSLIDE RISK ASSESSMENT USING DIGITAL ELEVATION MODELS" by Amanda McLean in partial fulfillment of the requirements for the degree of Master of Science.

Dated: March 22, 2011

Supervisor: _____

Dr. Gordon A. Fenton

Readers: _____

Dr. Craig Lake

_____

Dr. William J. Phillips

DALHOUSIE UNIVERSITY

DATE: March 22, 2011

AUTHOR: Amanda McLean

TITLE: LANDSLIDE RISK ASSESSMENT USING DIGITAL ELEVATION MODELS

DEPARTMENT OR SCHOOL: Department of Engineering Mathematics

DEGREE: MSc CONVOCATION: May YEAR: 2011

Signature of Author

To my mom and dad, my dedicated cheerleaders,

and to Vamsi, my best friend,

for their unwavering support.

TABLE OF CONTENTS

Page

Page

LIST OF TABLES

Table **Page**

LIST OF FIGURES

Figure **Page**

ABSTRACT

Regional landslide risk, as it is most commonly defined, is a product of the following: hazard, vulnerability and exposed population. The first objective of this research project is to estimate the regional landslide hazard level by calculating its probability of slope failure based on maximum slope angles, as estimated using data provided by digital elevation models (DEM). Furthermore, it addresses the impact of DEM resolution on perceived slope angles, using local averaging theory, by comparing the results predicted from DEM datasets of differing resolutions. Although the likelihood that a landslide will occur can be predicted with a hazard assessment model, the extent of the damage inflicted upon a region is a function of vulnerability. This introduces the second objective of this research project: vulnerability assessment. The third and final objective concerns the impact of urbanization and population growth on landslide risk levels.

LIST OF ABBREVIATIONS AND SYMBOLS USED

CDF	Cumulative Distribution Function
$CIESIN$	Center for International Earth Science Information Network
DEM	Digital Elevation Model
GDP	Gross Domestic Product
GIS	Geographical Information System
$GRUMP$	Global Rural-Urban Mapping Project
$GTOPO$	Global 30 arc-second elevation model
ICG	International Centre for Geohazards
IMF	International Monetary Fund
LAS	Local Average Subdivision
NGI	Norwegian Geotechnical Institute
NGU	Geological Survey of Norway
PDF	Probability Density Function
$RFEM$	Random Finite Element Method
RMS	Root Mean Square
$SoVI$	Social Vulnerability Index
$SRTM$	Shuttle Radar Topography Mission
$UNDRO$	United Nations Disaster Relief Organization
USD	United States Dollar
a_c	fraction of clay slides triggered by anthropogenic activity
a_d	fraction of debris slides triggered by anthropogenic activity

a_e	fraction of earth (or sand) slides triggered by anthropogenic activity
a_r	fraction of rock slides triggered by anthropogenic activity
A_t	total area of the region under analysis
a_L	fraction of all landslides triggered by human activity
c	cohesion
c_l	fraction of slides that are clay
d	fraction of slides that are debris
d_c	cell size
D_f	fractal dimension
D	horizontal and vertical dimensions of the region under analysis
D_u	directional derivative in the direction of a unit vector $\underset{\sim}{u}$
e	fraction of slides that are earth (or sand)
F_d	development factor
F_{pd}	population density factor
$f_s(s)$	probability density function of the slope angles
F_i	failure event if the ith slope
F_1	failure of a single random slope
$F_s(s)$	cumulative distribution function of the slope angles
I	overall coping capacity as a normalized value
I_i^{all}	non-specific hazard coping capacity indicators
$I_i^{hazard,j}$	hazard-specific coping capacity indicators
L_i	latitudinal coordinate of point i
m	maintenance factor

n	number of vulnerability indicators
n_c	number of cells in the domain
n_i	number of slopes having slope angle s_i
n_p	number of people exposed to landslide hazard
n_s	number of slope angle intervals
n_t	number of slopes in the domain
N_{n_i}	the random number of slopes that fail out those slopes having slope angle s_i
p_f	probability of regional slope failure
p_{f_c}	probability of regional slope failure for clayey soil
$p_{f_{gs}}$	probability of regional slope failure for gravely sands
p_{f_2}	expected future probability of regional slope failure
p_{s_k}	proportion of the domain having the k^{th} soil type
q_i	probability of non failure of a slope having slope angle s_i
r	fraction of slides that are rock
r_{ki}	failure probability estimate of the k^{th} soil type at the i^{th} slope angle
R	landslide risk level
R_E	radius of the Earth
R_f	future expected landslide risk level
s_i	i^{th} slope angle
s_{min}	minimum slope angle
s_{max}	maximum slope angle
$s_{_T}$	slope angle as perceived at resolution T
S	ransom slope angle

S_j	random slope angle of the j^{th} slope
S_m	random maximum slope angle
S_{T_m}	locally averaged maximum slope angle
S_x	slope angle in the horizontal direction
S_{T_x}	locally averaged slope angle in the horizontal direction
S_y	slope angle in the vertical direction
S_{T_y}	locally averaged slope angle in the vertical direction
T_{crit}	horizontal and vertical dimensions of the averaging domain at the critical scale
T_x	horizontal dimension of an averaging cell
T_y	vertical dimension of an averaging cell
T_1	horizontal and vertical dimensions of a GTOPO averaging cell
T_2	horizontal and vertical dimensions of a SRTM averaging cell
$\underset{\sim}{u}$	unit vector
v	landslide vulnerability level
v_i	vulnerability rank of each individual vulnerability indicator
v_f	expected future landslide vulnerability level
v_t	total vulnerability score of the region
w_i	weight of each individual vulnerability indicator
$Z(x, y)$	actual surface elevation at the surface location (x, y)
$Z_T(x, y)$	locally averaged surface elevation at the surface location (x, y)
$Z_T(i)^o$	observed locally averaged elevation at point i
$Z_T(i)$	true locally averaged elevation at point i
α	constant

α_i	weight of a non hazard-specific coping capacity indicator
β_i	weight of a hazard-specific coping capacity indicator
Δf	change in frequency of human-induced landslides
Δlat	difference between two latitudinal points on the Earth's surface
$\Delta long$	difference between two longitudinal points on the Earth's surface
Δp	population increase, computed as a fraction of the existing population
Δs	incremental slope value
ϵ_i	DEM elevation measurement error at point i
γ_i	relevance of hazard to coping capacity analysis
$\gamma_Z(T)$	1D variance function
$\gamma_Z(T,T)$	2D variance function
$\mu_{S_{T_m}}$	mean value of the locally averaged maximum slope angles
ϕ	friction angle
$\underset{\sim}{\nabla} Z_T$	gradient of $Z_T(x,y)$
$\rho_Z(\tau)$	1D elevation correlation function over the distance τ
$\rho_{Z_T}(2T)$	locally averaged 1D elevation correlation function over the distance $2T$
$\rho_Z(\tau_x,\tau_y)$	2D elevation correlation function over the distance (τ_x, τ_y)
σ	normal stress
σ_{S_T}	standard deviation of the locally averaged slope angles
$\sigma_{S_{T_m}}$	standard deviation of the locally averaged maximum slope angles
σ_ϵ	standard deviation of the vertical measurement error
σ_Z	point scale standard deviation of an elevation dataset
σ_{Z_T}	locally averaged standard deviation of an elevation dataset

τ	shear stress
τ_x	horizontal component of the distance between two points in the soil domain
τ_y	vertical component of the distance between two points in the soil domain
θ_R	point scale correlation length of ground strength parameters
θ_Z	point scale correlation length of an elevation dataset
θ_{Z_x}	horizontal component of the point scale correlation length of an elevation dataset
θ_{Z_y}	vertical component of the point scale correlation length of an elevation dataset

ACKNOWLEDGEMENTS

Financial support for this thesis came from the National Sciences and Engineering Research Council of Canada (grant IPS1-363060), the International Centre for Geohazards (ICG), and the Norwegian Geotechnical Institute. The author would like to express her sincere gratitude to each of these organizations for their help with this research. Additionally, the author would like to thank her thesis supervisory committee members, Dr. Craig Lake and Dr. William J. Phillips, as well as her supervisor at ICG, Dr. Farrokh Nadim, for their input and support. Finally, the author would like to convey her deepest gratitude to her supervisor at Dalhousie University, Dr. Gordon A. Fenton, whose invaluable guidance, patience and encouragement made this experience so enjoyable and enriching, and without whom none of it would have been possible.

CHAPTER 1

Introduction

1.1 Landslide Risk

Landslide events can be devastating, causing irreparable damage and loss of life. Given the unstable nature of the current environment, these natural disasters are increasing in frequency in many regions around the globe (Nadim et al., 2006). Thus, there is a pressing need to improve techniques for landslide risk management. Landslide risk refers to the probability that a region will undergo significant levels of damage from a landslide. More specifically, this risk, R, is a function of both hazard and vulnerability (UNDRO, 1979; Nadim et al., 2006), and can be calculated as:

$$R = p_f \cdot v \cdot n_p \tag{1.1}$$

where p_f represents the regional probability of a slope failure (i.e. hazard), ranked from 0 (not possible) to 1 (certain); the vulnerability, v, represents the physical and socioeconomic fragilities of the affected communities in terms of degree of loss, ranked from 0 (no loss) to 1 (complete loss); and n_p represents the number of people exposed to potential landslides.

The hazard level measures a region's physical susceptibility to landsliding. Some common indicators used to measure landslide susceptibility include maximum slope angles, lithology, soil moisture levels, precipitation patterns and seismic activity (Nadim et al., 2006). Maximum slope angles are one of the most important of these indicators because the potential for instability, resulting from the downward gravitational pull on an inclined soil mass, increases significantly with steepening slope. Maximum slope angles can be derived from digital elevation models (DEMs) which use remote sensing techniques to measure surface elevations. Consider a remote

sensing device which records average surface elevation over some areal domain of size $D \times D$, broken up into n_c cells. As the size of each individual cell decreases, the number of cells required to cover the domain increases. A maximum slope angle can be computed for each cell using the average surface elevations provided for that cell together with its neighbouring cells. Smaller cells require less local averaging and, as such, a reduction in the DEM's cell size corresponds to an increase in the amount of data available to describe the topography of the terrain. Thus, small cells provide more accurate slope estimates than large cells. For example, if the averaging dimension is 100 m, then variations within this domain having scale less than 100 m will be largely unnoticeable. In other words, small slopes (say, of extent 10 m) will not be resolved by this sensing device even if they are extremely steep – the small slopes are 'smoothed out'. Therefore, the perceived slope angle (i.e. the angle identified at a specific resolution) is very sensitive to the cell size.

The vulnerability level, v, measures a region's ability to cope with, and recover from, the repercussions of a landslide. More specifically, vulnerability can be broken down into two components: physical vulnerability and societal societal vulnerability. Physical vulnerability measures the relative resistance of buildings, the community's level of dependence upon the land for sustenance and the population density. Societal vulnerability assesses the socioeconomic milieu of a region in order to understand how much impact a landslide is expected to have on a given population. Demographic (e.g., age, urban population), social (e.g., education level, level of integration), economic (e.g., dependence on land for primary source of income, GDP per capita, building type), preparedness (e.g., quality of medical services, insurance and disaster funds) and administrative (e.g., regulation control, hazard evaluation, early warning systems, emergency response) types of indicators (Stinführer et al., 2009; Roberts et al., 2009; Lahidji, 2008; Tapsell et al., 2005; Cutter et al., 2003) all play important roles in determining a region's vulnerability to the impacts of landslides.

Once the hazard and vulnerability levels of a region have been successfully measured, and the population of the region exposed to landslide hazard has been estimated, a complete risk assessment framework can be formulated. A region deemed to have a high level of landslide risk will likely

contain a considerable number of people exposed to potential landslides, have high levels of slope instability and be highly vulnerable to loss in the event of a landslide. Any one of these factors alone does not imply a high probability of landslide-induced damage, i.e. risk. For example, a highly populated, indigent region is very vulnerable to harm in the event of a landslide, but if they are located in lowlands where there is essentially no landslide hazard, their landslide risk level is extremely low. Similarly, it is possible for region located nearby several unstable slopes to also have an extremely low landslide risk level. This would be the case if, for example, the infrastructure in the region was well-built and of high quality, the population density was low and consisted of primarily wealthy, physically fit individuals, and the community had extensive disaster funds, effective warning systems and emergency response procedures in place.

The current risk level of a region is the key (and often only) component in most analyses. However, it is important to also consider how the risk level is expected to change in the foreseeable future. Population growth and urbanization are important factors that should be considered. For example, as regions urbanize, more land is modified to meet the additional needs of the new population. Land use changes such as deforestation and expansion of developments and transportation routes become more common (Nadim et al., 2006). In addition, increased populations require more natural resources, such as water, for industrial and agricultural purposes, and often meet these needs in an unsustainable manner which permanently depletes the resources. These activities put significant levels of stress on the environment and, in many situations, decrease the stability of surrounding slopes.

1.2 Research Objectives

The objectives of this research project are threefold: (1) to perform a landslide hazard assessment using digital elevation models, (2) to perform a landslide vulnerability assessment, and (3) analyze the effects of population increase on landslide risk levels. The outcomes of all three objectives are interrelated and, when combined, produce a complete landslide risk assessment model applicable for existing and future populations.

Objective 1: Landslide hazard assessment using DEMs

The first issue addressed in this landslide hazard analysis is the effect of digital elevation model resolution on perceived slope angles. A relationship is derived between resolution and perceived slope angles using local averaging theory. Once the effects of local averaging are understood, they can be used to back-figure the distribution of slope angles, as perceived at any resolution. This thesis is concerned with landslide hazard analysis at the critical scale. The critical scale refers to the minimum scale at which we are concerned with slope failure, i.e. the minimum size that a landslide would have to be to result in noticeable damage to the surroundings. For example, if slope failure occurs in one cell of size 1 m $\times$ 1 m but not in the surrounding cells, it is unlikely that the amount of displaced soil would be hazardous, however, if a slope failure occurred in a 1000 m $\times$ 1000 m cell, it could be very hazardous. Thus, we know the critical scale must lie somewhere between 1 m $\times$ 1 m and 1000 m $\times$ 1000 m. The critical scale will vary from region to region as the amount of damage inflicted by a landslide depends upon the type of surroundings, e.g. the amount of material required to damage a wooden house or a farm is significantly lower than the amount required to damage a steel building.

Next, the conditional probability of local slope failure is evaluated. The total probability theorem, which is a function of the distribution of maximum slope angles and the conditional probability of local slope failure, is then used to determine the regional probability of slope failure, i.e. the probability that at least one slope in the region fails, which is used to define the regional hazard level. This methodology is described in detail in Chapter 3 and applied to two different test sites in Chapter 4.

Hypothesis: As the resolution of a DEM increases, the mean and standard deviation of the perceived maximum slope angles also increase. This hypothesis is based on the fact that DEM resolution is inversely proportional to the degree of local averaging. Therefore, high resolution DEMs are expected to smooth out fewer slopes and observe greater variability between the highest and lowest elevation points than low resolution models.

Objective 2: Landslide vulnerability assessment

The ability of a region to effectively cope with, and recover from, a landslide event is best estimated by addressing the physical and socioeconomic fragilities within that region. This research measures landslide vulnerability levels with an indicator-based vulnerability model. This model is composed of thirteen indicators, each weighted according to their degree of relevance to the model, and ranked from 1 (lowest degree of vulnerability) to 5 (highest degree of vulnerability), based on the conditions of the region.

The physical indicators, which include building type, urban population and rural population, provide direct measures of damage levels, whereas the socioeconomic indicators measure the coping capacity of a region. The socioeconomic indicators considered in this research include age, education level, level of integration, GDP per capita, quality of medical services, insurance and disaster funds, regulation control, hazard evaluation, early warning systems and emergency response procedures.

Although the long term impacts on a society due to injuries, lost lives and a weakened economy are hard to predict, the indicators presented in this model, when combined, provide a reasonable means of assessment. This model is described in detail in Chapter 5.

Objective 3: The effect of population increase on landslide risk levels

The third objective of this thesis is to evaluate the effects of an increasing population on landslide risk levels. The frequency of human-induced landslides is dependent upon a number of factors, including slope lithology, human interference with the natural landscape, population density and community resources. Typically, an increase in population leads to an increase in the frequency of human-induced landslides in a region. As a population grows and urbanizes, more resources, such as water, food and infrastructure, are required to fulfill all of their needs. Therefore, land use change becomes more and more common, natural resources are often over-exploited and as a result slope stability levels frequently suffer and more landslides ensue.

An empirical model describing the effect of an increasing population on the frequency of human-induced landslides, and the impact of this change on landslide risk, is developed in Chapter 5 and tested in Chapter 7.

CHAPTER 2

Literature Review

2.1 Landslide Hazard Assessment using DEMs

While maximum slope angles, as estimated using digital elevation models (DEMs), are one of the most important indicators used in landslide hazard analyses, the accuracy of the perceived slope angles is highly dependent upon the resolution of the model. This scale issue, associated with low resolution models, arises due to local averaging over the DEM cells. Although many papers allude to the impact of resolution on perceived slope angles, they rarely present a way of quantifying this effect. In other words, little progress has been made towards a model that overcomes these scaling issues, particularly one that does so using a relationship between the perceived slope angle and degree of local averaging.

In order to overcome the issues associated with resolution and successfully use digital elevation models for landslide hazard analyses, several issues must be considered: 1) the best method for computation of maximum slope angles from elevation data, and 2) the effect of DEM resolution on perceived slope angles.

1) Computation of maximum slope angles

Jones (1998) identified eight frequently used slope calculation algorithms and evaluated them individually on the basis of their root-mean square (RMS) errors. Under the assumption that the terrain surface has high spatial correlation, the *second-order finite-difference* algorithm, also referred to as Fleming and Hoffer's Method (Fleming and Hoffer, 1979), was found to perform the best, with the minimum RMS error between the predicted and actual slopes. Fleming and Hoffer's

Method, which uses four grid points, calculates a gradient in the x direction between cells $(i-1, j)$ and $(i+1, j)$ and another in the y direction between cells $(i, j-1)$ and $(i, j+1)$ (see Figure [2.1]). The remaining algorithms were ranked from best to worst as follows: *one over distance squared*, *one over distance*, *third-order finite-difference*, *constrained quadratic surface*, *diagonal Ritter's* (a modified version of second-order finite-difference), *three-point simple*, and finally, *maximum downward gradient*.

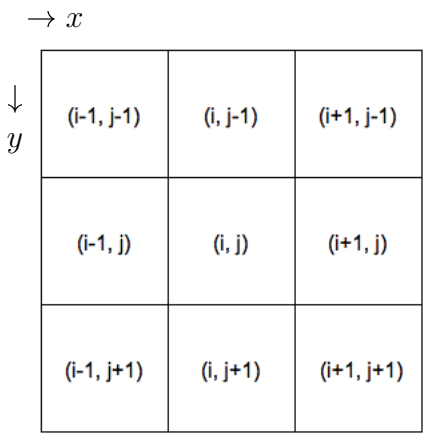

Figure 2.1 Elevation grid from a digital elevation model.

Zhang et al. (1999) also identified and compared common slope calculation algorithms, all of which utilize some form of numerical differentiation, i.e. the difference in elevation between two points divided by their separation distance, based on a 3×3 grid of cells. The first method considered, 1) *maximum drop* (also known as Jones' maximum downward gradient), calculates eight slope values, from (i, j) to each of its neighbouring cells (see Figure [2.1]), and defines S_m as the maximum of the eight slope estimates. The remaining methods considered were: 2) *linear regression*, 3) *full quadratic equation*, 4) *partial quadratic equation*, and 5) *third-order finite difference*. Methods 2 through 5 each calculate the slopes in the x and y directions (S_x and S_y) and define the maximum slope angle as $S_m = \sqrt{S_x^2 + S_y^2}$.

Zhang et al. (1999) found that methods 2 through 5 all had very similar RMS errors, and were significantly more accurate than method 1. Thus, in an effort to obtain the most accurate results possible, it would be inadvisable to choose method 1 (i.e. maximum drop).

Similarly, Raaflaub and Collins (2006) compared eight slope calculation algorithms: *three-point plane* (also known as three-point simple), *four-point closest neighbour* (also known as second-order finite-difference), *four diagonal neighbours* (also known as diagonal Ritter's), *eight neighbours unweighted* (also known as third-order finite-difference), *one over distance squared*, *maximum downhill gradient*, *multiple downhill neighbours*, and *maximum adjacent gradient*. Each of these algorithms employs between one and eight of the neighbouring cells in its slope estimate. Raaflaub and Collins (2006) concluded that the algorithms which use four of the neighbouring cells provide the most accurate results, in agreement with Jones' preference for the second-order finite-difference method (referred to as four-point closest neighbour by Raaflaub et al.), followed by the algorithms utilizing eight of the neighbouring cells. The remaining methods, i.e. two and three point algorithms, produced significantly more error in their slope estimates, and Raaflab and Collins felt that they should not be used in applications whereby accurate slope estimates are required.

2) Effect of DEM Resolution on Perceived Slope Angles

It was hypothesized in Chapter 1 that low resolution DEMs often overlook sudden changes in elevation and as a result, smooth out small, steep slopes. This smoothing effect leads to an underestimation of the maximum slope angles.

As part of a study on landslides and avalanches, Nadim et al. (2006) created a landslide hazard map which used a 'slope factor' based on slope angles derived from DEM datasets. Since the regions under analysis encompassed a significant portion of the globe, they were forced to use two different DEMs. The higher resolution dataset, applied to regions between 60° North and 60° South, had a 3 arc-second resolution with 90 m × 90 m cells. Only lower resolution models were available outside of these boundaries, thus the second dataset, used above 60° North, had a 30 arc-second resolution with 1000 m × 1000 m cells (Jaedicke, 2010; NGI, 2010). Nadim et al. (2006) recognized that the slope angles computed with the low resolution data were underestimated and tried to develop a relationship between the angles perceived by the DEMs at these two scales.

They did so by comparing the slopes computed by the lower resolution data against the higher resolutions data in two test regions; 1) Norway and 2) the Alps in the Balkan region of southern Europe. The resulting slope histograms derived at the two DEM resolutions were used to define a relationship between the slopes perceived by the 30 arc-second and 3 arc-second resolution DEMs. For instance, $8 - 10^\circ$ slope angles computed with the 30 arc-second data were assigned to the same hazard class as were $12 - 18^\circ$ slopes computed with the 3 arc-second data. Although this work by Nadim et al. (2006) addresses the issues associated with low resolution data, it does so using a very rough approximation. If a more accurate calibration technique existed, it would greatly improve the overall reliability of their model.

Zhang et al. (1999) also addressed the effect of resolution on maximum perceived slope angles. Firstly, they analyzed several DEMs (30, 10, and 5 arc-second resolutions) in eastern Asia as well as finer resolution datasets with 200 m, 30 m, and 20 m cell sizes in southeastern Spain and found that, as expected, high resolution DEMs produce steeper maximum slopes than low resolution DEMs.

Secondly, under the assumption that topography is, in general, fractal in nature (Peitgen and Saupe, 1988), Zhang et al. (1999) developed a relationship between the slope angle, S, and the corresponding scale (i.e. cell size), d_c, using the variogram technique,

$$S = \alpha d_c^{(1-D_f)} \tag{2.1}$$

where α is a constant and D_f is the fractal dimension. The variogram technique states that the statistical variation of the elevation between data points varies with the distance between them. However, as it stands, this method is not capable of estimating the spatial pattern of slopes as the values of α and D_f are assumed constant throughout the entire DEM. Zhang et al. (1999) addressed this problem using data from two of their test regions. First, they grouped the cells into a series of subareas. Next, they used high resolution DEMs to calculate α and D_f for each subarea in order to determine how significantly the values varied throughout the domain. They found that α varied the most, from 0.59 to 2023.1, while the value of D_f still varied considerably, from 1.03

to 1.96. In an attempt to overcome this issue, and use eq. [2.1] to estimate high resolution slopes from low resolution DEMs, Zhang et al. (1999) developed a method to calculate local fractal parameters from low resolution data. This methodology revolved around the assumption that while α and D_f vary in different subareas, they are highly dependent upon the standard deviation of the elevations. Zhang et al. (1999) concluded that the standard deviation of the elevations also varies significantly between subareas but decreases only slightly from high to low resolutions. By developing regression equations for the derivation of slope angles from the elevation data, they identified a relationship between the standard deviation of the elevation and α, as well as another relationship between the standard deviation and D_f. Thus, these two relationships, together with eq. [2.1], established a means of estimating the constant, α, the fractal dimension, D_f, and the scaled slope, S, at any resolution, i.e. any grid size, d_c. While the resulting scaled slope values were found, by Zhang et al. (1999), to be relatively good approximations of the true slopes in most areas, the fractal theory methodology tended to break down in regions where the elevation changed rapidly. Zhang et al. (1999) concluded that, in low resolution DEMs, the scaling properties of the slope were affected if the relative elevation changed considerably within a DEM cell. The fractal scaling properties of the slope angles are unable to account for this type of situation. While this only accounted for a small percentage of slopes within Zhang et al.'s (1999) test regions (e.g., 6% in eastern Asia and 4.3% in Guadalentin Basin, Spain), it could seriously underestimate the regional probability of slope failure in an area prone to landsliding. Therefore, it is important to consider the effects of local averaging within DEM cells for landslide hazard analyses.

Another consequence of using slope angles computed from low resolution DEMs is the effect that they have on the standard deviation of the resulting slope angles (i.e. one of the parameters required to evaluate the regional probability of slope failure). It was hypothesized in Chapter 1 that the standard deviation of slopes angles perceived by a DEM increases with increasing resolution. Smaller cells, associated with high resolution DEMs, are capable of resolving more detail and thus are more likely to observe a larger variance between the highest and lowest elevation points, thus predicting a larger range of slope angles. Underestimation of the standard deviation of the slopes, by

low resolution DEMs, presents a serious issue as this value is required to determine the distribution of maximum slope angles throughout a region, a necessary parameter for regional landslide hazard analysis. For instance, slope angles, as perceived by multiple DEMs, were examined by Chang and Tsai (1991) with cells ranging from 8m to 80 m in size, by Claessens et al. () with cell variations of 10 to 100 m, by Deng et al. () with cells from 5 m to 480 m, and by Chow and Hodgson (), on micro-scale terrain, with 2 m to 10 m cell dimensions. The results of each of these experiments indicated that higher resolution models map more terrain variance and steeper mean maximum slope angles than low resolution models.

As evidenced above, the correlation between DEM resolution and perceived maximum slope angles has been identified by a vast number of researchers. However, these papers do not consider local averaging theory as a means for quantifying the impacts of DEM resolution on slope angles. In fact, most of them only provide qualitative analyses of this resolution issue. Furthermore, most of the papers described above focus on small scale regions, usually with respect to hydrological modeling, which is unsuitable for large scale landslide hazard assessment problems, such as the one addressed by this thesis.

2.2 Landslide Vulnerability Assessment

While a significant number of papers discuss the subject of landslide vulnerability, the majority of these papers: 1) group landslides together with all other natural disasters, and/or 2) present only a rough outline for analysis, lacking any specific guidelines. For instance, most vulnerability models are composed of a set of vulnerability indicators, which must be individually evaluated and often weighted, yet most offer no explicit guidelines for evaluation or weighting (Roberts et al., 2009; Tapsell et al., 2005; Cutter et al., 2003). Thus, there is a pressing need for an unambiguous landslide-specific vulnerability model.

Roberts et al. (2009) attempt to combine the strengths typically associated with *natural* and *social* science vulnerability analyses into their vulnerability assessment framework for natural hazards. Natural sciences generally focus on the assessing vulnerability quantitatively, by considering

measurable factors such as structural damage to the built environment and loss of life. On the other hand, social sciences tend to analyze societies at large, and as such, present more qualitative analyses. The model presented by Roberts et al. (2009) consists of five vulnerability components (physical, health, economic, administrative and environmental), each broken down into three or four subcomponents (see Figure [2.2]).

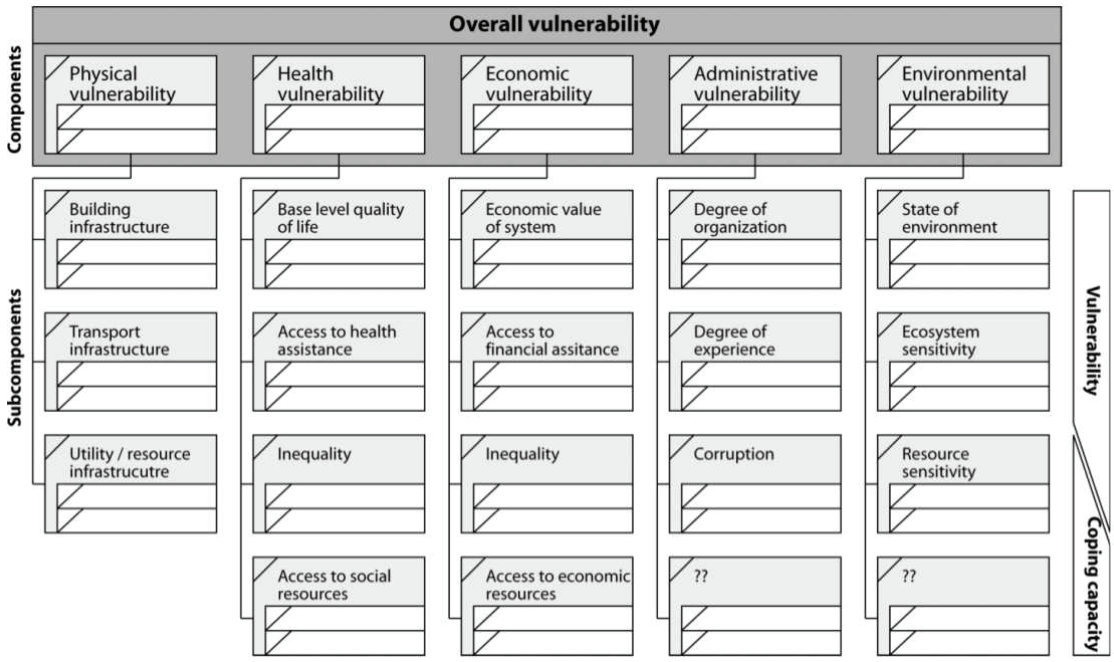

Figure 2.2 Components of the conceptual model for quantification of vulnerability (Roberts et al., 2009).

These subcomponents are considered in local context and designed to be individually weighted between 0 and 1. The goal of this weighting technique is to allow for various subcomponents to be combined and/or left out of the analysis all together. Roberts et al. (2009) do not actually weight the subcomponents themselves, however, they suggest that it should initially be done using expert judgment and later updated using back analysis with past disaster case studies. Roberts et al. (2009) also differentiated between coping capacity and vulnerability types of subcomponents, which they found to improve conceptual understanding. However, they acknowledged that this differentiation was often a hindrance during analysis.

Tapsell et al. (2005) developed an indicator-based methodology to evaluate vulnerability and resiliency levels to floods within Europe. While this models addresses floods, rather than landslides, there is a lot of overlap between the two, as they often occur together. Thus, many of the indicators described by Tapsell et al. (2005) are directly relevant to the landslide vulnerability assessment model presented in this thesis. The following indicators, assigned a (+) to denote an increase in vulnerability levels or a (-) sign to denote a decrease in vulnerability levels, were considered:

- Age – children and very elderly (+)
- Gender – women (+)
- Employment (-)
- Unemployment (+)
- Occupation (± depending upon whether skilled or unskilled, also linked to income and financial status)
- Education level (higher education level -, lower education level +)
- Family/household composition (large families +, single parents +, single person households +, home owner -, renter +, etc.)
- Nationality/ethnicity (non-white +, new migrants +)
- Type of housing (single storey accommodation +, mobile housing +)
- Number of rooms (low number indicates overcrowding +)
- Rural/urban (low income rural +, high density urban +)
- Levels of risk awareness and preparedness (high awareness -, low +)
- Previous flood experience (no experience +)
- Access to decision-making (increased access -)
- Trust in authorities (no +, yes -)
- Long-term-illness or disability (+)

- Length of residence (linked to prior experience, short residence +)
- Serviced by flood warning system (yes -, no +)
- Type of flood (indicates potential damage levels)
- Flood return period (indicates potential damage levels)

However, Tapsell et al. (2005) did not address issues such as combining and weighting indicators. Therefore, they did not present a conclusive model capable of assigning a final regional vulnerability score.

Cutter et al. (2003) developed a county-level social vulnerability index (SoVI) for natural disasters in the United States based on 11 independent indicator variables, reduced from 42 using a factor analysis approach. They performed a statistical analysis on the final 11 indicators to determine the amount of variance explained by each and the inter-variable correlations which resulted in the following ranking (see Figure [2.3]), from most-to-least important.

Cutter et al. (2003) assigned each of the indicators a 'factor score' (i.e. similar to weight) indicative of its level of importance to the model and calculated the total SoVI score for each county as the sum of the factors influencing the region. The SoVI levels were categorized relative to the mean US value (see Figure [2.4]), counties with a SoVI score greater than +1 standard deviation were considered the most vulnerable and those with greater than -1 standard deviation the least vulnerable; the SoVI ranged from -9.6 to 49.51 throughout the US with mean vulnerability score of 1.54 and a standard deviation of 3.38. The counties with the highest levels of vulnerability (i.e. standard deviations greater than +1) were found to contain a geographic mix of highly urbanized counties, large Hispanic and/or Native American populations, and socially dependent populations (e.g., those lacking education).

Factor	Name	Percent Variation Explained	Dominant Variable	Correlation
1	Personal wealth	12.4	Per capita income	+0.87
2	Age	11.9	Median age	−0.90
3	Density of the built environment	11.2	No. commercial establishments/mi^2	+0.98
4	Single-sector economic dependence	8.6	% employed in extractive industries	+0.80
5	Housing stock and tenancy	7.0	% housing units that are mobile homes	−0.75
6	Race—African American	6.9	% African American	+0.80
7	Ethnicity—Hispanic	4.2	% Hispanic	+0.89
8	Ethnicity—Native American	4.1	% Native American	+0.75
9	Race—Asian	3.9	% Asian	+0.71
10	Occupation	3.2	% employed in service occupations	+0.76
11	Infrastructure dependence	2.9	% employed in transportation, communication, and public utilities	+0.77

Figure 2.3 Dimensions of social vulnerability (Cutter et al., 2003).

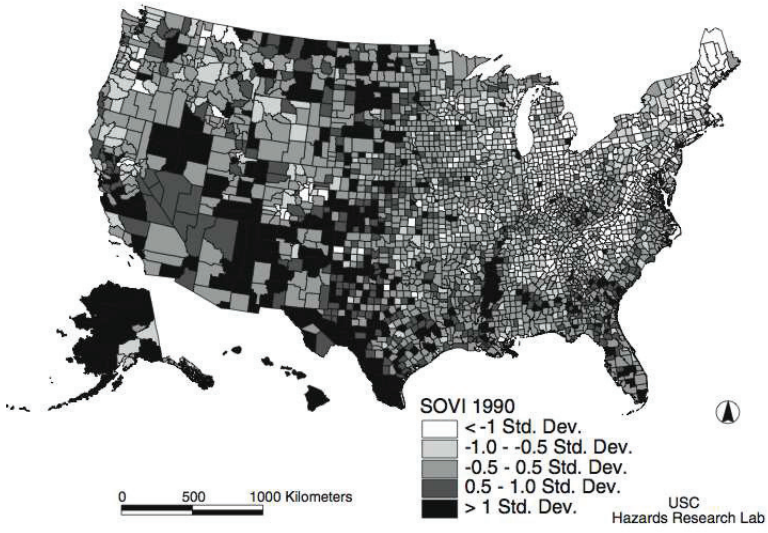

Figure 2.4 Comparative vulnerability of U.S. counties based on the social vulnerability index (SoVI) (Cutter et al., 2003).

In contrast to the models described above, some papers do provide guidelines for evaluating vulnerability indicators. However, most of these papers focus on a specific aspect of vulnerability,

rather than addressing the issue as a whole. For example, Lahidji (2008) focuses on the development of a model to measure the coping capacity of a region in the event of a natural disaster. While most of his criteria are widely applicable for any type of event, he has also included several hazard-specific indicators that focus on one or more of the following types of natural disasters: wildfires, avalanches, tsunamis, volcanoes, droughts, typhoons, *landslides*, floods and earthquakes. In order to assess the coping capacity, Lahidji (2008) used existing data (governance and development indicators) to quantify the legal and regulatory framework, environmental sustainability, infrastructure equipment, macroeconomic activity and social safety net, then developed questionnaires to address the remaining indicators:

- Hazard evaluation
- Consequences and vulnerability assessment
- Awareness-raising activities
- Sectoral regulations
- Structural defenses
- Continuity planning
- Early warning
- Emergency response
- Insurance and disaster funds
- Reconstruction and rehabilitation planning

The purpose of these questionnaires is to provide a means of ranking each of the indicators, from 1 to 5, based on their relationship to coping capacity. Rank 1 indicates that the indicator has not been considered in the region and thus, denotes a low coping capacity (e.g. for hazard evaluation: there has been no monitoring or forecasting of past events), while level 5 indicates a high level of consideration and thus, a high capacity to cope with a natural disaster should one occur (e.g. detailed hazard mapping and analysis has been completed). In addition to ranking,

each indicator is supposed to be weighted based on its degree of relevance to the model. However, Lahidji (2008) did not discuss how to select appropriate weights. Finally, Lahidji (2008) developed an equation to evaluate the overall coping capacity as a normalized value, I,

$$I = \sum_i \left(\alpha_i \cdot I_i^{all}\right) + \sum_i \sum_j \left(\beta_i \cdot \gamma_j \cdot I_i^{hazard,j}\right) \tag{2.2}$$

where α_i represents the weights of all non-specififc hazard indicators I_i^{all}, β_i represents the weights of hazard-specific indicators $I_i^{hazard,j}$, γ_j represents the weight (i.e. relevance of hazard j (e.g. landslides, floods, or wildfires) for the country), calculated in terms of exposure, and $\sum \alpha_i = \sum \beta_i = \sum \gamma_i = 1$.

2.3 The Effect of Population Increase on Landslide Risk Levels

In many regions around the globe, the frequency of landslides is noticeably increasing (Nadim et al., 2006). One of the main factors attributing to this increased occurrence of landslides is growing levels of urbanization and, as a result, increased amounts of land-use change. As Nadim et al.'s (2006) study on landslides and avalanches noted, when the population of a region increases, land that was once left in its natural state is often developed. These land-use changes typically include deforestation, expansion of developments and transportation routes and/or over-exploitation of natural resources (e.g., water supplies), which often leads to greater levels of instability in soil surfaces. As a result, existing slopes become increasingly unstable and more likely to fail. Furthermore, due to the large amount of urbanization occurring, especially in developing regions, borders to land that was once considered uninhabitable (e.g., in the mountains) is constantly being extended.

The SafeLand project (Nadim et al., 2010), which analyzes landslide risk throughout Europe, focused on many factors associated with landslide risk, including the effects of population increase. One of the case studies examined involved a series of more than 400 superficial landslides in the Alpes-Maritimes, in France, induced by heavy rainfall. Although, naturally induced, in the sense

that the landslides were initiated by rainfall, the extent of the disaster was largely attributed to land-use changes (i.e. anthropogenic activity). This region, which was once sparsely populated with an expanse reserve of water resources, has been urbanized and its water resources have since been over-exploited. Due to the nature of these land-use changes, slope stability levels have significantly decreased and, as a result, the region has become much more susceptible to sliding.

Work project 1.4 of the SafeLand project (Nadim et al., 2010) identified various other landslides induced, partly or fully, by human activity (see Figure [2.5]).

Location	Date	Material type	Main cause	Consequences
Lyon, France	13 Nov. 1930	Marly sand & backfill layers	Lack of maintenance of the old water canalization network, which led to increased pore water pressure in the superficial layers.	39 deaths (23 rescuers buried by the 2nd event) and 15 mill. old French francs
Switzerland	15 Oct. 2000	Karsts, scree deposits and moraines	Breaking of water canalization that created several debris flows.	No fatality, but significant farming damages.
Switzerland	1 Sept. 2002	Moraine, sandstone and marls	Permanent water saturation caused instability due to broken pipe.	3 houses destroyed killing 3 people.
Quebec city, Canada	19 Sept. 1889	Sedimentary rocks (Utica slate formation)	Unfavourable geometry of discontinuities + slope cutting + water infiltration due to leak in drainage pipe.	40 people died in their destroyed houses.
Wales, United Kingdom	21 Oct. 1966	Coal mining debris	Spoil heap destabilized by modification of the geometry.	School and 18 houses destroyed killing 116 children and 28 adults.
Switzerland	14 March 1922	Rock	Geometry of slopes and discontinuity sets were favourable for toppling. The general stability of the slope was disturbed and worsened by the quarry.	No fatality, but significant material damage.
Switzerland	11 Sept. 1889	Slate	Unfavourable geometry of discontinuities + critical slope cutting.	115 fatalities.
South West Alberta, Canada	29 April 1903	Rock	Unfavourable geometry of discontinuities + mining activities.	70 deaths and significant material damage.
Møre and Romsdal, Norway	26 March 2008	Rock	Bad slope design and inadequate slope stabilization.	5 fatalities and significant material damage.
Switzerland	9 Jan. 2001	Shaly sandstones	Road cut.	Significant damages of the infrastructure.
Trøndelag, Norway	13 March2009	Quick clay	Blasting during road construction.	No casualty, but significant economic damage.
Trøndelag, Norway	29 April 1978	Quick clay	Building works (head charge with excavation material) leading to retrogressive sliding.	One casualty and significant economic damage.
Menton, France	Winter 2000	Superficial soils	Heavy rainfall event on a territory where land-use has changed. Bad management of water flows.	400 shallow landslides and mudflows within few days; no fatalities; 10 M€ of urgent work.

Figure 2.5 Case studies of human-induced landslides in Europe (Nadim et al., 2010).

These examples illustrate the negative effects that a population can have on slope stability, thereby indicating the potential of increased populations to instigate a higher frequency of human-induced landslides.

CHAPTER 3

Landslide Hazard Assessment using DEMs

The assessment of regional landslide hazard is critically dependent upon the distribution of slope angles throughout the region. The equilibrium state of any terrain is a flat plane. The farther a terrain is away from a flat plane, i.e. the steeper the slope, the more likely the terrain is to fail in order to achieve this equilibrium state. Thus, maximum slope angles are an important indicator for slope stability. Other intrinsic factors such as soil composition and moisture level, as well as extrinsic factors such as precipitation and seismic activity, also highly influence slope stability levels (Nadim et al., 2006). The landslide model presented in this thesis estimates maximum slope angles from digital elevation models and uses these results together with the regional ground strength parameters to predict the probability of regional slope failure. Moreover, with a few minor adjustments, the landslide model presented here can be easily adapted to estimate snow avalanche hazard levels. However, this thesis will only consider landslides.

3.1 Probability of Slope Failure

Let F_1 be the event that a single randomly selected slope, having random slope angle S, fails. The total probability theorem allows the probability of F_1 to be calculated as

$$\mathrm{P}[F_1] = \int_{s_{min}}^{s_{max}} \mathrm{P}\left[F_1 \mid S = s\right] \cdot f_S(s)ds \tag{3.1}$$

where $\mathrm{P}\left[F_1 \mid S = s\right]$ is the conditional probability of slope failure given the slope angle and the integral is evaluated over all possible slope angles, s. The function $f_s(s)$ is the probability density

function of the slope angles. The integral in eq. [3.1] will be evaluated numerically by discretizing the possible slope angles into a series of ranges, s_i, where

$$s_i = \left[s_i - \frac{\Delta s}{2}, s_i + \frac{\Delta s}{2} \right] \tag{3.2}$$

and the incremental value Δs is

$$\Delta s = \left[\frac{(s_{max} - s_{min})}{n_s} \right] \tag{3.3}$$

where s_{min} and s_{max} are the minimum and maximum slope angles and n_s is the total number of slope angle intervals considered. For example, if $s_{min} = 0^\circ$ and $s_{max} = 90^\circ$, and n_s is selected to be 90, then $\Delta s = 1^\circ$ and the set of slope angle ranges becomes [0°, 0.5°), [0.5°, 1.5°), . . ., [89.5°, 90°). Under this discretization scheme, it is convenient to simply round the continuous random slope variable, S, to the midpoint of each range, e.g., one of $s_i = 0^\circ, 1^\circ, 2^\circ, \ldots, 90^\circ$, where the first and last intervals are taken at their endpoints.

This research will deal with the slope angles in units rise/run (i.e. in m/m). Thus, the range of slope angles would become [tan 0°, tan 0.5°), [tan 0.5°, tan 1.5°), . . ., [tan 89.5°, tan 90°), which can be simplified by rounding to the midpoint of each range such that, s_i = tan 0°, tan 1°, tan 2°, . . ., tan 90°.

Under this discretization, eq. [3.1] becomes

$$\mathrm{P}[F_1] \approx \sum_{s_i = s_{min}}^{s_{max}} \mathrm{P}\left[F_1 \mid S = s_i\right] \cdot \mathrm{P}[S = s_i] \tag{3.4}$$

where $P[S = s_i]$ is the probability that the randomly selected slope angle is s_i.

3.2 Regional Landslide Hazard Level

Given the probabilities, $\mathrm{P}\left[F_1 \mid S = s_i\right]$ and $\mathrm{P}[S = s_i]$, it is possible to estimate the probability of failure of a randomly selected slope (having a random slope angle with distribution $f_S(s)$). However, a region is generally composed of several, perhaps a very large number, of individual slopes. The question, in this case, is how to define the *regional* hazard level. In this research,

landslide failure of a region will be defined as occurring if one or more slopes in the region fail. The regional hazard level will be defined as the probability of this event, that is, the probability of one or more slopes in the region failing. Therefore, attention should now be turned to calculating the probability of *at least* one slope failure throughout an entire region of some areal extent, A_t. If the area is large, then it will consist of possibly very many separate slopes, $j = 1, 2, \ldots, n_t$, where n_t is the number of slopes in the region. Each of these slopes will have some random slope angle S_j.

For simplicity, assume that a typical slope in the region has areal dimensions $T \times T$ (T might be considered to be the minimum dimension below which slope failure is not a threat). If this is so, then the number of slopes having slope angle s_i in the region will be

$$n_i = n_t \cdot \mathrm{P}[S = s_i] = \frac{A_t \cdot \mathrm{P}[S = s_i]}{T^2} \tag{3.5}$$

Letting N_{n_i} be the random number of slopes that fail out those slopes having slope angle s_i, then the probability that one or more of these slopes fail is $\mathrm{P}\left[N_{n_i} \geq 1\right]$. As this probability increases, the general landslide hazard level of the region will also increase. Assuming independence between the n_i slopes, each having slope angle s_i, and that the probability of slope failure is constant at $\mathrm{P}[S = s_i]$, then the probability of at least one slope failure from these slopes is given by

$$\begin{aligned} \mathrm{P}\left[N_{n_i} \geq 1\right] &= 1 - \mathrm{P}\left[N_{n_i} = 0\right] \\ &= 1 - q_i^{n_i} \end{aligned} \tag{3.6}$$

where q_i is the probability of non-failure of a slope having slope angle s_i,

$$q_i = 1 - \mathrm{P}\left[F_1 \mid S = s_i\right] \tag{3.7}$$

Note that the assumption that slopes fail independently with constant failure probability, $\mathrm{P}\left[F_1 \mid S = s_i\right]$, means that N_{n_i} follows a binomial distribution.

The assumption that the slopes fail independently is admittedly not very reasonable. For example, if an earthquake strikes the region, it is more likely that several slopes will fail – the

common factor being the seismic cause. However, the assumption of independence is *conservative*, in the sense that it leads to a higher probability of failure than if the slope failures are positively correlated (i.e., if one fails, others are more likely to fail). This can be illustrated as follows; consider two slopes each having failure probability p. Suppose that if one slope fails, the probability of failure of the other becomes αp, where $\alpha > 1$ if slope failures are positively correlated. In this case, the probability of failure of at least one slope is

$$\begin{aligned} \mathrm{P}\left[F_A \cup F_B\right] &= \mathrm{P}\left[F_A\right] + \mathrm{P}\left[F_B\right] - \mathrm{P}\left[F_A \mid F_B\right] \mathrm{P}\left[F_B\right] \\ &= 2p - \alpha p^2 \end{aligned} \tag{3.8}$$

where F_i is the failure event of the i$^t h$ slope ($i = A, B$). If $\alpha = 1$ (independence), then

$$\mathrm{P}\left[F_A \cup F_B\right] = 2p - p^2 \tag{3.9}$$

It can be seen that $(2p - \alpha p^2) < (2p - p^2)$ when $\alpha > 1$, by virtue of the fact that $\alpha p^2 > p^2$, so the assumption of independently failing slopes gives a higher failure probability. The same principle extends to multiple slopes. If the landslide hazard is to be investigated under an earthquake, then all that needs changing in the model presented in this thesis is to find $\mathrm{P}\left[F_1 \mid S = s_i\right]$ under seismic loading (Section 3.4 introduces an approach for evaluating $\mathrm{P}\left[F_1 \mid S = s_i\right]$ under static loading conditions, i.e., selfweight only).

Equation [3.6] provides a conservative measure of the landslide susceptibility over a region. It should be noted that this measure depends on the size of the region, A_t. As A_t goes to infinity, the number of slopes involved also goes to infinity, and the regional probability of slope failure goes to one, $\mathrm{P}\left[N_{n_i} \geq 1\right] \rightarrow 1$. This makes sense in that it is to be expected that at least one slope failure will occur in very large areas. This issue, however, suggests that another measure of landslide hazard might involve a unit area slope failure probability. However, such a measure is left for future work.

As mentioned above, the regional landslide hazard level, p_f, is defined as the probability of failure of at least one slope throughout the region, A_t, which can be computed using the total

probability theorem over the range of possible slope angles,

$$\begin{aligned} p_f &= \sum_{s_i=s_{min}}^{s_{max}} \mathrm{P}\left[N_{n_i} \geq 1\right] \cdot \mathrm{P}\left[S = s_i\right] \\ &= \sum_{s_i=s_{min}}^{s_{max}} \left(1 - q_i^{n_i}\right) \cdot \mathrm{P}\left[S = s_i\right] \end{aligned} \tag{3.10}$$

3.3 Digital Elevation Models

Geographic information system (GIS) databases are becoming increasingly common and available at ever higher resolution levels. Of particular value in determining landslide hazard levels are digital elevation models (DEM), in which the elevation of the land is determined, usually by remote sensing, at a series of points. Most DEMs involve determining some sort of average elevation over some spatial dimension, the latter of which defines its resolution.

Consider a remote sensing device which records average surface elevation over some areal domain of size $T \times T$. If $Z(x, y)$ is the actual surface elevation at the surface location (x, y), where x and y are coordinate axes which may be aligned with the edges of the DEM but lie in the plane of the surface, then the local average elevation, $Z_T(x, y)$ over a domain of size $T \times T$ is given by

$$Z_T(x, y) = \frac{1}{T^2} \int_{y-T/2}^{y+T/2} \int_{x-T/2}^{x+T/2} Z(s, r)\, ds\, dr \tag{3.11}$$

Evidently, averaging over a cell may smooth over a lot of variation within the averaging domain and significantly reduce the range of slope angles identified. This statement is in agreement with the hypothesis presented in Chapter 1, which stated that as the resolution of a DEM increases (i.e. cell size decreases), the amount of averaging decreases and the standard deviation of the perceived slope angles increases.

3.3.1 Averaging Dimensions

When dealing with DEMs applied at a global scale, the exact cell size is dependent upon its geographic coordinates (Zhang et al., 1999). Due to the spherical nature of the Earth, the DEM cell size will change the most near the poles and least near the equator. The precise dimensions can be computed using the Haversine formula (Smith et al., 2007):

$$T = 2R_E \arcsin \sqrt{\sin^2\left(\frac{\Delta_{lat}}{2}\right) + \cos(L_1) \cdot \cos(L_2) \cdot \sin^2\left(\frac{\Delta_{long}}{2}\right)} \tag{3.12}$$

where R_E is the radius of the Earth, which is approximately 6371 km (NIMA, 2000), L_1 and L_2 are the latitudinal coordinates on the Earth's surface of the cell edges, Δ_{lat} is the difference between the two latitudinal coordinates and Δ_{long} is the difference between two longitudinal coordinates.

3.3.2 Elevation Data

Elevation data provided by digital elevation models can be used to estimate the distribution of slope angles, $P[S = s_i]$, throughout a region. However, the accuracy of the resulting slope angles measured by a DEM is dependent upon its resolution. Since the resolution is inversely related to the degree of local averaging, low resolution DEMs experience high levels of local averaging and as such, overlook much of the variation within a domain. As a result, low resolution DEMs often underestimate regional landslide hazard levels.

The landslide hazard model presented in this thesis requires data from two digital elevation models of differing resolutions. The slope angles perceived at each resolution will undergo different degrees of local averaging and therefore differ somewhat from the true slope angle. The amount of error is related to the DEM resolution. Local averaging theory, when applied to data provided by two DEMs, can be used to back-figure the distribution of slope angles at any resolution. In this research, interest is focused on a critical scale, where the critical scale refers to the minimum dimension at which a single slope failure is deemed to be potentially hazardous. For example, a failure of a slope of 1 m $\times$ 1 m would not likely be hazardous, whereas failure of a 1000 m $\times$ 1000 m slope could be very hazardous.

Let T_1 represent the averaging domain of one of the DEMs, and T_2 the averaging domain of the other. Each of these datasets experiences some degree of local averaging, the extent of which is dependent upon the cell size T (which will typically be equal to one of T_1 or T_2). Based on local averaging theory (Fenton and Griffiths, 2008), a relationship can be derived between the standard deviation of elevation data averaged over each DEM cell, σ_{Z_T}, and the standard deviation of the elevation data at the point scale, σ_Z.

$$\sigma_{Z_T}^2 = \sigma_Z^2 \cdot \gamma_Z(T,T) \tag{3.13}$$

where $\gamma_Z(T,T)$ is the 2D variance function, which describes the amount that the variance is reduced when the elevation is averaged over the cell domain, $T \times T$. The value of $\gamma_Z(T,T)$ decreases from one to zero as T increases. Since it is a multiplicative factor, a high value of $\gamma_Z(T,T)$ indicates a low degree of local averaging.

There are a number of commonly used variance functions (see e.g., Fenton and Griffiths, 2008), each derived from a corresponding common correlation function. In this research the Gaussian correlation function is adopted to govern the correlations between DEM elevations. One of the advantages of the Gaussian correlation structure, over others such as the Markovian correlation structure, is that it is mean square differentiable, meaning that its derivates have finite variance. Mean square differentiability simplifies the model mathematically by ensuring that the slope variance remains finite (which would generally be true).

If $Z_T(x,y)$ has a Gaussian correlation structure, its correlation function, $\rho_Z(\tau_x,\tau_y)$, and variance function, $\gamma_Z(T_x,T_y)$, are as follows (Fenton and Griffiths, 2008)

$$\begin{aligned}
\rho_Z(\tau_x,\tau_y) &= \exp\left\{-\pi\left[\left(\frac{\tau_x}{\theta_{Z_x}}\right)^2+\left(\frac{\tau_y}{\theta_{Z_y}}\right)^2\right]\right\} \\
&= \exp\left\{-\pi\left(\frac{\tau_x}{\theta_{Z_x}}\right)^2\right\}\exp\left\{-\pi\left(\frac{\tau_y}{\theta_{Z_y}}\right)^2\right\} \\
&= \rho_Z(\tau_x)\rho_Z(\tau_y)
\end{aligned} \tag{3.14}$$

and

$$\gamma_Z(T_x, T_y) = \frac{\theta_{Z_x}^2 \theta_{Z_y}^2}{\pi^2 T_x^2 T_y^2} \left(\frac{\pi |T_x|}{\theta_{Z_x}} \text{erf} \left\{ \frac{\sqrt{\pi} |T_x|}{\theta_{Z_x}} \right\} + \exp \left\{ \frac{-\pi T_x^2}{\theta_{Z_x}^2} \right\} - 1 \right) \cdot$$
$$\left(\frac{\pi |T_y|}{\theta_{Z_y}} \text{erf} \left\{ \frac{\sqrt{\pi} |T_y|}{\theta_{Z_y}} \right\} + \exp \left\{ \frac{-\pi T_y^2}{\theta_{Z_y}^2} \right\} - 1 \right)$$
$$= \gamma_Z(T_x) \gamma_Z(T_y) \tag{3.15}$$

where T_x and T_y are the directional cell dimensions, e.g., typically one of $T_x = T_y = T_1$ or T_2. The point scale correlation length, θ_Z, is used to describe the degree of linear dependence between data points. For example, if for any two points separated by distance τ, when the elevation of one doubles, the elevation of the other does as well, then points separated by distance τ are strongly correlated. This typically occurs when τ is small, i.e. points are close together. The correlation length, θ_Z, may be roughly viewed as the separation distance beyond which the two points will be largely uncorrelated. Thus, the smaller the correlation length, the more erratic the distribution of peaks in a mountainous region (due to more independence between elevations).

Note that the correlation function given by eq. [3.14] is separable, which means that the variance function is also separable. Furthermore, if $\theta_{Z_x} = \theta_{Z_y} = \theta_Z$, then the correlation function is also isotropic. Assuming isotropy, the correlation function simplifies as follows:

$$\rho_Z(\tau_x, \tau_y) = \exp \left\{ -\frac{\pi}{\theta_Z^2} \left(\tau_x^2 + \tau_y^2 \right) \right\} \tag{3.16}$$

Letting $\tau = \sqrt{\tau_x^2 + \tau_y^2}$ be the absolute distance between any two points, the correlation function can be expressed as

$$\rho_Z(\tau) = \exp \left\{ -\pi \left(\frac{\tau}{\theta_Z} \right)^2 \right\} \tag{3.17}$$

The corresponding variance function can now be expressed as

$$\gamma_Z(T, T) = \gamma_Z^2(T) \tag{3.18}$$

where

$$\gamma_Z(T) = \frac{\theta_Z^2}{\pi T^2} \left(\frac{\pi T}{\theta_Z} \text{erf} \left\{ \frac{\sqrt{\pi} T}{\theta_Z} \right\} + \exp \left\{ \frac{-\pi T^2}{\theta_Z^2} \right\} - 1 \right) \tag{3.19}$$

Given two DEM datasets, the following relationships emerge from equations [3.13], [3.18] and [3.19]

$$\sigma_{Z_{T_1}} = \sigma_Z \cdot \gamma_Z(T_1) \tag{3.20a}$$

$$\sigma_{Z_{T_2}} = \sigma_Z \cdot \gamma_Z(T_2) \tag{3.20b}$$

The ratio of these two standard deviations is

$$\frac{\sigma_{Z_{T_1}}}{\sigma_{Z_{T_2}}} = \frac{\gamma_Z(T_1)}{\gamma_Z(T_2)} = \left[\frac{\frac{\theta_Z^2}{\pi T_1^2}\left(\frac{\pi T_1}{\theta_Z}\text{erf}\left\{\frac{\sqrt{\pi}T_1}{\theta_Z}\right\} + \exp\left\{\frac{-\pi T_1^2}{\theta_Z^2}\right\} - 1\right)}{\frac{\theta_Z^2}{\pi T_2^2}\left(\frac{\pi T_2}{\theta_Z}\text{erf}\left\{\frac{\sqrt{\pi}T_2}{\theta_Z}\right\} + \exp\left\{\frac{-\pi T_2^2}{\theta_Z^2}\right\} - 1\right)} \right] \tag{3.21}$$

which is a function of the correlation length, θ_Z, and T_1, T_2, $\sigma_{Z_{T_1}}$ and $\sigma_{Z_{T_2}}$. The last four are either known or can be estimated from the DEM dataset. Thus, eq. [3.21] has only one unknown, the correlation length θ_Z. Therefore, the point scale correlation length, θ_Z, can be determined by solving eq. [3.21] for θ_Z. This value of θ_Z can then be plugged back into eq. [3.19], separately for each DEM (i.e. T_1 and T_2), in order to calculate the values of $\gamma_Z(T_1)$ and $\gamma_Z(T_2)$. Finally, the following equation, which is simply a rearrangement of eq. [3.13], can be used to calculate the point scale standard deviation of the elevation data, σ_Z,

$$\sigma_Z = \frac{\sigma_{Z_T}}{\gamma_Z(T)} \tag{3.22}$$

using the values of σ_{Z_T} and $\gamma_Z(T)$ at either resolution. This value of σ_Z is important for determining the distribution of maximum slope angles throughout the region $D \times D$, as illustrated in the next section.

3.3.3 Distribution of Slope Angles

Assuming that the average elevation over each cell, $T \times T$, is taken at the center of the cell (see eq. [3.11]) and that average elevations are recorded at regular intervals separated by distance T, the DEM produces a regular grid of adjacent average elevations. The slopes through a particular

cell in the two coordinate directions, x and y, can be estimated using second-order finite-difference approximations (the approach favored by Raaflaub and Collins (2006) and Jones (1998))

$$S_{Tx}(x,y) = \frac{Z_T(x+T,y) - Z_T(x-T,y)}{2T} \tag{3.23a}$$

$$S_{Ty}(x,y) = \frac{Z_T(x,y+T) - Z_T(x,y-T)}{2T} \tag{3.23b}$$

where the equations are modified for the cells along the edge of the DEM. For example, $S_{Tx}(x,y)$ is evaluated as $\frac{Z_T(x,y)-Z_T(x-T,y)}{T}$ along the right edge.

These slopes angles, $S_{Tx}(x,y)$ and $S_{Ty}(x,y)$, represent the values of the slopes as perceived at a given DEM resolution, and are expressed in terms of rise over run.

3.3.4 Effects of Resolution on Perceived Slope Angles

1) Standard deviation of locally averaged slope angles

According to theory for the derivative process of threshold excursions in one dimension, given stationary $Z_T(x,y)$, both $S_{Tx}(x,y)$ and $S_{Ty}(x,y)$ have zero mean (i.e. the underlying ground surface is approximately flat) and the following variances (Fenton and Griffiths, 2008)

$$\begin{aligned}\text{Var}\left[S_{T_x}\right] &= \frac{1}{(2T)^2}\text{Var}\left[Z_T(x+T,y) - Z_T(x-T,y)\right] \\ &= \frac{1}{4T^2}\left\{2\text{E}\left[Z_T^2\right] - 2\text{E}\left[Z_T(x+T,y)\cdot Z_T(x-T,y)\right]\right\}\end{aligned} \tag{3.24}$$

Given the following relationships

$$\sigma_Z^2 = \text{E}\left[Z_T^2\right] - \text{E}^2[Z_T] \tag{3.25}$$

$$\sigma_Z^2\rho_{Z_T}(2T) = \text{E}\left[Z_T(x+T,y)\cdot Z_T(x-T,y)\right] - \text{E}^2[Z_T] \tag{3.26}$$

where $\text{E}[Z_T]$ represents the expected value of Z_T (and so on), equation [3.24] can be simplified to

$$\begin{aligned}\text{Var}\left[S_{T_x}\right] &= \frac{1}{4T^2}\left[2\sigma_Z^2 + 2\text{E}^2[Z_T] - 2\sigma_Z^2\rho(2T) - 2\text{E}^2[Z_T]\right] \\ &= \frac{1}{4T^2}\left[2\sigma_Z^2 - 2\sigma_Z^2\rho(2T)\right]\end{aligned}$$

$$= \frac{\sigma_Z^2}{2T^2}\left[1 - \rho_{Z_T}(2T)\right] \tag{3.27}$$

where $\rho_{Z_T}(2T)$ is the Gaussian 2D correlation function (see eq. [3.17]) of the locally averaged data

$$\rho_{Z_T}(2T) = \exp\left[-\pi\left(\frac{2T}{\theta_{Z_T}}\right)^2\right] \tag{3.28}$$

and θ_{Z_T} is the locally averaged correlation length, which needs to be determined.

Furthermore, the variance in each of the x and y directions are assumed to be approximately equal, i.e. $\text{Var}\left[S_{T_x}\right] = \text{Var}\left[S_{T_y}\right] = \text{Var}\left[S_T\right] = \sigma_{S_T}^2$, and the standard deviation of the locally averaged slope angles can be evaluated as

$$\sigma_{S_T} = \frac{\sigma_Z}{T\sqrt{2}}\sqrt{\left[1 - \exp\left[-\pi\left(\frac{2T}{\theta_{Z_T}}\right)^2\right]\right]} \tag{3.29}$$

Stationarity, or statistical homogeneity, of $Z_T(x, y)$ implies that its mean, variance and correlation structure are independent of position. In other words, the mean and variance are constant over space and the correlation structure depends on relative positions. In this research, stationarity has been assumed.

a) Standard deviation of slope angles at the critical scale

As previously mentioned in Section 3.3.2, the critical scale refers to the minimum size at which a single slope failure is considered hazardous. Also, as previously mentioned, the slope variance increases as the cell size decreases. Thus, interest is really in these small cell sizes. However, there is no point in considering cell sizes below the critical scale since slope failures at those scales are not hazardous. The critical scale then is the scale which this research will concentrate on as the best indicator of landslide hazard. As will be shown, the correlation length between elevations is very much greater than the critical resolution for the two test regions considered. Therefore, the correlation length and standard deviation of the elevation data at the critical scale are approximately equal to the values computed at the point scale, i.e. $\theta_{Z_{T_{crit}}} \simeq \theta_Z$ and $\sigma_{Z_{T_{crit}}} \simeq \sigma_Z$. As a result,

eq. [3.29] can be used to solve for the standard deviation of the slope angles, i.e.

$$\sigma_{S_{T_{crit}}} = \frac{\sigma_{Z_{T_{crit}}}}{T_{crit}\sqrt{2}} \sqrt{\left[1 - \exp\left[-\pi\left(\frac{2T_{crit}}{\theta_{Z_{T_{crit}}}}\right)^2\right]\right]}$$
$$\simeq \frac{\sigma_Z}{T_{crit}\sqrt{2}} \sqrt{\left[1 - \exp\left[-\pi\left(\frac{2T_{crit}}{\theta_Z}\right)^2\right]\right]} \tag{3.30}$$

where T_{crit} is selected based upon expert judgement and will vary from region to region.

b) Standard deviation of slope angles at the DEM scales

The hazard level perceived by each of the DEMs is less than that at the critical scale. Therefore, it is not required to computed the hazard level at each of DEM resolutions. However, it is useful to compare the hazard levels perceived by each of the DEMs with the hazard level estimated at the critical scale. Through this comparison it is possible to determine which DEMs are accurate enough for landslide hazard analysis on specific types of terrain. For example, if a DEM of some resolution $T \times T$ produces slope estimates within 5% of those at the critical scale in several mountainous test regions, it could potentially be considered accurate enough for all landslide hazard analyses in mountainous regions. This would allow future hazard assessments to proceed faster, as they would not require two DEMs and calculations at the critical scale. Instead, a DEM of resolution $T \times T$ would be considered adequate. However, eq. [3.29] cannot be used to calculate the standard deviations of the slope angles at the DEM resolutions, as done for the critical scale, because the correlation lengths of the locally averaged data, θ_{Z_T}, are unknown. Thus, the standard deviation of the slope angles, σ_{S_T}, must be evaluated through a statistical analysis of the DEM datasets.

The distribution of slope angles, in each of the x and y directions, is considered normal, with mean zero and standard deviation estimated directly from the data. If the elevation data are normally distributed, the assumption of normality for the slope distribution is also reasonable since the slope is the derivative of the elevation, which is a difference (see eq. [3.23]).

3.3.5 Maximum Slope Angles

The gradient of $Z_T(x, y)$ is the vector whose components are $\frac{\partial Z_T}{\partial x}$ and $\frac{\partial Z_T}{\partial y}$

$$\underset{\sim}{\nabla} Z_T = \frac{\partial Z_T}{\partial x} i + \frac{\partial Z_T}{\partial y} j \tag{3.31}$$

where $\underset{\sim}{\nabla} Z_T$ is the gradient of $Z_T(x, y)$. The vector $\underset{\sim}{\nabla} Z_T$ indicates the direction of the slope, and its length $|\underset{\sim}{\nabla} Z_T|$ indicates the steepness. More specifically, the directional derivative, D_u, in the direction of a unit vector $\underset{\sim}{u}$ is

$$D_u Z_T = \underset{\sim}{\nabla} Z_T \cdot \underset{\sim}{u} \tag{3.32}$$

The slope $D_u Z_T$ is largest when $\underset{\sim}{u}$ is parallel to $\underset{\sim}{\nabla} Z_T$, and the maximum slope, $S_{Tm}(x, y)$, is the length of the gradient of $Z_T(x, y)$ (Strang, 1991), i.e. for $u = \underset{\sim}{\nabla} Z_T / |\underset{\sim}{\nabla} Z_T|$, the maximum slope is

$$\begin{aligned} S_{Tm}(x, y) = \underset{\sim}{\nabla} Z_T \cdot \underset{\sim}{u} &= \frac{|\underset{\sim}{\nabla} Z_T|^2}{|\underset{\sim}{\nabla} Z_T|} = |\underset{\sim}{\nabla} Z_T| \\ &= \sqrt{\frac{\partial Z_T}{\partial x}^2 + \frac{\partial Z_T}{\partial y}^2} \end{aligned}$$

Therefore, by assuming that each DEM cell is taken to be a plane whose center (x, y) is at the average elevation, $Z_T(x, y)$, the maximum slope angles can be determined from the values obtained in each of the x and y directions

$$S_{Tm}(x, y) = \sqrt{S_{Tx}^2(x, y) + S_{Ty}^2(x, y)} \tag{3.33}$$

If the slope angles are normally distributed, as assumed above, then the maximum slope angles, S_{Tm}, follow a Rayleigh distribution, if the following are true:

1) The two components are independent and identically normally distributed. As mentioned above, the assumption of normality is reasonable if the elevations are normally distributed. The assumption of independence is more difficult to show, but has been found to be reasonable by the author for the two cases considered in Chapter 4 (correlation between the directional slopes has been found to be less than about 20%).

2) The two components have common variances, Var$[S_T]$ = Var$\left[S_{T_x}\right]$ = Var$\left[S_{T_y}\right]$. As will be shown in Chapter 4, this assumption is reasonable.

3) The two components have zero means. This means that the average ground surface over the areal domain, $D \times D$, is assumed to be flat, so that the mean slope is zero. As will be shown in Chapter 4, this is approximately true for both domains studied.

The mean and variance of Rayleigh distributed random variables can be estimated using the following equations (Fenton and Griffiths, 2008)

$$\mu_{S_{Tm}} = \sigma_{S_T}\sqrt{\left(\frac{1}{2}\pi\right)} \tag{3.34}$$

$$\sigma_{S_{Tm}} = \sqrt{\sigma^2_{S_T}\left(2 - \frac{1}{2}\pi\right)} \tag{3.35}$$

The cumulative distribution function (CDF) of the Rayleigh distribution is given by

$$F_S(s) = \mathrm{P}\left[S \leq s\right] = 1 - \exp\left(-\frac{s^2}{2\sigma^2_{S_T}}\right) \tag{3.36}$$

which is a function of the variance of the slope angle at a given resolution T. There will exist two slope angles, s_{T_1} and s_{T_2}, such that the exceedence probabilities at the two resolutions, T_1 and T_2, will be equal, i.e.,

$$1 - \exp\left(-\frac{s^2_{T_1}}{2\sigma^2_{S_{T_1}}}\right) = 1 - \exp\left(-\frac{s^2_{T_2}}{2\sigma^2_{S_{T_2}}}\right) \tag{3.37}$$

This can be used to develop a relationship between the slope angles corresponding to a fixed exceedence probability at different resolutions,

$$s_{T_2} = \left(\frac{\sigma_{S_{T_2}}}{\sigma_{S_{T_1}}}\right) \cdot s_{T_1} \tag{3.38a}$$

where the values of $\sigma_{S_{T_1}}$ and $\sigma_{S_{T_2}}$ have already been calculated in Section 3.3.4. Eq. [3.38] can also be modified to compare s_{T_1}, or s_{T_2}, with $s_{T_{crit}}$

$$s_{T_{crit}} = \left(\frac{\sigma_{S_{T_{crit}}}}{\sigma_{S_{T_1}}}\right) \cdot s_{T_1} = \left(\frac{\sigma_{S_{T_{crit}}}}{\sigma_{S_{T_2}}}\right) \cdot s_{T_2} \tag{3.38b}$$

Equation [3.36] can be used to determine the distribution of the maximum slope angles, P $[S_{Tm} = s_i]$ (recall that the event $S_{Tm} = s_i$ means that the slope is within $\Delta s/2$ of s_i),

$$\begin{aligned} \mathrm{P}\left[S_{Tm} = s_i\right] &= \mathrm{P}\left[S_{Tm} \leq \left(s_i + \frac{\Delta s}{2}\right)\right] - \mathrm{P}\left[S_{Tm} \leq \left(s_i - \frac{\Delta s}{2}\right)\right] \\ &= \left[1 - \exp\left(-\frac{\left(s_i + \frac{\Delta s}{2}\right)^2}{2\sigma_{S_T}^2}\right)\right] - \left[1 - \exp\left(-\frac{\left(s_i - \frac{\Delta s}{2}\right)^2}{2\sigma_{S_T}^2}\right)\right] \\ &= \exp\left(-\frac{\left(s_i - \frac{\Delta s}{2}\right)^2}{2\sigma_{S_T}^2}\right) - \exp\left(-\frac{\left(s_i + \frac{\Delta s}{2}\right)^2}{2\sigma_{S_T}^2}\right) \end{aligned} \tag{3.39}$$

3.4 Conditional Probability of Slope Failure

To assess the conditional probability of slope failure, P $\left[F_1 \mid S_{Tm} = s_i\right]$, the spatial and temporal variability of the ground strength must be considered. One way of doing this is to model the ground as a random field and then use finite element analysis, which takes into account the site-specific soil properties and geometries, to compute the corresponding probability of failure for a given slope angle. This can be accomplished using the 2-D stochastic slope stability analysis program, Rslope2d, developed by G.A. Fenton and D.V. Griffiths (Griffiths and Fenton, 2004). To test for failure, Rslope2d implements an algorithm which generates a random field, assigns property values to each element, applies gravity loading, then monitors the stress at all Gauss points (Griffiths and Fenton, 2004). If there is excess stress at any point, the program attempts to redistribute it to those nearby in order to satisfy the maximum allowable stress limitations, as governed by the Mohr-Coulomb failure criterion

$$\tau = c + \sigma \tan \phi \tag{3.40}$$

where τ is the shear stress of the soil, c the cohesion, σ the normal stress and ϕ the friction angle. However, if after the maximum number of iterations, Rslope2d is not able to successfully redistribute the stress, the slope is considered to have failed (Griffiths et al., 2009). This technique is referred to as the random finite-element method (RFEM) because it combines elastoplastic finite-element analysis with a random field generator, simulated via the Local Average Subdivision (LAS) method (Fenton and Vanmarke, 1990).

Once the ground strength parameters required for Rslope2d (friction angle, dilation angle, cohesion, unit weight, elastic modulus and Poisson's ratio) are acquired, the program is used to determine the probability of slope failure for a specific slope angle, s_i. The likelihood of failure increases as the slope steepens. Rslope2d is only able to calculate the failure probabilities at integer slope ratios (e.g., $s_i = \frac{1}{3}, \frac{1}{2}, 1$), but the remaining slope angles can be interpolated through regression analysis. This regression equation, i.e. the conditional probability of slope failure equation, can then evaluate the probability of slope failure for any slope angle, s_i.

Given the fact that the ground strength parameters will likely vary throughout the domain under analysis, a range of soil conditions can be considered. For example, if a region is composed primarily of quick clay and dense sand, then Rslope2d would be implemented twice, once to obtain the failure probability for the quick clay and once to obtain the failure probability for the dense sand. The final domain-wide failure probability would be a weighted average of these two probabilities, the weights being the relative proportions of the two soil types. In general, for a region composed of n_s different soil types, the domain-wide slope failure probability would be given by the total probability theorem as

$$\mathrm{P}\left[F_1 \mid S_{Tm} = s_i\right] = \sum_{k=1}^{n_s} p_{s_k} r_{ki} \tag{3.41}$$

where p_{s_k} is the proportion of the domain having the k^{th} soil type and r_{ki} is Rslope2d's estimate of the failure probability of the k^{th} soil type at the i^{th} slope angle.

3.5 Landslide Hazard Assessment Model

The landslide hazard level is assessed based on the regional probability of slope failure, as described by eq. [3.10] in Section 3.2. The hazard level is considered to be equal to the probability of one or more slope failures over the region D $\times$ D,

$$p_f = \sum_{s_i=s_{min}}^{s_{max}} \left(1 - q_i^{n_i}\right) \cdot \mathrm{P}\left[S_{Tm} = s_i\right] \tag{3.42}$$

where

$$q_i = 1 - \mathrm{P}\left[F_1 \mid S_{Tm} = s_i\right] = 1 - \sum_{k=1}^{n_s} p_{s_k} r_{ki}$$

$$\mathrm{P}\left[S_{Tm} = s_i\right] = \exp\left(\frac{-\left(s_i - \frac{\Delta s}{2}\right)^2}{2\sigma_{S_T}^2}\right) - \exp\left(\frac{-\left(s_i + \frac{\Delta s}{2}\right)^2}{2\sigma_{S_T}^2}\right)$$

CHAPTER 4

Application of the Landslide Hazard Assessment Model

4.1 Chamonix, France

The first case study selected by this research to illustrate an application of the methodology proposed in Chapter 3 for regional landslide hazard analysis is located in the Alps, near Chamonix, France. This is a mountainous region, 54 km × 58 km in size, composed of terrain ranging from 459 m to 4784 m in elevation, which has been previously mapped by two different digital elevation models: 1) the global 30 arc-second elevation (GTOPO) model, and 2) the shuttle radar topography mission (SRTM) model with 3 arc-second resolution. There is a significant difference in level of detail perceived by the two models (see Figures [4.1] and [4.2]).

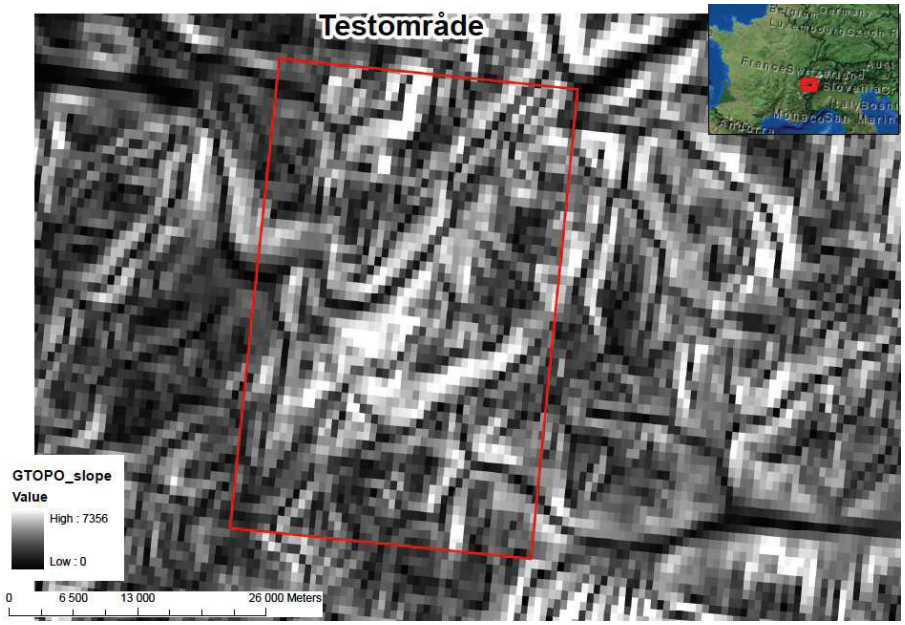

Figure 4.1 GTOPO coverage of Alps test region (NGI, 2010).

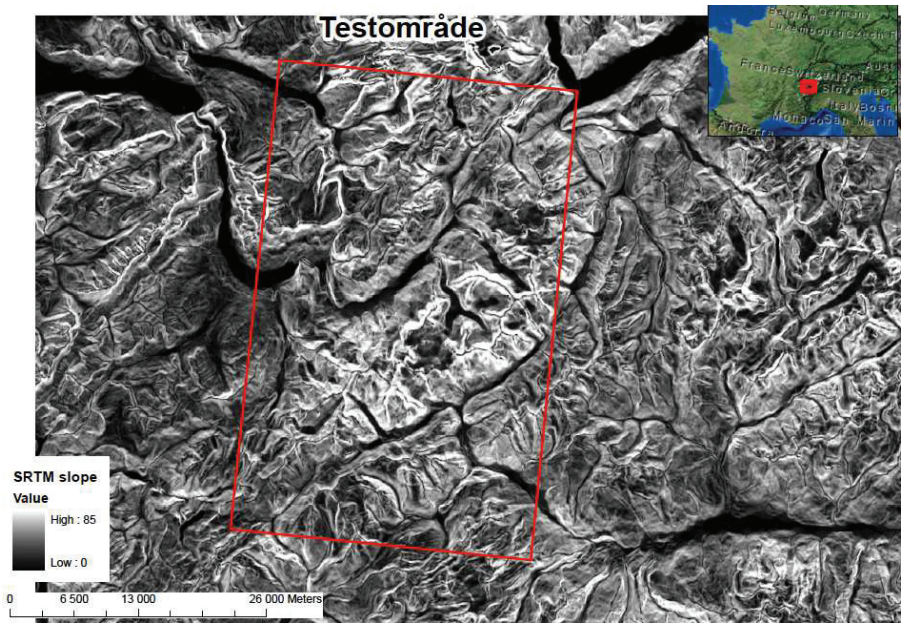

Figure 4.2 SRTM coverage of Alps test region (NGI, 2010).

The DEM data used in this application was supplied by the Norwegian Geotechnical Institute (NGI, 2010).

4.1.1 Averaging Dimensions

Although the 'standard' dimensions for each GTOPO and SRTM cell are 1000 m × 1000 m and 90 m × 90 m respectively, the actual size of the cells varies across the globe and is dependent upon the geographical position of the test region. The latitudinal and longitudinal coordinates of the test region, presented in Table [4.1], can be used by eq. [3.12] to calculate the averaging dimensions, T_1 (GTOPO) and T_2 (SRTM), of each DEM.

Since the test site is small, with respect to the Earth, each cell is assumed to be the same size. The latitudinal coordinates L_1 and L_2, used in eq. [3.12] to solve for the averaging dimension T, have been chosen at the border of the DEM's central cell. The latitudinal coordinates which correspond to the central cell are, for the GTOPO DEM: $L_1 = 45.87497°$ and $L_2 = 45.88329°$, and for the SRTM DEM: $L_1 = 45.87913°$ and $L_2 = 45.87829°$. Thus, the averaging dimensions

for the two DEMs are as follows:

$$T_1 = 1129.0 \text{ m} \tag{4.1a}$$

$$T_2 = 112.9 \text{ m} \tag{4.1b}$$

Table 4.1 Digital elevation model measurement parameters for test site 1.

	GTOPO	SRTM
Number of columns	48	470
Number of rows	52	514
Lower left corner latitude (decimal degrees)	45.68333	45.68333
Lower left corner longitude (decimal degrees)	6.67500	6.68167
Cell size = Δ_{lat} = Δ_{long} (decimal degrees)	0.00833	0.00083

The values of T_1 and T_2 are calculated again, but this time with L_1 and L_2 selected such that they border: 1) the lower left corner cell, and 2) the upper right corner cell (see Table [4.2]). The fact that these values are as far as possible from the center cell, yet extremely close in magnitude, validates the assumption that the size of all cells throughout the domain are approximately equal.

Table 4.2 Averaging dimensions of test site 1.

	Lower left corner	Upper right corner
T_1	1130.28 m	1127.74 m
T_2	113.03 m	112.77 m

4.1.2 Elevation Data

The standard deviations of the elevations in the GTOPO and SRTM datasets are estimated, using the histogram presented in Figure [4.3], to be: $\sigma_{Z_{T_1}}$ = 678.08 m and $\sigma_{Z_{T_2}}$ = 702.57 m. As expected, the standard deviation of the low resolution model (GTOPO) is smaller than the standard deviation of the high resolution model (SRTM). These results support the hypothesis

made in Chapter 1, which stated that as the resolution of a DEM increases, the amount of local averaging decreases and thus, the variance of the elevation data (and correspondingly, the derived slope angles) increases.

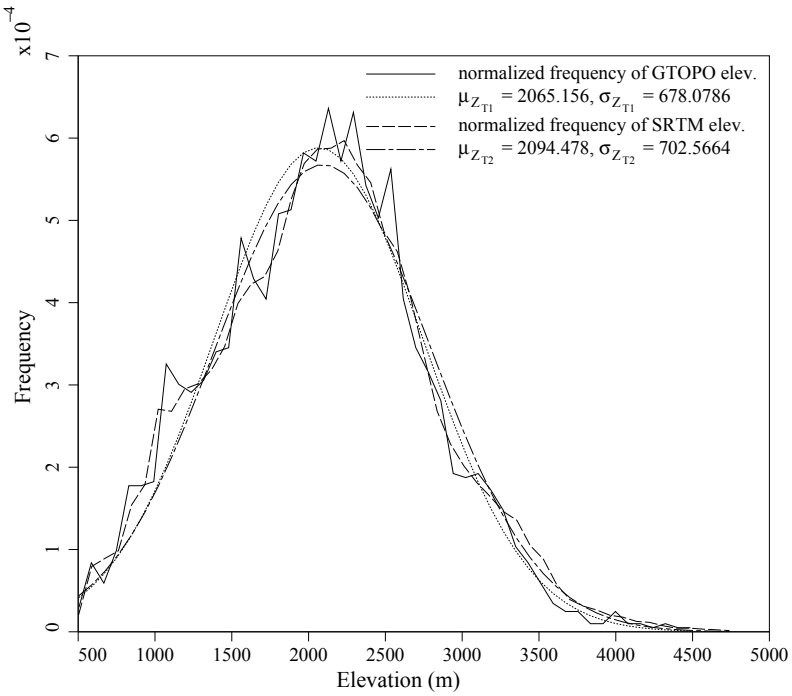

Figure 4.3 Histogram of elevation data collected by the GTOPO and SRTM DEMs for test site 1.

The point scale correlation length and point scale standard deviation, of the elevation data, must be calculated in order to determine the distribution of maximum slope angles throughout the domain, a requirement for the regional landslide hazard analysis.

Point scale correlation length

The point scale correlation length of the elevation data is determined by substituting the standard deviation values, $\sigma_{Z_{T_1}}$ and $\sigma_{Z_{T_2}}$ (from Figure [4.3]), into eq. [3.21], as follows

$$\frac{678.08}{702.57} = \frac{\gamma_Z(T_1)}{\gamma_Z(T_2)} = \left[\frac{\left(\frac{\theta_Z^2}{\pi 1129.0}\right)\left(\frac{\pi 1129.0}{\theta_Z}\text{erf}\left\{\frac{\sqrt{\pi}1129.0}{\theta_Z}\right\} + \exp\left\{\frac{-\pi 1129.0^2}{\theta_Z^2}\right\} - 1\right)}{\left(\frac{\theta_Z^2}{\pi 112.9}\right)\left(\frac{\pi 112.9}{\theta_Z}\text{erf}\left\{\frac{\sqrt{\pi}112.9}{\theta_Z}\right\} + \exp\left\{\frac{-\pi 112.9^2}{\theta_Z^2}\right\} - 1\right)} \right]$$

$$\theta_Z = 4260 \text{ m} \tag{4.2}$$

This value of θ_Z implies that, throughout the domain, elevation points separated by more than 4260 m are negligibly correlated with one another.

Point scale standard deviation

The variance functions are evaluated using eq. [3.19] with the point scale standard deviation of the elevation data, θ_Z, and the averaging domains, T_1 and T_2, as

$$\gamma_Z(T_1) = \frac{4260^2}{\pi 1129.0^2}\left(\frac{\pi 1129.0}{\theta_Z}\text{erf}\left\{\frac{\sqrt{\pi}1129.0}{4260}\right\} + \exp\left\{\frac{-\pi 1129.0^2}{4260^2}\right\} - 1\right)$$
$$= 0.9648 \tag{4.3a}$$
$$\gamma_Z(T_2) = \frac{4260^2}{\pi 112.9^2}\left(\frac{\pi 112.9}{\theta_Z}\text{erf}\left\{\frac{\sqrt{\pi}112.9}{4260}\right\} + \exp\left\{\frac{-\pi 112.9^2}{4260^2}\right\} - 1\right)$$
$$= 0.9996 \tag{4.3b}$$

which can be substituted into eq. [3.22] in order to estimate the point scale standard deviation

$$\sigma_Z = \sigma_{Z_1} = \sigma_{Z_2} = \frac{678.08}{0.9648} = \frac{702.57}{0.9996} = 702.83 \text{ m} \tag{4.4}$$

The standard deviation of the elevation data, at the point scale, should be higher than the locally averaged values computed for each of the DEMs because it is unaffected by local averaging and thus, observes the entire range of elevation points throughout the domain. As evidenced by Figure [4.3], the standard deviation values of the locally averaged elevation data are indeed smaller than the point scale value of σ_Z computed in eq. [4.4].

4.1.3 Effects of Resolution on Perceived Slope Angles

Standard deviation of slope angles at the critical scale

As previously described in Section 3.3.2, this research is concerned with landslide hazard analysis at the critical scale. The critical scale refers to the minimum size cell that could contain a landslide capable of inflicting a considerable amount of damage on the surroundings. The

magnitude of the critical scale depends on the characteristics of the region being analyzed. Some regions are more vulnerable to landslide damage than others and, in these regions, a smaller landslide would constitute a hazardous classification than in other less vulnerable regions. Questions such as: how strong is the infrastructure within the test region? how close is the infrastructure located to potentially hazardous slopes?, should be considered in order to determine an appropriate critical scale. For this case study, a critical scale of 10 m has been chosen arbitrarily.

The standard deviation of the slope angles at the critical scale, $\sigma_{S_{T_{crit}}}$, can be determined using eq. [3.30]. For this, the values of the correlation length and standard deviation at the critical scale averaging length must be known. As discussed in Section 3.3.4, when the point correlation length is significantly larger than the scale under consideration, there will be little difference between the point scale and critical scale values. This means that $\theta_{Z_{T_{crit}}}$ = 4260 m and $\sigma_{Z_{T_{crit}}}$ = 702.83 m, can be assumed, and the resulting value of $\sigma_{S_{T_{crit}}}$ is given by

$$\sigma_{S_{T_{crit}}} = \frac{702.83}{10\sqrt{2}} \sqrt{\left[1 - \exp\left[-\pi\left(\frac{2(10)}{4260}\right)^2\right]\right]} = 0.413545 \simeq 0.414 \qquad (4.5)$$

Although the averaging dimension of the critical scale was chosen arbitrarily, it should be noted that it does not affect the resulting value of $\sigma_{S_{T_{crit}}}$ by very much. The value of $\sigma_{S_{T_{crit}}}$ changes only marginally with varying values of T_{crit}. For example, if T_{crit} were chosen to be a smaller value, e.g., 1 m, then $\sigma_{S_{T_{crit}}}$ = 0.413553, or a larger value, e.g., 20 m, then $\sigma_{S_{T_{crit}}}$ = 0.413524.

Standard deviation of slope angles at the DEM scales

Since the values of the locally averaged correlations lengths, $\theta_{Z_{T_1}}$ and $\theta_{Z_{T_2}}$, are unknown, i.e. only $\theta_{Z_{T_{crit}}}$ had been approximated by the point scale correlation length, the standard deviation of the slope angles at the DEM scales, $\sigma_{S_{T_1}}$ and $\sigma_{S_{T_2}}$, cannot be estimated with eq. [3.29]. Instead, the values of $\sigma_{S_{T_1}}$ and $\sigma_{S_{T_2}}$ are estimated based on a statistical analysis of the DEM datasets. The slope angles in each of the x and y directions, computed with equations [3.23a] and [3.23b], are plotted in Figures [4.4] to [4.7] and the standard deviations are estimated from the histograms.

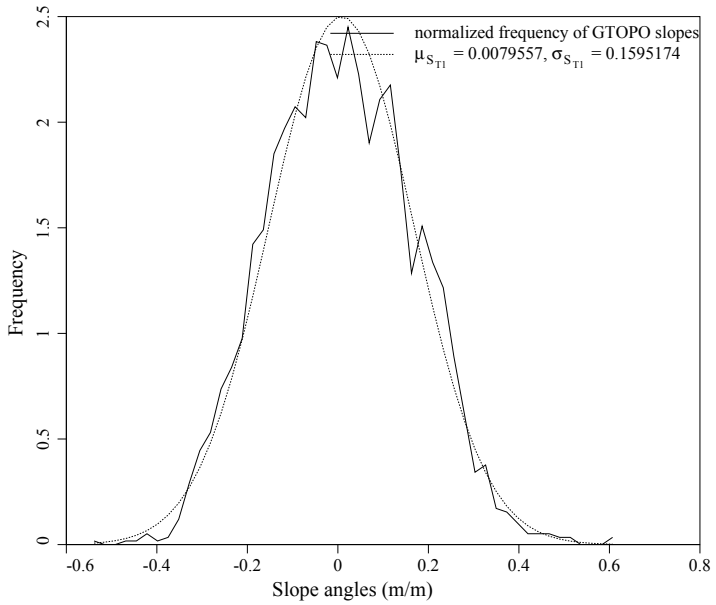

Figure 4.4 GTOPO slope angles in the x direction for test site 1.

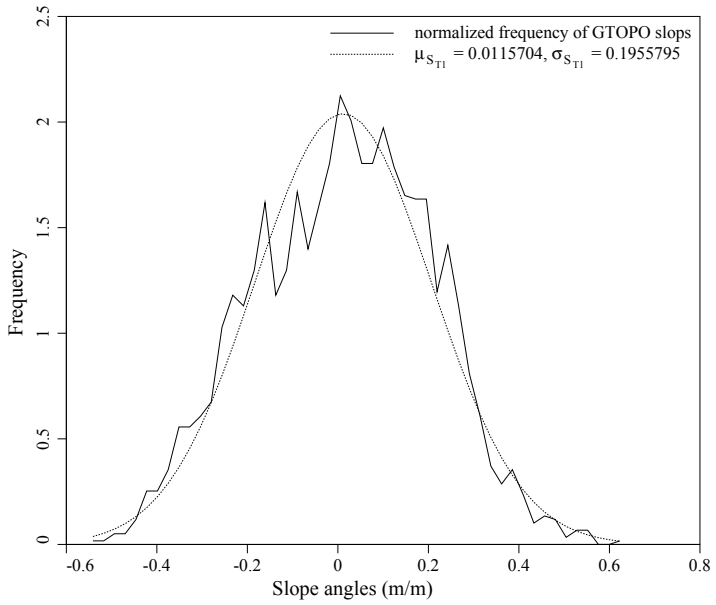

Figure 4.5 GTOPO slope angles in the y direction for test site 1.

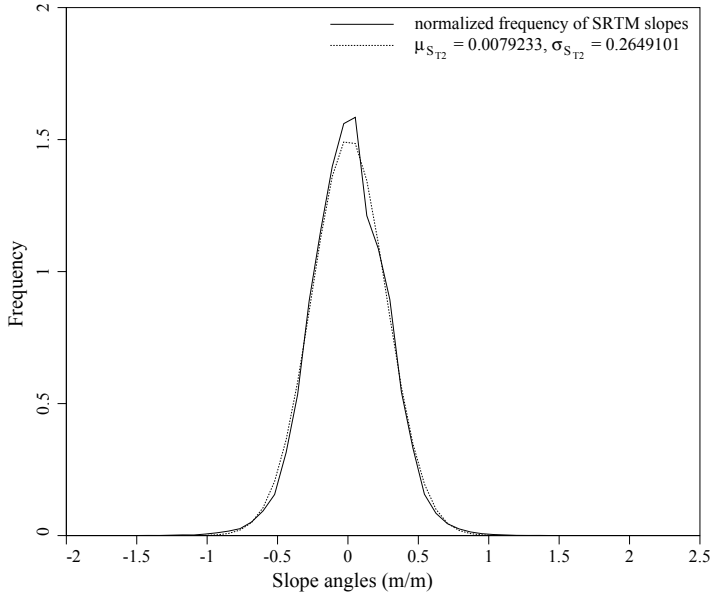

Figure 4.6 SRTM slope angles in the x direction for test site 1.

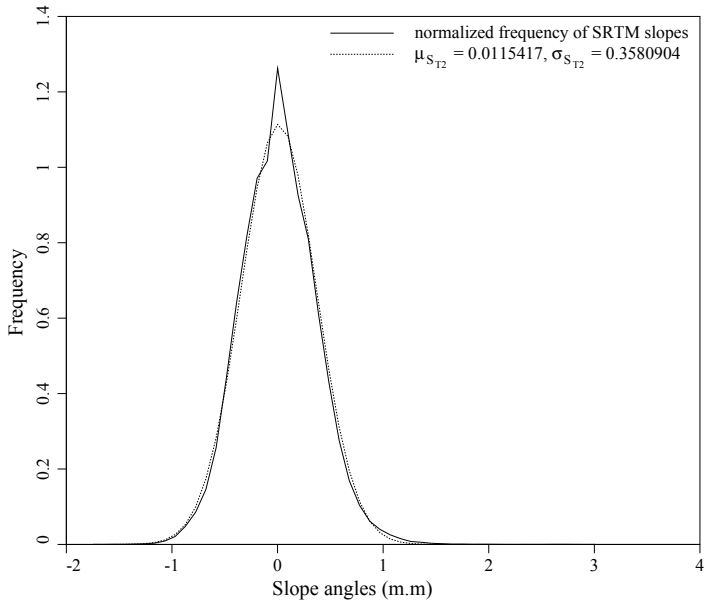

Figure 4.7 SRTM slope angles in the y direction for test site 1.

The mean slopes, as indicated in Figures [4.4] to [4.7], are approximately equal to zero. This agrees with the assumption made in Section 3.3.4, which stated that the average ground surface of the domain is approximately flat. Furthermore, the standard deviations: 1) $\sigma_{S_{T_{1x}}}$ and $\sigma_{S_{T_{1y}}}$, and 2) $\sigma_{S_{T_{2x}}}$ and $\sigma_{S_{T_{2y}}}$, are approximately equal, which also agrees with the assumption of common variances made in Section 3.3.4.

The common standard deviations, estimated from the slope histograms, are as follows:

$$\sigma_{S_{T_1}} \simeq \left(\frac{\sigma_{S_{T_{1x}}} + \sigma_{S_{T_{1y}}}}{2} \right) = \frac{(0.1595173 + 0.1955793)}{2} \simeq 0.178 \qquad (4.6a)$$

$$\sigma_{S_{T_2}} \simeq \left(\frac{\sigma_{S_{T_{2x}}} + \sigma_{S_{T_{2y}}}}{2} \right) = \frac{(0.2649167 + 0.3580654)}{2} \simeq 0.311 \qquad (4.6b)$$

Since the STRM DEM has a higher resolution, it should experience less local averaging and perceive a larger range of slope angles than the GTOPO DEM. Equations [4.6a] and [4.6b] indicate that $\sigma_{S_{T_2}} > \sigma_{S_{T_1}}$, which agrees with the above hypothesis stating that the SRTM DEM should perceive a higher slope variance.

4.1.4 Maximum Slope Angles

The maximum slope angle of each cell throughout the domain is evaluated using eq. [3.33] and the values of S_{Tx} and S_{Ty} calculated with equations [3.23a] and [3.23b]. These maximum slope angles follow a Rayleigh distribution if the directional slope angles follow a normal distribution. The normal distribution is shown in Figures [4.4] to [4.7] to be a very reasonable assumption.

Equations [3.34], [3.35] and [3.39] can then be used, with the values of σ_{S_T} estimated in Section 4.1.3, to compute the mean, $\mu_{S_{Tm}}$, and standard deviation, $\sigma_{S_{Tm}}$, of the maximum slope angles, at each of the three resolutions (see equations [4.7a] to [4.8c]). These values are not required to compute the regional hazard level, however, they can be used to validate the hypothesis posed in Chapter 1. It was originally hypothesized that both the mean and standard deviation of

the maximum slope angles would increase with increasing resolution. The results presented in equations [4.7a] to [4.8c] support this hypothesis.

$$\mu_{S_{Tm_1}} = 0.178\sqrt{\left(\frac{1}{2}\pi\right)} = 0.223 \tag{4.7a}$$

$$\mu_{S_{Tm_2}} = 0.311\sqrt{\left(\frac{1}{2}\pi\right)} = 0.390 \tag{4.7b}$$

$$\mu_{S_{Tm_{crit}}} = 0.414\sqrt{\left(\frac{1}{2}\pi\right)} = 0.519 \tag{4.7c}$$

$$\sigma_{S_{Tm_1}} = \sqrt{0.178^2\left(2 - \frac{1}{2}\pi\right)} = 0.117 \tag{4.8a}$$

$$\sigma_{S_{Tm_2}} = \sqrt{0.311^2\left(2 - \frac{1}{2}\pi\right)} = 0.203 \tag{4.8b}$$

$$\sigma_{S_{Tm_{crit}}} = \sqrt{0.414^2\left(2 - \frac{1}{2}\pi\right)} = 0.271 \tag{4.8c}$$

Furthermore, by setting the minimum possible slope angle to $\tan 0^\circ$ and the maximum possible slope angle to $\tan 90^\circ$, with an incremental step of $\tan 1^\circ$, equations can be developed to define the distribution of maximum slope angles throughout the domain, again at each of the three resolutions (see equations [6.9a] to [4.9c] and the probability density functions (PDF) in Figure [4.8]).

$$\mathrm{P}\left[S_{Tm_1} = s_i\right] = \exp\left(-\frac{\left(s_i - \frac{\tan 1^\circ}{2}\right)^2}{0.06337}\right) - \exp\left(-\frac{\left(s_i + \frac{\tan 1^\circ}{2}\right)^2}{0.06337}\right) \tag{4.9a}$$

$$\mathrm{P}\left[S_{Tm_2} = s_i\right] = \exp\left(-\frac{\left(s_i - \frac{\tan 1^\circ}{2}\right)^2}{0.19344}\right) - \exp\left(-\frac{\left(s_i + \frac{\tan 1^\circ}{2}\right)^2}{0.19344}\right) \tag{4.9b}$$

$$\mathrm{P}\left[S_{Tm_{crit}} = s_i\right] = \exp\left(-\frac{\left(s_i - \frac{\tan 1^\circ}{2}\right)^2}{0.34279}\right) - \exp\left(-\frac{\left(s_i + \frac{\tan 1^\circ}{2}\right)^2}{0.34279}\right) \tag{4.9c}$$

where s_i varies from $\tan 0^\circ$ to $\tan 90^\circ$ in steps of size $\tan 1^\circ$.

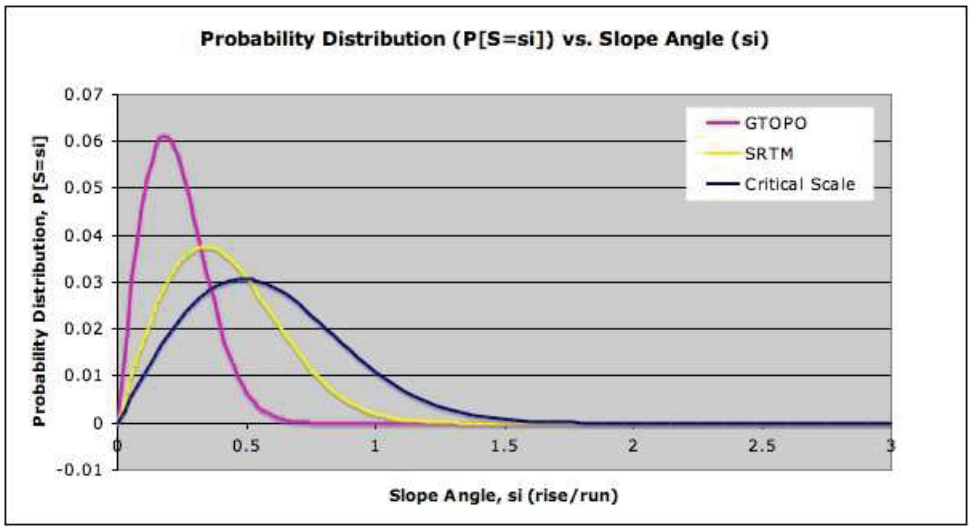

Figure 4.8 GTOPO, SRTM and critical probability density functions for test site 1.

When the GTOPO DEM (i.e. the lowest resolution model considered in this application) perceives a slope to be of some angle s_{T_1}, that angle has most likely been underestimated as a result of local averaging. The angle, s_{T_2}, perceived by the SRTM DEM, and $s_{T_{crit}}$, estimated at the critical scale, are also likely underestimated, but to lesser and lesser degrees. Using eq. [3.38], the relationships between the resolutions and perceived slope angles can be written as

$$s_{T_1} = \left(\frac{0.178}{0.311}\right) s_{T_2} = \left(\frac{0.178}{0.414}\right) \cdot s_{T_{crit}} \tag{4.10}$$

For example, according to eq. [3.36], at approximately 25% probability of occurrence, the GTOPO DEM perceives the slope angle to be less than or equal to

$$\mathrm{P}[S \leq s] = 0.25 = 1 - \exp\left(\frac{-s^2}{2(0.178)^2}\right) \rightarrow s \simeq 0.135 \simeq 7.689^\circ \tag{4.11a}$$

whereas the SRTM DEM perceives the slope angle to be less than or equal to

$$\mathrm{P}[S \leq s] = 0.25 = 1 - \exp\left(\frac{-s^2}{2(0.311)^2}\right) \rightarrow s \simeq 0.236 \simeq 13.274^\circ \tag{4.11b}$$

and local averaging theory estimates that the angle, at the critical scale, is less than or equal to

$$\mathrm{P}[S \leq s] = 0.25 = 1 - \exp\left(\frac{-s^2}{2(0.414)^2}\right) \rightarrow s \simeq 0.314 \simeq 17.434^\circ \tag{4.11c}$$

The cumulative distribution functions (CDF), at all three resolutions, are plotted against the slope angle, s_i, in Figure [4.9].

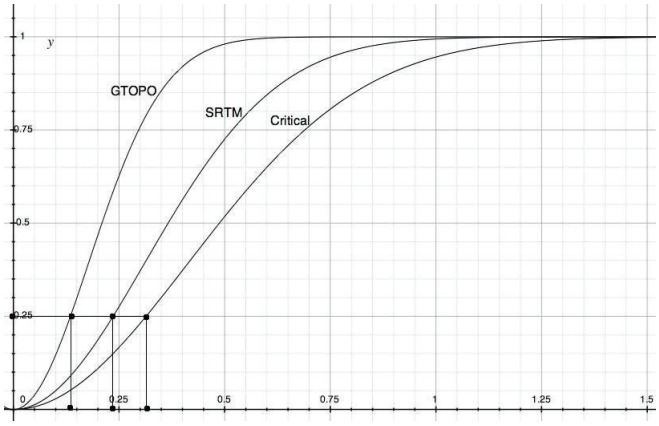

Figure 4.9 GTOPO, SRTM and critical cumulative distribution functions for test site 1.

The slope angles, perceived at the three resolutions, are compared with one another at various probabilities of occurrence, to elucidate the effects of local averaging on the perceived slope angles. The results are presented in m/m in Table [4.3] and in degrees in Table [4.4].

Table 4.3 Comparison of slope angles (m/m) perceived, for a given probability of occurrence, at three different resolutions.

P $[S \leq s_i]$	GTOPO DEM (s_{T_1})	SRTM DEM (s_{T_2})	Critical Scale ($s_{T_{crit}}$)
0.10	0.081710	0.142763	0.190044
0.20	0.118912	0.207763	0.276572
0.30	0.150339	0.262671	0.349665
0.40	0.179917	0.314349	0.418458
0.50	0.209579	0.366175	0.487448
0.60	0.240964	0.421010	0.560444
0.70	0.276213	0.482596	0.642427
0.80	0.319354	0.557972	0.742767
0.90	0.381982	0.667395	0.888430
0.99	0.540204	0.943840	1.256430

Table 4.4 Comparison of slope angles (degrees) perceived, for a given probability of occurrence, at three different resolutions.

P $[S \leq s_i]$	GTOPO DEM (s_{T_1})	SRTM DEM (s_{T_2})	Critical Scale ($s_{T_{crit}}$)
0.10	4.671247	8.124792	10.760403
0.20	6.781336	11.736950	15.459930
0.30	8.549754	14.717455	19.272923
0.40	10.199347	17.450475	22.707253
0.50	11.836674	20.111443	25.986815
0.60	13.547931	22.831562	29.268175
0.70	15.440818	25.761771	32.717778
0.80	17.711081	29.160299	36.603737
0.90	20.905955	33.718965	41.618846
0.99	28.378098	43.345103	51.483505

As evidenced in Table [4.4], the relationship between the slope angles, when viewed in degrees, is not linear, as the transformation from m/m to degrees is not linear. The discrepancy amongst steeper slopes is by far the most significant, which is due to the higher averaging effect on smaller and steeper slopes.

4.1.5 Conditional Probability of Slope Failure

The ground strength parameters, required for Rslope 2d, vary in value from region to region. For example, the ground strength parameters of clay are significantly different than those of gravely sand. The region being analyzed, for landslide hazard, should be examined and the ground strength parameters should be obtained via field and lab tests. However, since the purpose of this case study is to illustrate how to apply the methodology outlined in Chapter 3, there was no actual field or lab work carried out. Instead, the ground strength parameters have been assigned arbitrarily for this illustrative example. The Alps test site is considered to be composed of approximately 20% clay and 80% gravely sand. These two types of soils will initially be considered separately, then the results will be combined to obtain an effective failure probability for the entire site.

The specific parameters, used to estimate the strength of the soil, required for Rslope2d include: friction angle, dilation angle, cohesion, unit weight, elastic modulus and Poisson's ratio. The distribution parameters, as well as the distribution type, are required for each of the soil parameters. Typical values for various types of soil are presented in Tables [4.5] to [4.8]. The values selected for this case study, based on the properties of clay and gravely sand, are identified in Tables [4.9] and [4.10] (see Appendix A for the input format of Rslope2d).

Friction angle

Table 4.5 Typical internal friction angles ϕ for soils in a natural state (Liu, 2009).

Soil type	ϕ (degrees)
Loose rounded-grained sand	27-30
Medium rounded-grained sand	30-35
Dense rounded-grained sand	35-38
Loose angular-grained sand	30-35
Medium angular-grained sand	35-40
Dense angular-grained sand	40-45
Gravel with some sand	34-48
Silts	26-35

The friction angle of clay is taken to have a bounded distribution with mean 26° and a standard deviation of 5°. The gravely sand is taken to have a bounded distribution with mean 40° and a standard deviation of 5°. The bounded distribution was selected because the friction angle is constrained to be less than 90°. Therefore, it cannot be represented by a limitless distribution (e.g., lognormal).

Dilation angle

Dilatancy is a measure of the change in soil volume as a result of shear loading. A high angle of soil dilation indicates a more stable slope (Manzari and Nour, 2000). Since this is a very difficult

parameter to measure, this analysis will use a conservative assumption of zero degrees and assume a deterministic distribution for the entire domain.

Cohesion

Soils are essentially frictional materials and over time continued shearing causes the soil particles to approach a purely frictional state where $c = 0$ (Aysen, 2005). The same approximation, of zero stress cohesion, was also made by Stark et al. (2005) in their analysis of the drained shear strength parameters of landslides. Therefore zero cohesion is used as a deterministic parameter throughout the entire analysis.

Unit weight

Table 4.6 Typical values of unit weight γ for soils in a natural state (Liu, 2009).

Soil type	γ (KN/m^3)
Loose uniform sand	14.5
Dense uniform sand	18
Loose angular-grained silty sand	16
Dense angular-grained silty sand	19
Stiff clay	17
Soft clay	11.5 – 14.5
Soft organic clay	6 – 8
Loess	13.5
Glacial till	21

The unit weight of clayey type soils is assumed to follow a lognormal distribution with a mean value of 13 KN/m^3 and a standard deviation of 1.5 KN/m^3. The unit weight of gravely sands is also assumed to follow a lognormal distribution but with a mean value of 18 KN/m^3 and a standard deviation of 1 KN/m^3. The lognormal distribution was selected for the unit weight parameter because it is non-negative and it is capable of modeling all possible types of soils as it has no upper bound.

Elastic modulus

Table 4.7 Typical values of elastic modulus E_s for soils in a natural state (Geotechnical Info, 2007).

Soil type	E_s (tsf)	E_s (KPa)
Very soft clay	$5 - 50$	$479 - 4,788$
Soft clay	$50 - 200$	$4,788 - 19,152$
Medium clay	$200 - 500$	$19,152 - 47,880$
Stiff clay, silty clay	$500 - 1000$	$47,880 - 95,761$
Sandy clay	$250 - 2000$	$23,940 - 191,521$
Clay shale	$1000 - 2000$	$95,761 - 191,521$
Loose sand	$100 - 250$	$9,576 - 23,940$
Dense sand	$250 - 1000$	$23,940 - 95,761$
Dense sand and gravel	$1000 - 2000$	$95,761 - 191,521$
Silty sand	$250 - 2000$	$23,940 - 191,521$

The elastic modulus is assigned a lognormal distribution with a mean value of 20,000 KPa and a standard deviation of 15,000 KPa for clayey soils, and a lognormal distribution with a mean value of 125,000 KPa and a standard deviation of 75,000 KPa for gravely sands.

Poisson's ratio

Poisson's ratio is assumed to be deterministic with a value of 0.3 for the entire domain.

Table 4.8 Typical values of Poisson's ratio μ for soils in a natural state (Rowe, 2001).

Soil type	μ
Saturated soil, undrained loading	0.5
Clay, drained loading	$0.2 - 0.4$
Dense sand, drained loading	$0.3 - 0.4$
Loose sand, drained loading	$0.1 - 0.3$
Peat, drained loading	$0 - 0.1$

In summary, the ground strength parameters for Rslope2d are as follows:

Table 4.9 Ground strength parameters of clayey soils.

Ground Stength Parameters	Approximations		
	Mean	Standard Deviation	Distribution Type
Friction angle (degrees)	26	5	bounded
Dilation angle mean (degrees)	0	0	deterministic
Cohesion (kN)	0	0	deterministic
Unit weight (kN/m^3)	13	1.5	lognormal
Elastic modulus (kPa)	20000	15000	lognormal
Poisson's ratio	0.3	0	deterministic

Table 4.10 Ground strength parameters of gravely sand.

Ground Stength Parameters	Approximations		
	Mean	Standard Deviation	Distribution Type
Friction angle (degrees)	40.0	5.0	bounded
Dilation angle mean (degrees)	0	0	deterministic
Cohesion (kN)	0	0	deterministic
Unit weight (kN/m^3)	18	1	lognormal
Elastic modulus (kPa)	125000	75000	lognormal
Poisson's ratio	0.3	0	deterministic

In addition to the regional ground strength parameters, Rslope2d requires information concerning the geometry of the slope. Although there may be many slopes under analysis, located throughout the entire domain, and the exact properties of each are unknown, a generalization must be made in order to implement Rslope2d. This study is primarily interested in the effect that the slope angle has on the probability of slope failure, thus, the overall dimensions of the slope modeled are not that important. What is important is the ratio of the slope model dimensions to the soil property correlation length. A 'worst' case ratio is selected for this study (see, e.g., Griffiths and Fenton, 2004) which assumes a correlation length equal to one-tenth of the total distance. The

program Rslope2d will be run multiple times for each soil type, but the only variable that will be changed with each analysis is the slope gradient. Therefore, Rslope2d's results will illustrate how the probability of failure of a region changes with changing slope angles, i.e. $\mathrm{P}\left[F_1 \mid S_{Tm} = s_i\right]$.

Slope angle and dimensions

Rslope2d is only capable of calculating the probability of failure for integer slope gradients. Therefore, for this analysis, Rslope2d will be run three times, for slope gradients of 1/1 (45°), 2/1 (26.57°) and 3/1 (18.43°). Figure [4.10] illustrates the slope model dimensions selected for this analysis.

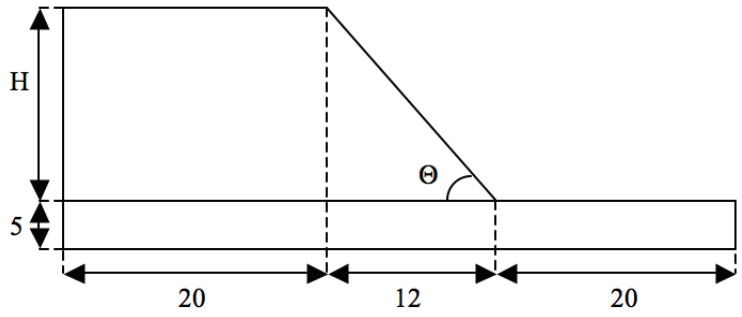

Figure 4.10 Slope model dimensions.

In Figure [4.10], H is the slope height and Θ is the slope angle. The width, w (into the page), is taken to be 40 units. Each unit is equal to 2.5 m × 2.5 m × 2.5 m, giving a slope volume, V, of somewhere between 180,000 m^3 and 420,000 m^3, depending on the angle of the slope.

$$V_{1/1} = \left[(12)(20)(40) + (5)(32)(40) + \frac{1}{2}(12)(12)(40) + (5)(20)(40)\right] 2.5^3 = 420,000 \text{ m}^3 \quad (4.12a)$$

$$V_{3/1} = \left[(4)(20)(40) + (5)(32)(40) + \frac{1}{2}(4)(4)(40) + (5)(20)(40)\right] 2.5^3 = 180,000 \text{ m}^3 \quad (4.12b)$$

where $V_{1/1}$ represents the largest possible slope under consideration, i.e. with a gradient of 1/1, and $V_{3/1}$ represents the smallest possible slope under consideration, i.e. with a gradient of 3/1. To put this into perspective, landslides with volumes greater than one million cubic meters occur about every 10 years in Canada while thousands of smaller slides occur annually (Natural Resources

Canada, 2009). So although the landslides considered in this analysis are relatively large, slides of this magnitude are quite common.

Correlation length of soil

According to the definition provided in Section 3.3.2, a correlation length is used to describe the degree of linear dependence between data points. The correlation length of the elevation data, θ_Z, as described in Chapter 3 and evaluated in Section 4.1.2 of this chapter, refers to the linear dependence between *elevation* points. However, Rslope2d is measuring the slope stability with respect to the ground strength parameters, therefore, its correlation length, θ_R, does not refer to the elevation of the region, but rather, the soil properties. The value of θ_R is used to estimate the maximum distance that two soil particles can be apart from one another while still being somewhat correlated. A large correlation length is indicative of a relatively homogenous soil mass (same properties everywhere). Determining the correlation length is difficult in practice, so in this analysis the soil is considered to have a correlation length of approximately one-tenth the total distance (Griffiths and Fenton, 2004), which is a 'worst' case, leading to the highest probabilities of slope failure. Under the assumption of isotropy, $\theta_R = \theta_{Rx} = \theta_{Ry}$, and given that the length of the slope being evaluated by Rslope2d is 52 units, at 2.5 m/unit, the value of θ for the soil is assumed to be:

$$\theta_R = \frac{(52)(2.5)}{10} = 13 \text{ m} \tag{4.13}$$

Conditional probability of failure

Based on the values presented in Table [4.9] and [4.10], Rslope2d calculates the conditional probabilities of failure, P $\left[F_1 \mid S_{Tm} = s_i\right]$, shown in Table [4.11], over a range of slope angles, s_i:

Table 4.11 Conditional probabilities of failure.

Slope angle, s_i	P $\left[F_1 \mid S_{Tm} = s_i\right]_c$	P $\left[F_1 \mid S_{Tm} = s_i\right]_{gs}$
1/3	0	0
1/2	0.351	0
1/1	1	1

In Table [4.11], the subscripts c and gs refer to the clayey and gravely sand ground strength parameters. Using regression analysis, the following conditional slope failure probability equations are fit to the results presented in Table [4.11]:

$$\mathrm{P}\left[F_1 \mid S_T = s_i\right]_c = -0.904 + 3.116 s_i - 1.212 s_i^2 \geq 0 \tag{4.14a}$$

$$\mathrm{P}\left[F_1 \mid S_T = s_i\right]_{gs} = -1.0 + 2.0 s_i \geq 0 \tag{4.14b}$$

With respect to the clayey soils, all slope ratios below 1/3 result in 0% probability of failure and all slope ratios over 1/1 result in 100% probability of failure. Therefore, the conditional probability of failure equation (eq. [4.14a]) only applies to slopes with ratios within the range of values: $(1/3, 1/1)$. In other words, the probability of failure is 0% (i.e. $p_f = 0$) for all slopes with ratio less than or equal to 1/3 and 100% (i.e. $p_f = 1$) for all slopes with ratio greater than or equal to 1/1. Similarly, with respect to the gravely sands, all slope ratios below 1/2 result in 0% probability of failure and all slope ratios over 1/1 result in 100% probability of failure. Thus, the conditional probability of failure equation (eq. [4.14b]) only applies to slopes with ratios within the range $(1/2, 1/1)$.

4.1.6 Hazard Evaluation

The regional landslide hazard level was defined in Section 3.2 as the probability that one or more slopes, in the region under analysis, fail. The probability that at least one slope in the Alps test region fails can be estimated using the conditional probability of failure equations, developed in equations [4.14a] and [4.14b], the maximum slope angle distributions, developed in equations [4.9a] to [4.9c], and the slope failure probability model, presented in eq. [3.42]. However, since the conditional probability of failure equations considered two types of soil, there will initially be two separate slope failure probability estimates. These two failure estimates can be combined based on the proportion of the domain having each type of soil (see eq. [3.41]).

$$p_f = 0.2 p_{f_c} + 0.8 p_{f_{gs}} \tag{4.15}$$

where,

$$p_{f_c} = \sum_{s_i=\tan 0^\circ}^{\tan 90^\circ} \left(1 - \left\{1.904 - 3.116 s_i + 1.212 s_i^2\right\}^{\frac{(3.136\times 10^9 m^2)}{T^2} \mathrm{P}[S=s_i]}\right) \cdot \mathrm{P}\left[S_{Tm} = s_i\right]$$

$$p_{f_{gs}} = \sum_{s_i=\tan 0^\circ}^{\tan 90^\circ} \left(1 - \left\{2.0 - 2.0 s_i\right\}^{\frac{(3.136\times 10^9 m^2)}{T^2} \mathrm{P}[S=s_i]}\right) \cdot \mathrm{P}\left[S_{Tm} = s_i\right]$$

$$\mathrm{P}\left[S_{Tm} = s_i\right] = \exp\left(\frac{-\left(s_i - \frac{\tan 1^\circ}{2}\right)^2}{2\sigma_{S_T}^2}\right) - \exp\left(\frac{-\left(s_i + \frac{\tan 1^\circ}{2}\right)^2}{2\sigma_{S_T}^2}\right)$$

The final regional hazard levels are estimated using eq. [4.15] with the values of σ_{S_T}, for each distribution, used in equations [4.5], [4.6a] and [4.6b]. The resulting regional slope failure probabilities are presented in Table [4.12].

Table 4.12 Regional slope failure probabilities for test site 1.

Resolution	p_{f_c}	$p_{f_{gs}}$	p_f
T_1 = 1129.0 m	0.166	0.009	**0.040**
T_2 = 112.9 m	0.561	0.277	**0.334**
T_{crit} = 10.0 m	0.721	0.484	**0.531**

The GTOPO DEM, which has the lowest resolution, estimates the lowest regional landslide hazard, 4.0%. The SRTM DEM, which is significantly more detailed than the GTOPO DEM, estimates a much higher 33.4% regional landslide hazard level. Finally, the model developed, using local averaging theory, at the critical scale of 10 m, predicted the highest hazard level of 53.1%. Therefore, it can be concluded that the lower the resolution of a DEM, the more likely it is to underestimate landslide hazard levels. This is a serious issue given that unrealistically low landslide hazard evaluations could result in inadequate levels of landslide preparation, in and around the region being analyzed, which could possibly lead to increased levels of damage in the event of a landslide.

The results given in Table [4.12] can also be interpreted as providing the relative failure probabilities of slopes of different sizes. For example, Table [4.12] suggests that slopes failures of

size 1129 m will occur 4.0% of the time, while small slope failures of size 10 m will occur 53.1% of the time. This information can be further used in a more detailed risk assessment which accounts for the frequency vs. consequence of slides of different sizes, although this is beyond the scope of the current study.

4.2 Southwestern Norway

The second test region considered in this thesis covers a domain of approximately 80 km × 215 km in southwestern Norway. It was selected to illustrate how the landslide hazard model is affected by regions that include water bodies whose elevations are either not recorded or erroneously recorded. The bodies of water are designated 'no-data' points in the DEM datasets and represented by either zeroes or negative numbers. Although no-data points may also be used to describe other abnormalities, the following assumptions have been made for this analysis:

1) all negative and zero DEM values represent no-data points;
2) all no-data points are associated with water surfaces; and
3) all slopes end at the edge of water bodies, i.e. underwater slopes are not considered in the analysis.

The missing data presents a serious issue for landslide hazard analyses: since the water bodies are not assigned elevation values, there is no way to know where the water surface is with respect to the surrounding land. This analysis is carried out, due to lack of data, under the assumption that all water bodies are at zero elevation. This assumption, however, can seriously affect the slope distribution and thus the resulting regional probability of slope failure.

This test site in southwestern Norway has been mapped with the same two digital elevation models as the first case study in the Alps (see Section 4.1): 1) the global 30 arc-second elevation (GTOPO) model, and 2) the 3 arc-second shuttle radar topography mission (SRTM) model, supplied by the Norwegian Geotechnical Institute (NGI, 2010). This test region is composed of complex terrain that ranges from 0 m to 1683 m in elevation. As is evidenced by the terrain view in Figure

[4.11] and the histogram in Figure [4.12], the elevation profile of this region is far from normally distributed.

Figure 4.11 Test region in southwestern Norway (iTouchMap, 2010).

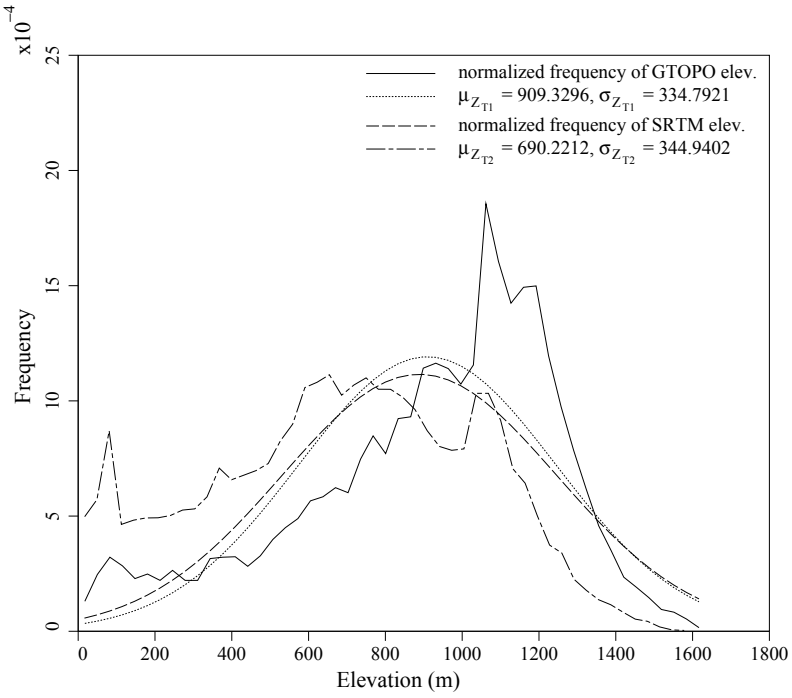

Figure 4.12 Histogram of elevation data collected by the GTOPO and SRTM DEMs for test site 2.

One of the requirements for accuracy of the regional landslide hazard model presented in this thesis is that the elevation profile be approximately normal. Therefore, this southwestern Norway dataset is not ideal and, if used as is, will be subject to a considerable amount of error. There are two possible alternatives for analysis of a region which encounters this type of problem: 1) divide the region into smaller subsets, such that the elevation profiles within each are approximately normal, or 2) zoom out and consider a larger region such that its elevation profile becomes normal.

This thesis approaches the issue of non-normality in the elevation data using the first of the aforementioned possibilities. To begin, the test site is broken up into four equal sections, cut horizontally, as the region appears to be composed of several long strips of consistent elevations (see Figure [4.13]). Normal histograms (Figures [4.14] to [4.17]) are constructed for each of the subsets to see if the elevation profiles appear adequately normal.

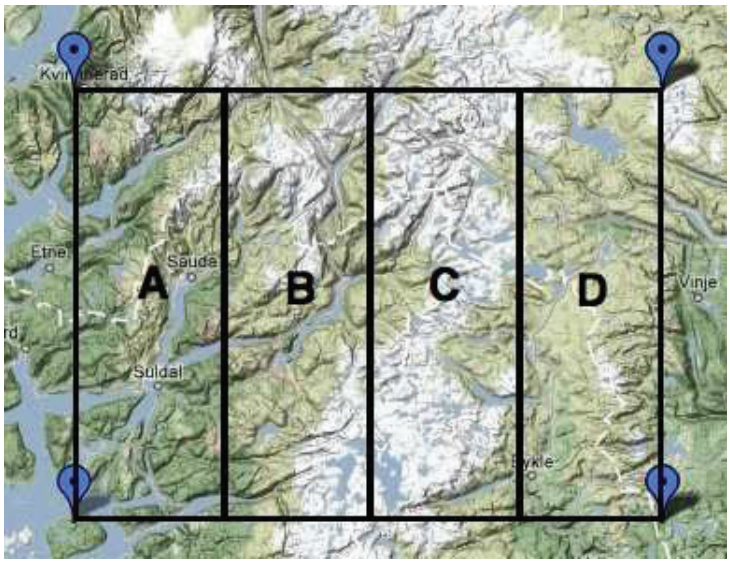

Figure 4.13 Subsets of test region in southwestern Norway (iTouchMap, 2010).

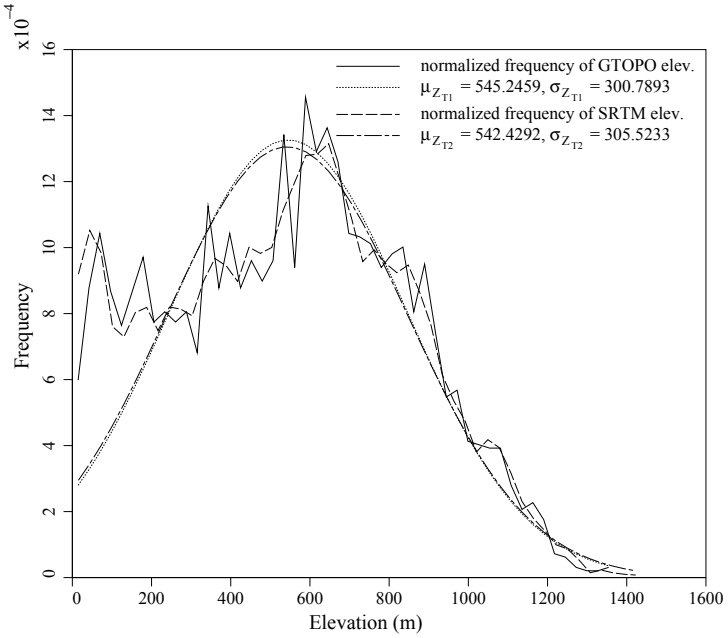

Figure 4.14 Normal histogram of elevation data for subset A.

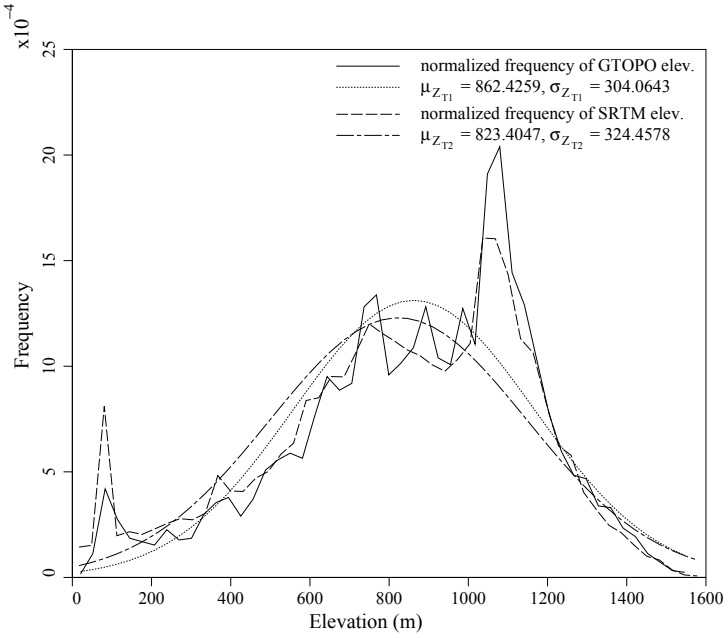

Figure 4.15 Normal histogram of elevation data for subset B.

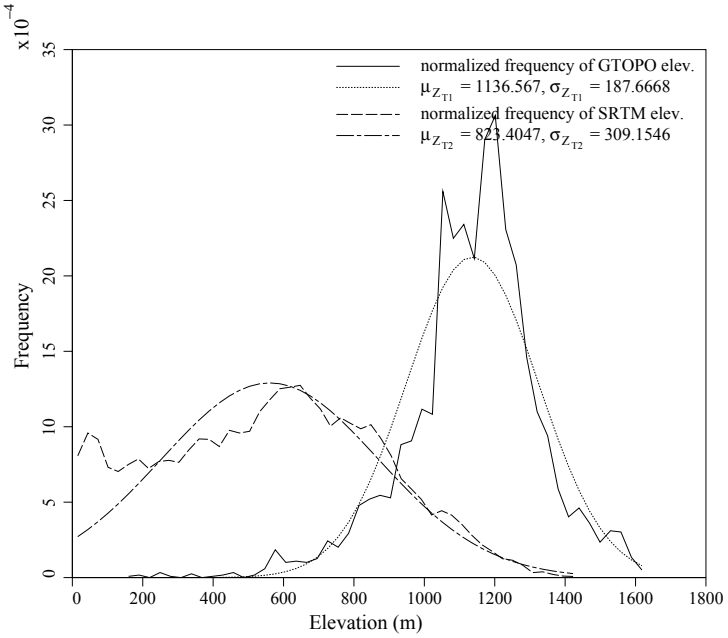

Figure 4.16 Normal histogram of elevation data for subset C.

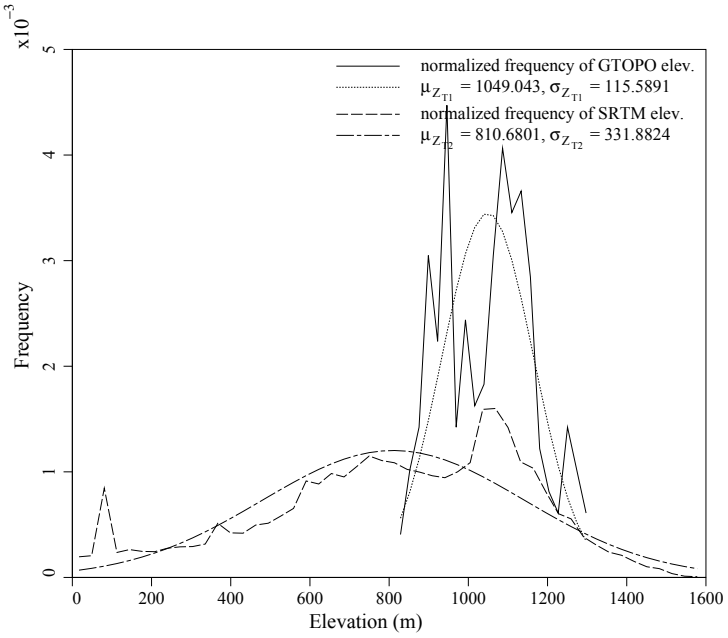

Figure 4.17 Normal histogram of elevation data for subset D.

It is interesting to note the differences between each of the histograms. For example, subset C contains a large number of high elevation points and interspersed amongst the peaks, many water bodies (see Figure [4.13]). The corresponding histogram of elevation points, shown in Figure [4.16], shows the data supplied by both of the DEMs. The elevations perceived by the two DEMs are vastly different. The SRTM DEM has almost twice as large a standard deviation as the GTOPO DEM. This large discrepancy in elevation profiles between the DEM models is likely due to the presence of water bodies, which are spread throughout the region. The sudden drops in elevation, from land to water surface, which are exacerbated by the lack of DEM data for the water surfaces, results in many erroneous and very steep slope estimates. These slopes are often small in spatial extent and thus, overlooked by the lower resolution GTOPO DEM.

If the goal of this application were to classify the hazard level of the entire 80 km $\times$ 215 km region in southwestern Norway, each subset would have to be analyzed and classified individually. However, the goal of this case study is simply to illustrate how the landslide hazard model reacts to a region with water bodies (i.e. 'no-data' points). Since each of the subsets fulfill this criterion individually, only one needs to be analyzed here. Subset C has been selected for analysis since it has a lot of water bodies and yet the resulting distributions are more normal than seen in the other subsets. However, it is important to note that the elevation profile of subset C is still slightly abnormal. Therefore, this analysis will not be as accurate as the first case study completed in Section 4.1.

4.2.1 Averaging Dimensions

As described in Section 4.1.1, the averaging dimensions of DEMs depend on the geographical position of the region under analysis. Thus, the averaging dimensions of the GTOPO (T_1) and SRTM (T_2) DEMs in this case study will differ from the values used in the Alps, even though the same DEM resolutions are used. The geographical position, in decimal degrees, and DEM dimensions of the southwestern Norway test site are presented in Table [4.13].

Table 4.13 Digital elevation model measurement parameters for test site 2.

	GTOPO	SRTM
Number of columns	208	2067
Number of rows	77	761
Lower left corner latitude (decimal degrees)	59.28333	59.28417
Lower left corner longitude (decimal degrees)	6.00833	6.01333
Cell size = Δ_{lat} = Δ_{long} (decimal degrees)	0.00833	0.00083

The averaging dimensions of the two DEMs can be determined with eq. [3.12] and the latitudinal coordinates of the central cell, which are: L_1 = 60.15000 ° and L_2 = 60.15833 ° for the GTOPO DEM, and L_1 = 60.14497 ° and L_2 = 60.14580 ° for the SRTM DEM.

$$T_1 = 1035.0 \text{ m} \tag{4.16a}$$

$$T_2 = 103.5 \text{ m} \tag{4.16b}$$

The averaging dimensions are calculated again, this time using the latitudinal coordinates associated with: 1) the lower left corner cell, and 2) the upper right corner cell, instead of the center cell. The values of T_1 and T_2, calculated for a specific cell, are very similar regardless of the position of that cell within the test region (see Table [4.14]). Therefore, the assumption made in Section 3.3.1, that the size of the cells throughout the entire domain are approximately equal, is reasonable.

Table 4.14 Averaging dimensions of test site 2.

	Lower left corner	Upper right corner
T_1	1040.44 m	1029.66 m
T_2	104.05 m	102.97 m

4.2.2 Elevation Data

Based on the distribution shown for subset C in Figure [4.16], the locally averaged standard deviations of the elevation data are: $\sigma_{Z_{T_1}}$ = 187.6668 m and $\sigma_{Z_{T_2}}$ = 309.1546 m. Table [4.15]

displays information about the number of no-data points, identified by each of the DEMs, within subset C of the southwestern Norway test region. Clearly, the GTOPO did not detect water bodies, while the finer resolution SRTM detected many and assigned them erroneous elevations.

Table 4.15 No-data DEM points present in subset C of test site 2.

	GTOPO DEM	SRTM DEM
Total number of elevation points	4,004	393,437
Number of no-data points	0	38,996
Number of valid points	4,004	354,441

Point scale correlation length

The point scale correlation length of the elevation data is determined by solving eq. [3.21] for θ_Z, as follows

$$\frac{187.69}{309.15} = \frac{\gamma_Z(T_1)}{\gamma_Z(T_2)} = \left[\frac{\left(\frac{\theta_Z^2}{\pi 1035.0}\right)\left(\frac{\pi 1035.0}{\theta_Z}\text{erf}\left\{\frac{\sqrt{\pi}1035.0}{\theta_Z}\right\} + \exp\left\{\frac{-\pi 1035.0^2}{\theta_Z^2}\right\} - 1\right)}{\left(\frac{\theta_Z^2}{\pi 103.5}\right)\left(\frac{\pi 103.5}{\theta_Z}\text{erf}\left\{\frac{\sqrt{\pi}103.5}{\theta_Z}\right\} + \exp\left\{\frac{-\pi 103.5^2}{\theta_Z^2}\right\} - 1\right)} \right]$$

$$\theta_Z = 840 \text{ m} \tag{4.17}$$

Thus, elevation points within subset C, separated by more than 840 m, are negligibly correlated with one another.

Point scale standard deviation

Using the value of θ_Z computed in eq. [4.17], the variance functions, $\gamma_Z(T_1)$ and $\gamma_Z(T_2)$, can be evaluated from eq. [3.19],

$$\gamma_Z(T_1) = \frac{840^2}{\pi 1035.0^2}\left(\frac{\pi 1035.0}{\theta_Z}\text{erf}\left\{\frac{\sqrt{\pi}1035.0}{840}\right\} + \exp\left\{\frac{-\pi 1035.0^2}{840^2}\right\} - 1\right)$$

$$= 0.6021 \tag{4.18a}$$

$$\gamma_Z(T_2) = \frac{840^2}{\pi 103.5^2}\left(\frac{\pi 103.5}{\theta_Z}\text{erf}\left\{\frac{\sqrt{\pi}103.5}{840}\right\} + \exp\left\{\frac{-\pi 103.5^2}{840^2}\right\} - 1\right)$$

$$= 0.99921 \tag{4.18b}$$

and then substituted into eq. [3.22] to compute the point scale standard deviation

$$\sigma_Z = \sigma_{Z_1} = \sigma_{Z_2} = \frac{187.69}{0.6021} = \frac{309.15}{0.9921} = 311.70 \text{ m} \tag{4.19}$$

The point scale standard deviation is higher than both of the locally averaged values (see Figure [4.16]). This is as expected since the point scale represents the most accurate measurements of elevation, and thus, observes the entire range of elevation values. The DEMs undergo local averaging and as a result, smooth out some of the rapidly changing terrain, thereby reducing the range of perceived elevations.

4.2.3 Effects of Resolution on Perceived Slope Angles

Standard deviation of slope angles at the critical scale

If the averaging dimension of the critical scale is set to 10 m, as initially assumed in Section 4.1.3, the standard deviation of the slopes angles, as perceived at the critical scale, can be computed using eq. [3.30] with the values of θ_Z and σ_Z determined in Section 4.2.2. As explained in more detail in Section 4.1.3, the critical scale refers to the minimum scale at which a single cell could contain a potentially hazardous landslide. As a result, for this research, the critical scale is the best indicator of overall landslide hazard. Again, parameters computed at the point scale are assumed to be approximately equal to those at the critical scale, i.e. $\theta_{Z_{T_{crit}}} = \theta_Z$ and $\sigma_{Z_{T_{crit}}} = \sigma_Z$, since the point scale correlation length is much larger than the critical scale. Using this approximation (of $\theta_{Z_{T_{crit}}}$ and $\sigma_{Z_{T_{crit}}}$), the standard deviation of the slope angles at the critical scale can be determined using eq. [3.30],

$$\sigma_{S_{T_{crit}}} = \frac{311.70}{10\sqrt{2}} \sqrt{\left[1 - \exp\left[-\pi\left(\frac{2(10)}{840}\right)^2\right]\right]} = 0.929725 \simeq 0.930 \tag{4.20}$$

Standard deviation of slope angles at the DEM scales

Since the values of the locally averaged correlations lengths, $\theta_{Z_{T_1}}$ and $\theta_{Z_{T_2}}$, are unknown, eq. [3.29] cannot be used to solve for the standard deviations of the slope angles. Instead, $\sigma_{S_{T_1}}$ and

$\sigma_{S_{T_2}}$ must be estimated through a statistical analysis of the DEM datasets. The slopes of each cell, calculated in both the x and y directions with equations [3.23a] and [3.23b], are plotted in Figures [4.18] to [4.21], in units m/m.

However, as shown in Figures [4.18] to [4.21], there are a few extreme values located unusually far from the mean. This problem is exacerbated as the resolution increases because high resolution models observe more of the extreme elevations (i.e. they smooth out fewer peaks). A transformation to degrees scales the extremes (i.e. $70^\circ = 2.747474$ while $85^\circ = 11.430052$ and $89^\circ = 57.289962$) and as a result, the slope profile is better represented by a normal distribution (see Figures [4.22] to [4.25]) when evaluated in degrees.

The transformation from rise over run to degrees is achieved via

$$S_T = \frac{\arctan(S_T) \cdot 180^\circ}{\pi} \tag{4.21}$$

The Anderson-Darling (AD) test is a method commonly used to measure the goodness-of-fit of a distribution to a dataset. The AD statistic essentially measures the 'distance' the data is away from the null hypothesis (normal distribution); the hypothesis is rejected if the AD statistic is too large (i.e. larger than about 0.75). Although the AD statistics shown in Figures [4.18] to [4.25] would seem to indicate that the test has failed, the distribution fit is reasonable and can be used to estimate probabilities with acceptable accuracy. The primary shortcoming of quantitative goodness-of-fit tests is that they tend to reject hypotheses for large sample sizes (Fenton and Griffiths, 2008) and in this case the sample sizes are exceptionally large (4,004 and 354,441 points), therefore the AD statistics cannot be used to assess reasonableness-of-fit in this model. However, by comparing the AD statistics of the histograms produced in units m/m (Figures [4.18] to [4.21]) with those produced in degrees (Figures [4.22] to [4.25]), it is clear that it is better to estimate the standard deviation values from the histograms plotted in degrees, as they have lower AD statistics.

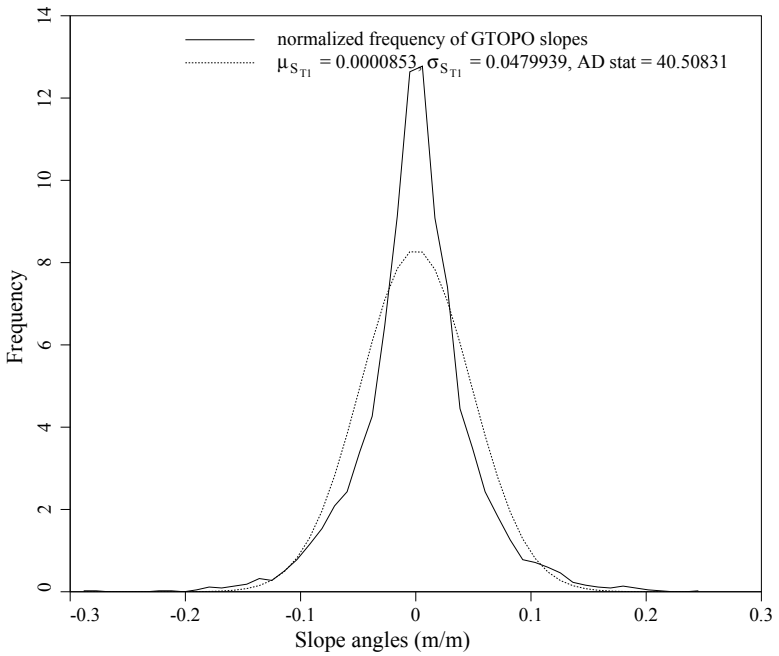

Figure 4.18 GTOPO slope angles in the x direction (m/m) for subset C.

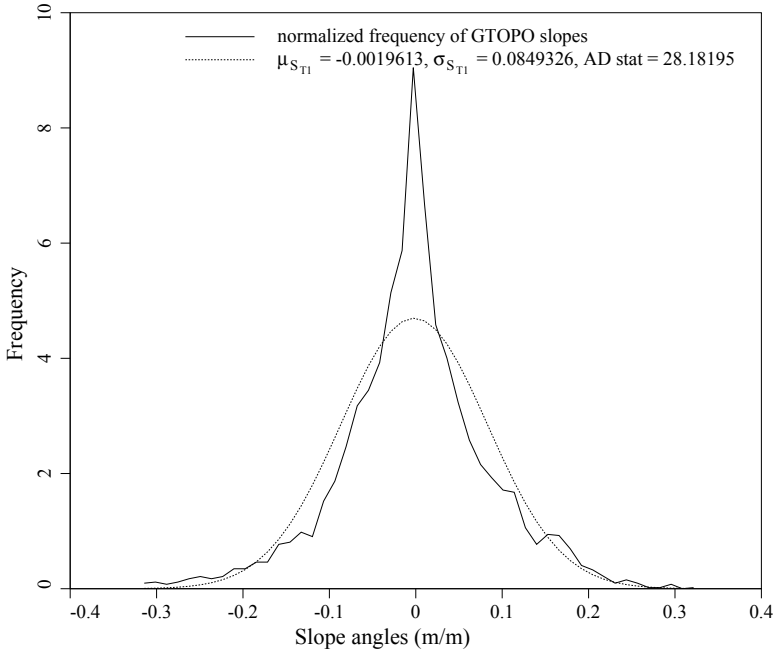

Figure 4.19 GTOPO slope angles in the y direction (m/m) for subset C.

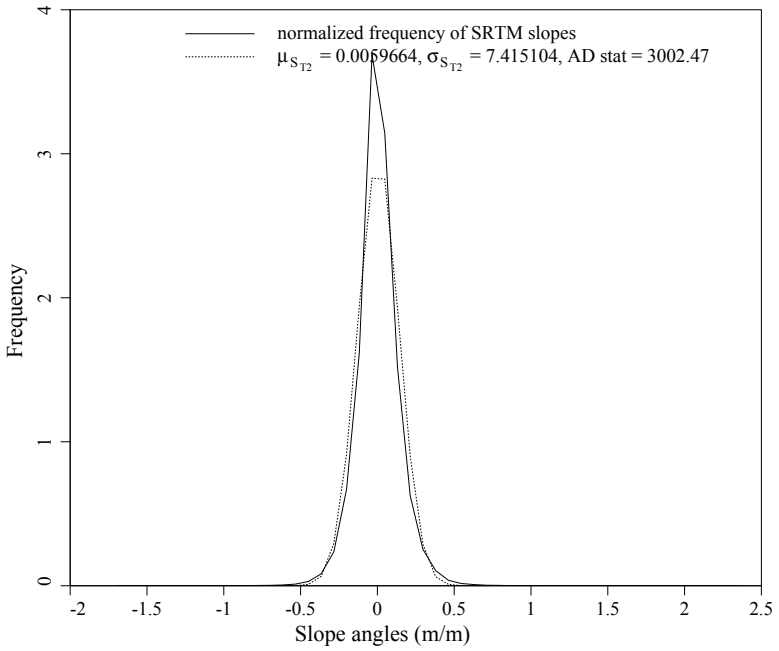

Figure 4.20 SRTM slope angles in the x direction (m/m) for subset C.

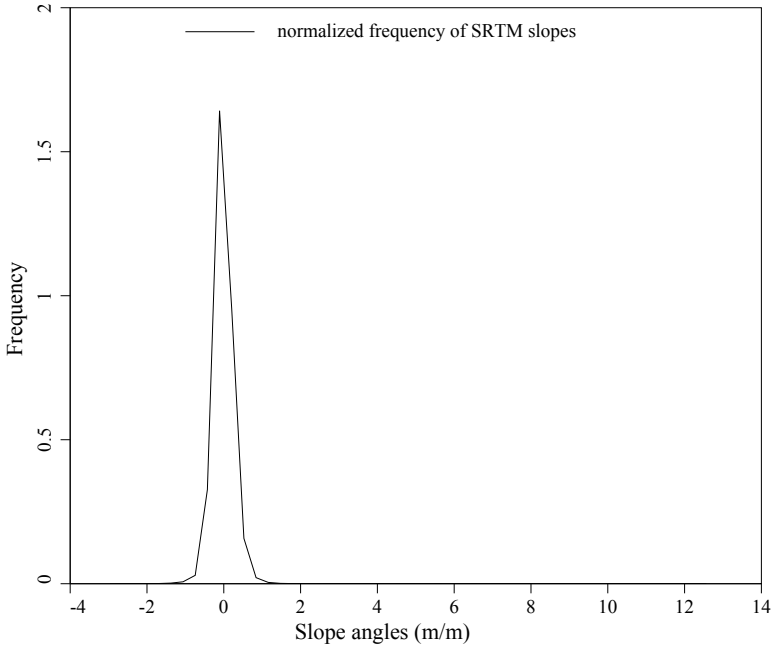

Figure 4.21 SRTM slope angles in the y direction (m/m) for subset C.

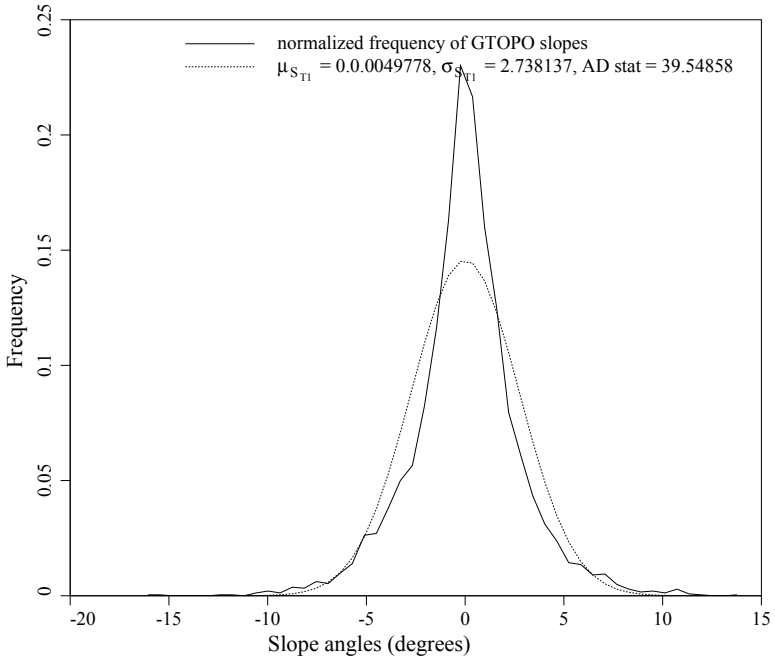

Figure 4.22 GTOPO slope angles in the x direction (degrees) for subset C.

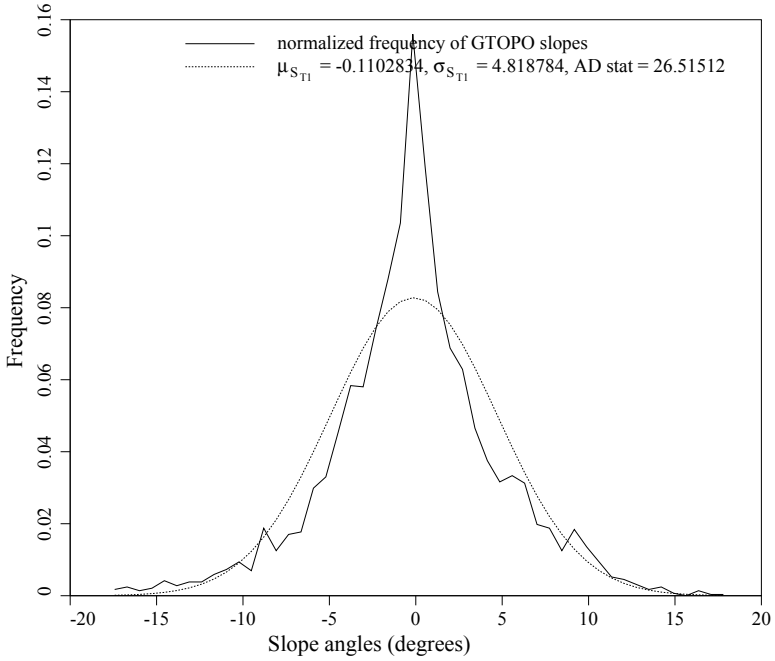

Figure 4.23 GTOPO slope angles in the y direction (degrees) for subset C.

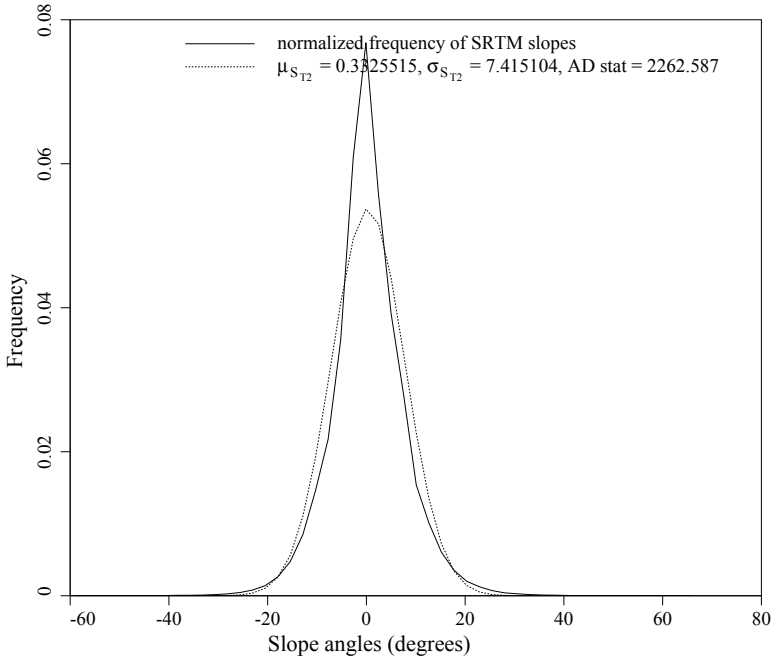

Figure 4.24 SRTM slope angles in the x direction (degrees) for subset C.

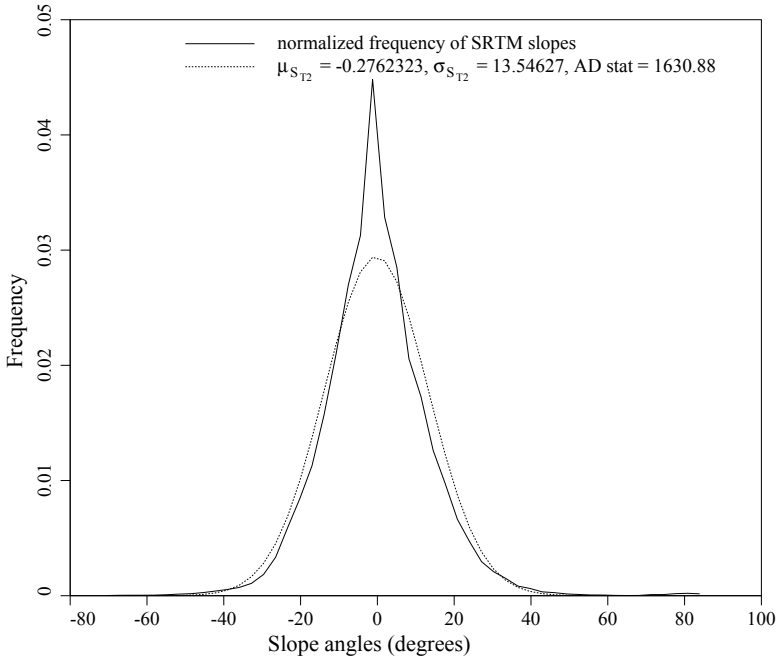

Figure 4.25 SRTM slope angles in the y direction (degrees) for subset C.

The mean value of each of the slope distributions, shown in Figures [4.18] to [4.25], is approximately equal to zero, again validating the assumption made in Section 3.3.4, which stated that the average ground surface of the domain is approximately flat. The standard deviations of the slope angles, for each DEM, are estimated from the histograms as the average of the standard deviations in the x and y directions. Once the standard deviations have been estimated from the histograms in Figures [4.22] to [4.25], the values are converted from degrees into units of m/m. This conversion is necessary because the standard deviations of the slopes are required to estimate the distribution of slope angles throughout the domain, and the slope distribution equation (eq. [3.39]) is defined in terms of m/m.

$$\sigma_{S_{T_1}} \simeq \left(\frac{\sigma_{S_{T_{1x}}} + \sigma_{S_{T_{1y}}}}{2} \right) = \frac{(2.738137 + 4.818784)}{2} = 3.77846^\circ \simeq 0.066 \qquad (4.22a)$$

$$\sigma_{S_{T_2}} \simeq \left(\frac{\sigma_{S_{T_{2x}}} + \sigma_{S_{T_{2y}}}}{2} \right) = \frac{(13.54627 + 7.415104)}{2} = 10.48069^\circ \simeq 0.185 \qquad (4.22b)$$

As evidenced from eq. [4.20] and equations [4.22a] and [4.22b] , the standard deviation of the slope angles is largest at the critical scale (0.930) and smallest at GTOPO scale (0.066). These results agree with the hypothesis made in Chapter 1, which stated that high resolution models should perceive higher slope variances than low resolution models, but they span a much wider range that observed in the Alps test site. This is most likely due to the missing data causing a rapid increase in apparently steep slopes as the resolution increases.

4.2.4 Maximum Slope Angles

The distribution of maximum slope angles throughout the domain follows a Rayleigh distribution if the directional slopes are normally distributed. The mean and standard deviations of these angles are estimated using equations [3.34] and [3.35];

$$\mu_{S_{Tm_1}} = 0.066\sqrt{\left(\frac{1}{2}\pi\right)} = 0.083 \qquad (4.23a)$$

$$\mu_{S_{Tm_2}} = 0.185\sqrt{\left(\frac{1}{2}\pi\right)} = 0.232 \qquad (4.23b)$$

$$\mu_{S_{Tm_{crit}}} = 0.930\sqrt{\left(\frac{1}{2}\pi\right)} = 1.166 \tag{4.23c}$$

$$\sigma_{S_{Tm_1}} = \sqrt{0.066^2\left(2 - \frac{1}{2}\pi\right)} = 0.0.043 \tag{4.24a}$$

$$\sigma_{S_{Tm_2}} = \sqrt{0.185^2\left(2 - \frac{1}{2}\pi\right)} = 0.121 \tag{4.24b}$$

$$\sigma_{S_{Tm_{crit}}} = \sqrt{0.930^2\left(2 - \frac{1}{2}\pi\right)} = 0.609 \tag{4.24c}$$

The distribution, using $\tan 0^\circ$ as the minimum possible angle, $\tan 90^\circ$ as the maximum possible angles and $\tan 1^\circ$ as the incremental step value, is modeled with eq. [3.39];

$$\mathrm{P}\left[S_{Tm_1} = s_i\right] = \exp\left(-\frac{\left(s_i - \frac{\tan 1^\circ}{2}\right)^2}{0.00871}\right) - \exp\left(-\frac{\left(s_i + \frac{\tan 1^\circ}{2}\right)^2}{0.00871}\right) \tag{4.25a}$$

$$\mathrm{P}\left[S_{Tm_2} = s_i\right] = \exp\left(-\frac{\left(s_i - \frac{\tan 1^\circ}{2}\right)^2}{0.06845}\right) - \exp\left(-\frac{\left(s_i + \frac{\tan 1^\circ}{2}\right)^2}{0.06845}\right) \tag{4.25b}$$

$$\mathrm{P}\left[S_{Tm_{crit}} = s_i\right] = \exp\left(-\frac{\left(s_i - \frac{\tan 1^\circ}{2}\right)^2}{1.72980}\right) - \exp\left(-\frac{\left(s_i + \frac{\tan 1^\circ}{2}\right)^2}{1.72980}\right) \tag{4.25c}$$

Furthermore, the PDFs, for each of the three resolutions, are plotted in Figure [4.26].

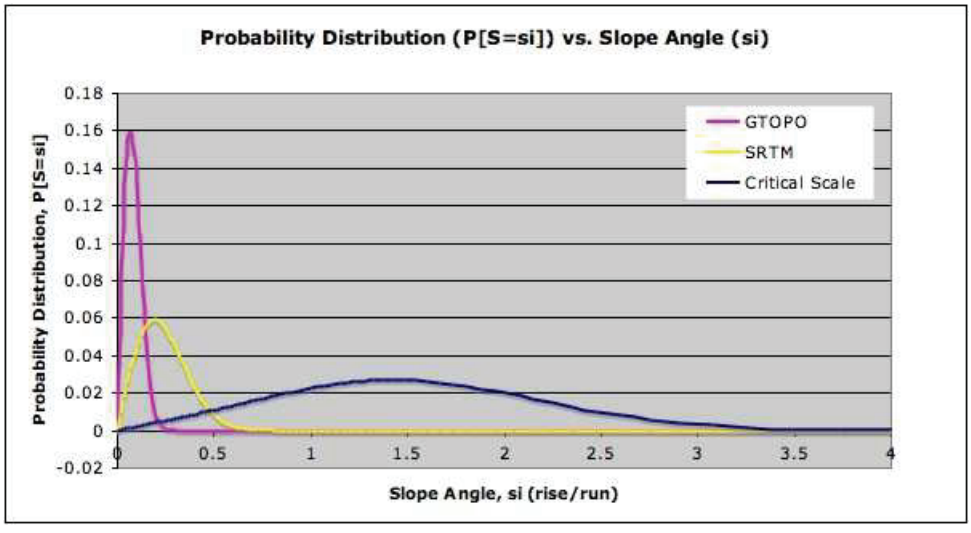

Figure 4.26 GTOPO, SRTM and critical probability density functions for subset C.

The relationships between the slope angles, as perceived at the three differing resolutions, are summarized below using eq. [3.38],

$$s_{T_1} = \left(\frac{0.066}{0.185}\right) \cdot s_{T_2} = \left(\frac{0.066}{0.930}\right) \cdot s_{T_{crit}} \tag{4.26}$$

4.2.5 Conditional Slope Failure Probability

The same ground strength parameters are used for this analysis as were used for the first test region (see Tables [4.9] and [4.10] in Section 4.1.5), i.e. it is assumed that this test region is also composed of 20% clayey soils and 80% gravely sands. Thus, equations [4.14a] and [4.14b], developed in Section 4.1.5 to describe the conditional probability of slope failure in the Alps for each of the soil types, are also used for this case study in southwestern Norway.

$$\mathrm{P}\left[F_1 \mid S_T = s_i\right]_c = -0.904 + 3.116 s_i - 1.212 s_i^2 \geq 0 \tag{4.27a}$$

$$\mathrm{P}\left[F_1 \mid S_T = s_i\right]_{gs} = -1.0 + 2.0 s_i \geq 0 \tag{4.27b}$$

To reiterate what was already mentioned in Section 4.1.5, the ground strength parameters used in this analysis do not represent the actual parameters of the test site, they have been chosen arbitrarily. The purpose of this application is simply to illustrate the steps involved in carrying out the regional landslide hazard model developed in Chapter 3.

4.2.6 Hazard Evaluation

The regional landslide hazard level, defined as the probability that one or more slopes in the region fail, can be evaluated using the conditional probability of failure equations ([4.27a] and [4.27b]), the maximum slope angle distributions, developed in equations [4.25a] to [4.25c], and the slope failure probability model, presented in eq. [3.42]. The final hazard level is estimated as,

$$p_f = 0.2 p_{f_c} + 0.8 p_{f_{gs}} \tag{4.28}$$

where,

$$p_{f_c} = \sum_{s_i=\tan 0^\circ}^{\tan 90^\circ} \left(1 - \left\{1.904 - 3.116 s_i + 1.212 S_i^2\right\}^{\frac{(4.3\times10^9 m^2)}{T^2}\mathrm{P}[S=s_i]}\right) \cdot \mathrm{P}\left[S_{Tm} = s_i\right]$$

$$p_{f_{gs}} = \sum_{s_i=\tan 0^\circ}^{\tan 90^\circ} \left(1 - \left\{2.0 - 2.0 s_i\right\}^{\frac{(4.3\times10^9 m^2)}{T^2}\mathrm{P}[S=s_i]}\right) \cdot \mathrm{P}\left[S_{Tm} = s_i\right]$$

$$\mathrm{P}\left[S_{Tm} = s_i\right] = \exp\left(\frac{-\left(s_i - \frac{\tan 1^\circ}{2}\right)^2}{2\sigma_{S_T}^2}\right) - \exp\left(\frac{-\left(s_i + \frac{\tan 1^\circ}{2}\right)^2}{2\sigma_{S_T}^2}\right)$$

The final hazard estimations are presented in Table [4.16].

Table 4.16 Regional slope failure probabilities for test site 2.

Resolution	p_{f_c}	$p_{f_{gs}}$	p_f
T_1 = 1035.0 m	0.000	0.000	**0.000**
T_2 = 103.5 m	0.188	0.024	**0.056**
T_{crit} = 10.0 m	0.937	0.866	**0.880**

Subset C contains land masses up to 1681 m in elevation, which, in many areas, apparently slope very abruptly down into water. Due to the lack of DEM data available for water surfaces, all water surfaces are considered to have zero elevation and the slopes from land to water then appear to be extremely steep. As a result, a lot of steep slopes, which are small in spatial extent, are measured at the critical scale and lead to a very high estimation of slope failure probability. In contrast, the low resolution DEM model overlooks almost all of these small slopes and predicts a negligible landslide hazard level. In order to improve the landslide hazard analysis in regions with 'no-data' DEM points, it is necessary to obtain elevation data for these regions. Typically, there are significantly more valid points than 'no-data' points in regions where landslide hazard analyses are desirable, thus, it is worthwhile to measure the 'no-data' regions using another method. For instance, in subset C of this test region 38,996 of the 393,437 elevation points are designated 'no-data' points, i.e. less than 10% of the entire region. If another GIS method were used to fill in these missing measurements, the landslide hazard analysis methodology, presented in Chapter 3, would provide much better results, as evidenced by the first case study which contained no missing data. However, this data correction exercise is beyond the scope of the current study.

4.2.7 Discussion of Results

Each of the test sites analyzed in this thesis were relatively large in size: 54 km $\times$ 58 km and 80 km $\times$ 215 km. Therefore, it is not surprising that the regional probabilities of slope failure were so high (up to 53.1% in the Alps, and 88.0% in southwestern Norway). If a community or organization wished to incorporate landslide hazard analyses into their landslide preparation and/or mitigation strategies, it would be prudent to divide such large domains into multiple subregions. For instance, there is as high as a 53.1% chance that at least one slope in the region examined in the Alps will fail, but whether or not it will affect any of the surrounding communities (e.g. Chamonix) is unknown. Perhaps only one slope within the 54 km $\times$ 58 km domain is expected to fail. Or perhaps thousands of slopes, evenly spread throughout the entire region, are highly unstable and thus, expected to fail. By breaking the analysis down into several smaller units, it would be much easier to pinpoint the most susceptible regions. In general, the size of the domain depends on the type of analysis. Community-level planning will require smaller domains than those at a national level. This model can be implemented for any study region, provided that the elevation profile within that region is approximately normal (if not, the methodology needs to employ a different final maximum slope distribution, i.e. rather than Rayleigh).

CHAPTER 5

Landslide Vulnerability Assessment

Vulnerability assessments[1] measure the physical and socioeconomic fragilities of the affected communities in terms of degree of loss, ranked from 0 (no loss) to 1 (complete loss). The degree of loss, or amount of *damage*, inflicted by a landslide is dependent upon much more than its magnitude and impact force. Damage refers to the amount of destruction caused to the physical infrastructure (e.g. buildings, agriculture, forests), the amount of harm to the population (e.g. injuries, deaths and emotional issues associated with such losses) and the impact on the economy (e.g. temporary business closures). If there are slopes which are susceptible to sliding, there may be a high risk of landslide *occurrence*, but if these slopes are isolated, there may be a minimal risk of landslide *damage*. The severity of the consequences resulting from a landslide are dependent upon the region's vulnerability level. A model, formed from a set of vulnerability indicators, is presented in this thesis as a means of predicting regional landslide vulnerability levels.

5.1 Vulnerability Indicators

The following indicators (Stinführer et al. (2009); Roberts et al., 2009; Lahidji, 2008; Tapsell et al., 2005; Cutter et al., 2003), separated by category, have been selected using the guidelines presented in Figure [5.1] for the vulnerability model.

1) demographic – (a) age, (b) urban population;

2) social – (a) education level, (b) level of integration;

[1] The research for this chapter was developed in equal parts by Amanda McLean and Unni Eidsvig at the International Centre for Geohazards, as part of the SafeLand project (2010). Some of the research discussed here appears in Work Project 2.2 of the SafeLand project (Eidsvig et al., 2010).

3) economic – (a) rural population, (b) GDP per capita, (c) building type;

4) recovery – (a) quality of medical services, (b) insurance and disaster funds; and

5) administrative – (a) regulation control, (b) hazard evaluation, (c) early warning systems, (d) emergency response.

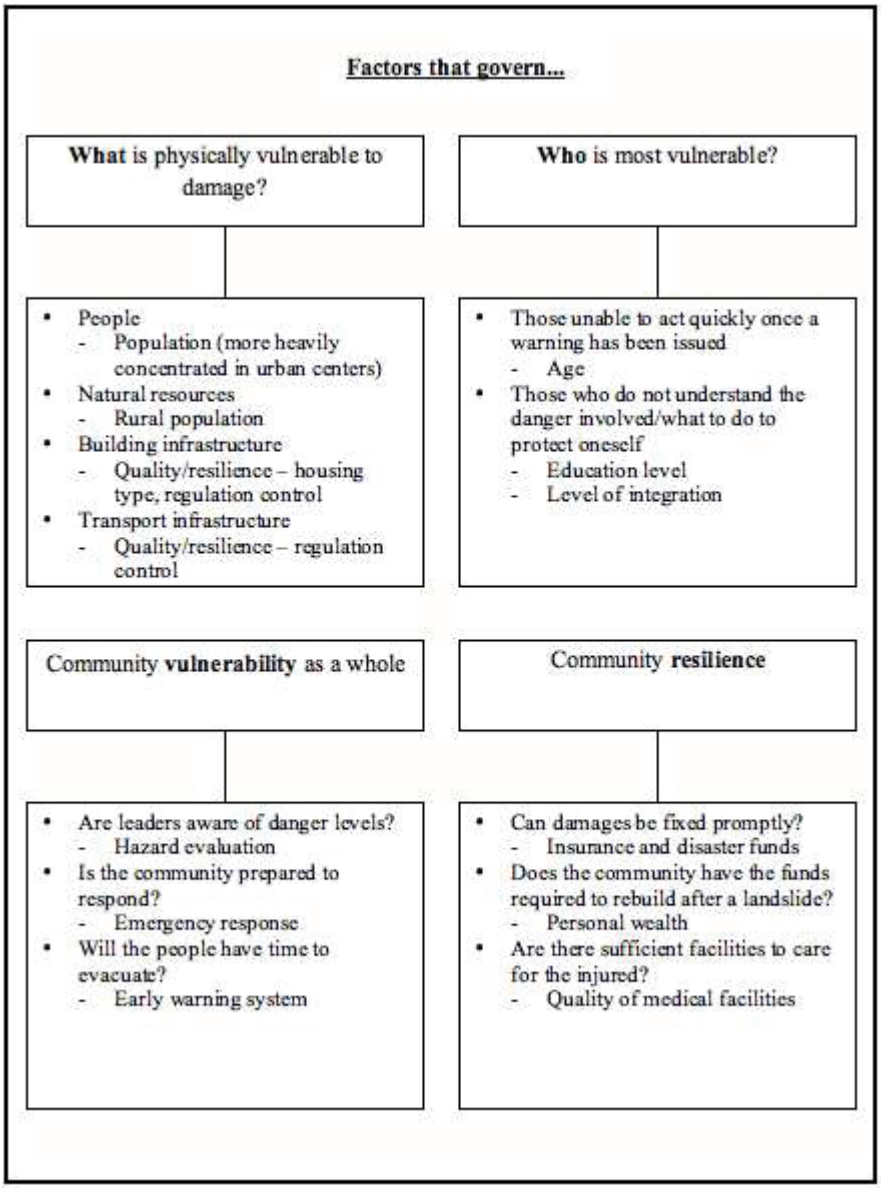

Figure 5.1 Selection process for vulnerability indicators.

Discussion of indicators

Each indicator is ranked and assigned a rank value based on the level of vulnerability the region faces. The rank values range from 1 to 5, where 1 indicates the lowest level of vulnerability and 5 indicates the highest level of vulnerability. This range (i.e. five possible rank values) is selected arbitrarily (it is normalized to the range 0 to 1 later).

1) a) Age: Young children (defined as under 5 years of age) and senior citizens (over 65 years of age) are typically more vulnerable to harm in the event of a landslide, as they are less able to protect themselves without assistance. The metric proposed for this indicator is based on a life expectancy of 75 years and assumes a uniform age distribution. Given such a distribution, 20% of the population is expected to fall into one of these two 'vulnerable' age categories; this is used as the reference point and given a rank of 1 (i.e. the lowest vulnerability since the fraction of the population in these 'vulnerable' age categories is only 20%). As the percentage of vulnerable peoples increase, so does the vulnerability ranking. (*Note: societal vulnerability indicator*)

b) Urban population: It is more difficult to evacuate and care for highly dense populations in the aftermath of a landslide and as such, these regions are considered to be more vulnerable to physical harm. Furthermore, densely populated regions typically coincide with densely built infrastructure, thus densely populated regions are also more vulnerable to economic losses resulting from damage to existing infrastructure. (*Note: physical vulnerability indicator*)

2) a) Education level: People with high levels of formal education generally prepare themselves better for potential disasters (e.g. landslides) than those without, especially if they have already experienced a similar disaster in the past. Stinführer et al. (2009) completed a case study in a post-flood region in Germany and found that after the disaster people with higher levels of formal education had less trust in public protection measures. As a result, the people with higher levels of education changed their own behaviour in order to protect themselves

against future floods more so than people with less education. (*Note: societal vulnerability indicator*)

b) Level of integration: In highly segregated regions, language and cultural barriers can impact the ability of certain groups to access both pre- and post- disaster support (e.g. awareness of preparedness strategies and disaster funding) (Cutter, 2003). (*Note: societal vulnerability indicator*)

3) a) Rural population: Rural populations are highly vulnerable to damage due to their lower average incomes and higher dependence on the surrounding natural resources (e.g., farming, fishing) for sustenance (Cutter, 2003). A population that is highly dependent upon the land for their primary source of income is considered more vulnerable to the economic damages associated with a landslide. (*Note: physical vulnerability indicator*)

b) GDP per capita: The average level of wealth within a region is indicative of its resiliency against the repercussions of a landslide. For example, if a wealthy community is warned of an impending disaster, the residents are better able to take extra safety precautions (e.g. temporary relocation) than residents of poorer regions. (*Note: societal vulnerability indicator*)

c) Building type: The materials used for buildings is indicative of how much impact they can withstand from a landslide without sustaining irreparable damage. The ranking system for this indicator refers to houses as having strong, medium or weak resistance. Strong resistance refers to thick brick, stone wall, and/or reinforced concrete constructions. Medium resistance refers to mixed concrete-timber and/or thin brick-wall constructions while weak resistance refers to simple timber and very light constructions (Heinimann, 1999). (*Note: physical vulnerability indicator*)

4) a) Quality of medical services: This indicator is categorized by the number of hospital beds per 1,000 people. Country-wide statistics provided by the World Bank's development indicators (2010) was used as the metric for this ranking system. However, the data may have to be

acquired independently if the region being analyzed is on a local, rather than national, scale. (*Note: societal vulnerability indicator*)

b) Insurance and disaster funds: Pre-existing funds set up to deal with damages following a landslide event significantly increases a community's level of resilience as it allows them to rebuild and move past the disaster in a much shorter time period; the more extensive the funding, the higher the level of resilience. (*Note: societal vulnerability indicator*)

5) a) Regulation control: This indicator takes into account the quality of infrastructure in the region. If there is a significant amount of control over construction guidelines, the community is more likely to consider the impacts of probable disasters in their designs. Therefore, buildings in landslide prone regions would be constructed in a manner which ensures maximal resistance to the expected impact forces. (*Note: societal vulnerability indicator*)

b) Hazard evaluation: If a region is aware of the likelihood of landslide occurrence they can (and are more likely to) prepare themselves for such an event. Moreover, they can adapt their mitigation and preparedness strategies to best suit their specific needs based on the results of a regional hazard assessment, e.g., by following the methodology presented in Chapter 3. (*Note: societal vulnerability indicator*)

c) Early warning systems: If a population is warned of an impending landslide, they can take the necessary safety precautions to protect themselves as best as possible from harm. However, it is important to ensure that the warnings are accurate and effectively delivered; if the warnings are not followed by the disaster, people will soon start to ignore them. Also, if the warnings are sent to risk managers, but do not reach the public, fewer benefits will be derived. (*Note: societal vulnerability indicator*)

d) Emergency response: Emergency response teams properly equipped to respond to landslide events can significantly reduce the amount of damage inflicted on a population by providing emergency treatment to injured persons, clean-up of potentially harmful debris and efficient

handling of damaged infrastructure. For instance, a landslide could potentially damage a sewerage system or water treatment plant, and if not seen to shortly thereafter, could lead to serious water contamination issues within the region. (*Note: societal vulnerability indicator*)

Damages associated with landslides span a wide timeframe; some have obvious impacts that are apparent immediately after the event (e.g. damaged infrastructure) while others have delayed impacts (e.g. business closures or increased levels of homelessness). The direct losses are best measured with physical vulnerability indicators, while indirect losses are better measured with societal indicators.

The physical indicators (i.e. building type, urban populations and rural population) provide direct measures of damage levels. For example, 'low' resistance buildings are much more likely to suffer significant amounts of damage than those of 'high' resistance, and the type and extent of damage expected depends on the populations present (i.e. urban or rural). Similarly, it is more likely that people and infrastructure will be damaged if a landslide occurs in a densely populated urban region, as they are present in higher numbers, but it is more likely that farms and agricultural products will be damaged if a landslide occurs in a rural region.

The remaining indicators listed above are considered societal, or socioeconomic, and they are used to measure the coping capacity of a region. The ability of a community to absorb significant damages associated with a landslide event and recover quickly indicates a high level of resilience, and thus, a low level of vulnerability. For example, a population with a low GDP per capita will have a difficult time restarting businesses that were closed due to damages. As a result, poorer populations are more likely to continue to lose money as a result of prolongued foreclosure than wealthier populations.

Indicator ranking metric

The ranking metric used for each of the vulnerability indicators is shown in Table [5.1].

Table 5.1 Vulnerability indicators.

1. Demographic indicators	
Classification of indicator vulnerability	**Rank (V_i)**
a. Age	
$<$ 20% population is either under 5 or over 65 years of age	1
$[20, 30)$% are either under 5 or over 65 years of age	2
$[30, 40)$% are either under 5 or over 65 years of age	3
$[40, 50)$% are either under 5 or over 65 years of age	4
$\geq$ 50% are either under 5 or over 65 years of age	5

b. Urban population	
Population density is $<$ 25 people/km^2	1
Population density is $[25, 50)$ people/km^2	2
Population density is $[50, 100)$ people/km^2	3
Population density is $[100, 200)$ people/km^2	4
Population density is $\geq$ 200 people/km^2	5

2. Social indicators	
Classification of indicator vulnerability	**Rank (V_i)**
a. Education level	
$\geq$ 30% of the eligible population (over 18 years of age) have (or are in the process of obtaining) a post-secondary education	1
$[20, 30)$% have a post-secondary education	2
$[10, 20)$% have a post-secondary education	3
$[5, 20)$% have a post-secondary education	4
$<$ 5% have a post-secondary education	5

b. Level of integration	
$<$ 5% of the population is not familiar with the majority language and culture	1
$[5, 10)$% are not familiar with the majority language and culture	2
$[10, 15)$% are not familiar with the majority language and culture	3
$[15, 25)$% are not familiar with the majority language and culture	4
$\geq$ 25% are not familiar with the majority language and culture	5

3. Economic indicators	
Classification of indicator vulnerability	**Rank (V_i)**
a. Rural population	
$<$ 10% population is dependent on the land for primary source of income	1
$[10, 25)$% depend on the land for primary source of income	2
$[25, 50)$% depend on the land for primary source of income	3
$[50, 75)$% depend on the land for primary source of income	4
$\geq$ 75% depend on the land for primary source of income	5

b. GDP per capita	
The GDP per capita is $\geq$ 50 thousand USD	1
The GDP per capita is $[30, 50)$ thousand USD	2
The GDP per capita is $[20, 30)$ thousand USD	3
The GDP per capita is $[10, 20)$ thousand USD	4
The GDP per capita is $<$ 10 thousand USD	5

c. Building type (Heinimann, 1999)	
The *majority* of the buildings are of **strong** resistance and there are *none* of **weak** resistance	1
The *majority* of the buildings are of **strong** resistance, and there are *some* of **weak** resistance	2
The *majority* of the buildings are of **medium** resistance	3
The *majority* of the buildings are of **weak** resistance, and there are *some* of **strong** resistance	4
The *majority* of the buildings are of **weak** resistance, and there are *none* of **strong** resistance	5

4. Recovery indicators	
Classification of indicator vulnerability	**Rank (V_i)**
a. Quality of medical services	
$\geq$ 4 hospital beds per 1,000 people	1
[3, 4) hospital beds per 1,000 people	2
[2, 3) hospital beds per 1,000 people	3
[1, 2) hospital beds per 1,000 people	4
$<$ 1 hospital beds per 1,000 people	5

b. Insurance and disaster funds (Lahidji, 2008	
Extensive coverage for private and public buildings, existence of government-sponsored landslide funds	1
Insurance coverage for the majority of private and public buildings, limited government-funding	2
Widespread landslide insurance in development phase, but not yet accessible to everyone	3
Incomplete support for victims of past landslide events	4
Little or no insurance provided	5

5. Administrative indicators	
Classification of indicator vulnerability	**Rank (V_i)**
a. Regulation control (Lahidji, 2008)	
Stringent guidelines (which take into account *all* landslide triggers) in place for all construction and land-use activities	1
Adequate guidelines (which take into account *most* landslide triggers) in place for all construction and land-use activities	2
Fairly effective regulations for new developments, however, potential problems with existing constructions and land-use activities	3
Some consideration of landslide risk during construction and land-use activities, but inadequate enforcement of regulations	4
No consideration of landslide risk in construction and land-use activities	5
b. Hazard evaluation (Lahidji, 2008)	
Detailed landslide hazard assessment completed for the entire region	1
Basic landslide hazard assessment completed for the entire region	2
Detailed landslide hazard assessment ongoing; some gaps	3
Basic landslide hazard assessment ongoing; some gaps	4
No landslide hazard assessment completed or in progress	5
c. Early warning systems (Lahidji, 2008)	
Advanced early warning systems used in coordination with emergency response procedures	1
Adequate early warning system coordinated with media announcements capable of reaching the majority of the population prior to the landslide	2
Fairly effective regulations for new developments, however, potential Basic early warning systems available to the public	3
Basic early warning systems available to the risk managers	3
No early warning system	5

d. Emergency response (Lahidji, 2008)	
All of the necessary specialized equipment and well-trained rescue professionals available throughout the *entire* region	1
All of the necessary specialized equipment and well-trained rescue professionals available in *portions* of the region; some equipment and rescue professionals available throughout the *entire* region	2
All of the necessary specialized equipment and well-trained rescue professionals available in *portions* of the region; some areas without access to sufficient resources	3
Some equipment and rescue professionals available in *portions* of the region; some areas without access to sufficient resources	4
Fragmented organization and scattered resources; predominance of voluntary responders	5

Indicator weighting scheme

Each of the indicators are individually weighted, on a scale of 1 to 3, based on their degree of relevance to the assessment. A score of 3 indicates the highest level of relevance to the vulnerability assessment. The total vulnerability score is computed as the sum of the weighted indicators (i.e. the indicator rank, from the above tables, times the weighting value) divided by the sum of the weights. For this model the weights have been assigned based on educated judgement, i.e. extensive literature review and feedback from SafeLand contributors, both within and outside of the Norwegian Geotechnical Institute and the International Centre for Geohazards.

The indicators deemed most influential include: (3c) building type, (5a) regulation control and (5b) hazard evaluation, and so they have each been assigned the highest weight of 3. The indicators: (1a) age, (3a) rural population, (3b) GDP per capita, (4b) insurance and disaster funds, (5c) early warning systems and (5d) emergency response were considered moderately influential and assigned weights of 2. Finally the remaining indicators: (1b) urban population, (2a) education level, (2b) level of integration and (4a) quality of medical services were regarded as least influential and each assigned a weight of 1.

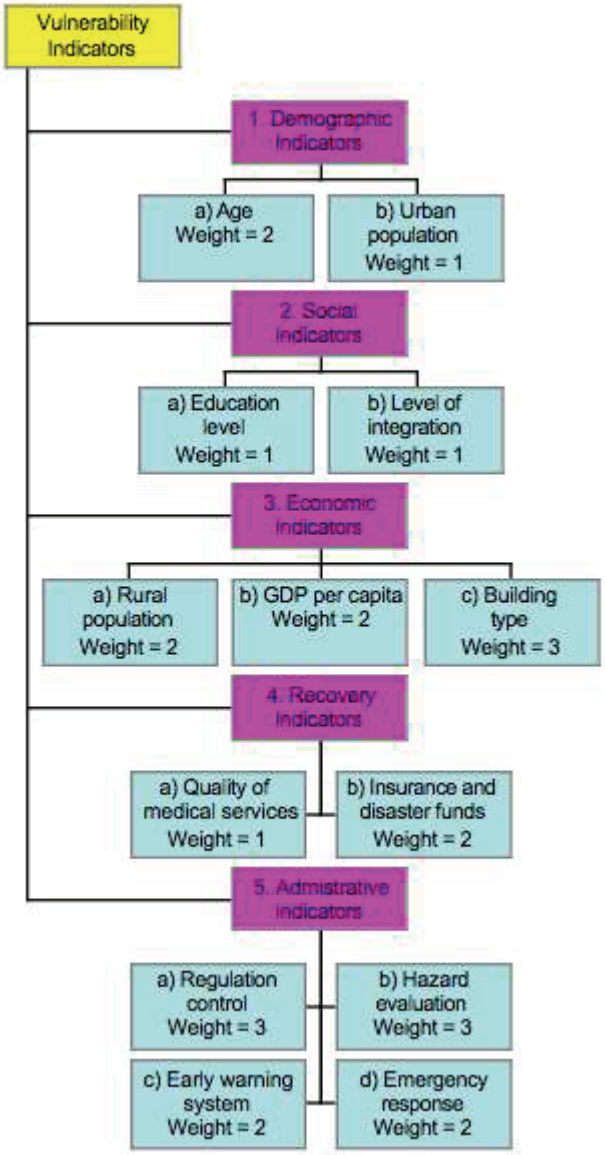

Figure 5.2 Overview of weighted vulnerability indicators.

5.2 Landslide Vulnerability Assessment Model

The landslide vulnerability model considers the combined results of the thirteen weighted indicators.

$$v_t = \frac{\sum_{i=1}^{n} [v_i \cdot w_i]}{\sum_{i=1}^{n} w_i} \tag{5.1}$$

where v_t is the total vulnerability score of the region, n is the number of indicators, w_i is the weighting value and v_i the vulnerability rank of each individual indicator.

However, in order to be incorporated into the risk model (along with the regional probability of slope failure, p_f) the total vulnerability score, v_t, should be normalized to lie between 0 to 1, where 0 is lowest possible score and 1 is the highest. This is achieved by dividing the total vulnerability score by the highest possible value of v_t (obtained by simply setting all ranks to 5). Thus, the final regional landslide vulnerability score is

$$v = \frac{\left(\frac{\sum_{i=1}^{13}[v_i \cdot w_i]}{25}\right)}{\left(\frac{[3(5\cdot3)+6(5\cdot2)+4(5\cdot1)]}{25}\right)} = \frac{\sum_{i=1}^{13}[v_i \cdot w_i]}{125} \tag{5.2}$$

CHAPTER 6

Existing and Future Landslide Risk Assessment

6.1 Existing Risk Levels

The likelihood that a landslide will occur can be predicted with a hazard assessment model (see Chapter 3), but the extent of the damage inflicted upon a region – physically, economically and mentally – is a function of vulnerability (see Chapter 5). These factors, together with the exposed population, define *risk*. The equation for risk (eq. [1.1]) presented in Chapter 1, is a product of hazard, p_f, vulnerability, v, and exposed population, n_p. This equation can be refined by substituting eq. [3.42] for p_f and eq. [5.2] for v. Thus, regional landslide risk, which is a measure of the expected loss, can be determined as follows

$$\begin{aligned} R &= p_f \cdot v \cdot n_p \\ &= \left[\sum_{s_i=s_{min}}^{s_{max}} \left\{ \left(1 - q_i^{n_i}\right) \cdot \left(\mathrm{P}\left[S_{Tm} = s_i\right]\right) \right\} \right] \left[\frac{\sum_{i=1}^{13} [v_i \cdot w_i]}{125} \right] \cdot n_p \end{aligned} \tag{6.1}$$

where,

n_p = the population of the region being analyzed (i.e. the population exposed to landslide risk)

$q_i = 1 - \mathrm{P}\left[F_1 \mid S = s_i\right]$

$\mathrm{P}\left[F_1 \mid S = s_i\right]$ = the conditional probability of failure of a slope having given angle s_i

n_i = the number of slopes in the region having slope angle s_i

$$\mathrm{P}\left[S_{Tm} = s_i\right] = \exp\left(\frac{-\left(s_i - \frac{\Delta s}{2}\right)^2}{2\sigma_{S_T}^2}\right) - \exp\left(\frac{-\left(s_i + \frac{\Delta s}{2}\right)^2}{2\sigma_{S_T}^2}\right)$$

v_i = the vulnerability ranking of each individual vulnerability indicator

w_i = the weight of each individual vulnerability indicator

Note that in eq. [6.1], the factor of 125 is as was used in Chapter 5. If the weights change, the factor of 125 will also change.

6.2 The Effect of Population Increase on Landslide Risk Levels

In order to understand the effects of population increase on landslide risk levels, it is important to break risk down into its components, i.e. hazard, vulnerability and exposed population. While the effect of population increase on the exposed population risk component is straightforward enough, i.e. the increase in n_p is proportional to the percentage increase in population, the effect on hazard and vulnerability requires a more thorough investigation.

6.2.1 The Effect of Population Increase on Landslide Hazard Levels

When the population of a region increases, several consequences are obvious and take place immediately thereafter. To begin with, an increase in population generally leads to an increase in occupied land space. As a result, more natural landscapes are modified – regions may be deforested, rural areas urbanized, vegetation species changed, etc. Furthermore, existing developments and infrastucture are often expanded, more roads, railways and buildings are constructed (Nadim et al., 2006) and there is an increased demand for food and water. These activities put significant levels of stress on the environment and consume large quantities of natural resources. If, as is the case in many parts of the world, natural resources are used unsustainably, they can become permanently depleted. The environmental stresses resulting from land use change and over-exploitation of natural resources (e.g., water) commonly influence slope geometries, soil moisture levels and the hydrological cycle, all of which lead to increased levels of slope instability.

The degree of influence of an increased population on the landslide hazard level of a region is addressed by analyzing its influence on the frequency of human-induced landslides. This

relationship, between population increase and human-induced landslide frequency, is dependent upon: 1) regional soil lithology and landslide triggers, and 2) the effect of human activity on regional slope stability levels.

1) Regional soil lithology and landslide triggers

Using whatever databases are available for the region under analysis, historical records of past landslides must be collected in order to identify the most common types of slope failures. These slopes are categorized by lithology as either clay (comprises both sensitive and non-sensitive clay slides), sand (or earth), debris (includes mud) or rock. Once collected, this data, used to categorize past landslides by lithology, can be used to estimate the fraction of future landslides expected to be clay, the fraction expected to be sand, and so on.

In order to estimate future landslide hazard levels, it is also important to understand why landslides occurred in the past, i.e. what were the triggering factors? This section of the research is concerned with the expected frequency of human-induced landslides, therefore the triggers for past landslides should be categorized as either natural or anthropogenic (note that partly human-induced slides are categorized as anthropogenic for this analysis). Unfortunately, many historical landslide records do not specify landslide triggers, therefore, this step is best completed with expert judgment. Leading natural scientists and engineers can provide reasonable estimates of the fraction of landslides induced by human activity versus the fraction induced by natural causes, again categorized by lithology. The results are, however, very region-specific. For instance, the majority of quick clay slides in Norway are human-induced, whereas in Sweden, most are the result of toe erosion caused by changing water levels. Therefore, regional experts should be consulted.

The data on past landslides, together with expert opinions, is sufficient to estimate the fraction of past landslides, in the region under analysis, that have been partly or fully induced by human activity, i.e.

$$a_L = c_l \cdot a_c + e \cdot a_e + d \cdot a_d + r \cdot a_r \tag{6.2}$$

where a_L is the fraction of past landslides that were induced by anthropogenic activity, c_l is the fraction of all future slides that are expected to be clay (similarly e, d, and r for sand (or earth), debris, and rock), and a_c is the fraction of future clay slides that are, according to experts, expected to be triggered by anthropogenic activity (similarly a_e, a_d, and a_r for earth, debris, and rock).

The value of a_L is important for understanding the effect of population increase on landslide hazard levels because human activity only influences the frequency of *human*-induced landslides. Therefore, the frequency of naturally-induced landslides (e.g., by earthquakes) is assumed constant regardless of population.

2) Effect of human activity on regional slope stability levels

Increased human presence, e.g., as a result of urbanization, does not have the same effect on landslide hazard levels in all regions. The effect of human activity on regional slope stability levels is widely variable and dependent upon factors such as the initial population density, the level of development and the skills and professional expertise of the incoming population. The relationship developed in this section, which describes the change in frequency of human-induced landslides as a result of population increase, includes multiplicative population density and development factors (as these factors increase, the frequency of expected human-induced landslides also increases), as well as another factor referred to as maintenance, m, which accounts for the positive influence of human activity on slope stability levels (i.e. the types of human activity that reduce landslide probability). The factor, m, enters into the model as part of a composite multiplicative 'human influence' indicator. The human influence indicator considers the negative effects of human activity on slope stability levels (i.e. the types of human activity that increase landslide probability) through the inclusion of Δp (the increase in population computed as a fraction of the existing population), as well as the positive effects of human activity on slope stability levels through the inclusion of $m \cdot \Delta p$. The human influence composite indicator is written as $\Delta p \cdot (1 - m)$ and it is directly proportional to the expected increase in frequency of human-induced landslides (the equation will be developed later in this section). Therefore, as the the value of m, which ranges from 0 to 1,

increases, the expected frequency of human-induced landslides decreases. Each of these factors is described in detail below.

a) Population density factor

A region can only support a finite number of people without being forced to overexploit its natural resources. Thus, in order to develop a relationship between the expected increased in human-induced landslide frequency (and resulting hazard level) and population increase, the initial population density of the region must be taken into consideration. Based on a constant rate of population growth, a region with a high initial population density will reach its maximum capacity before a region with a lower initial population density (i.e. a low initial population density implies, in most cases, more room for growth). In this research, a population density factor, F_{pd}, has been developed (se Table [6.1]) using country-wide statistics provided by the Global Rural-Urban Mapping Project (GRUMP) (CIESIN, 2007) as a metric.

Table 6.1 Population density factor.

Population density (per km^2)	Classification	F_{pd}
>1	Very low	1.00
[1 – 25)	Low	1.10
[25 – 50)	Moderate	1.20
[50 – 100)	Medium	1.30
[100 – 200)	High	1.40
$\geq$ 200	Very high	1.50

Note: The values selected for the population density factor (and all subsequent factors) have been assigned based on educated judgement of the author and other SafeLand contributors (Nadim et al., 2006). Thus, these factors should be calibrated by applying the model to several landslide-prone regions that have already experienced significant levels of population growth. This issue will be discussed further in Section 8.2.

b) Development factor

In most cases, a high level of economic development implies that a region has the resources required to employ professionals and ensure that proper regulations and guidelines are followed when altering natural landscapes, extracting natural resources, etc. This economic development indicator is incorporated into the model developed in this research using gross domestic product (GDP) per capita, as provided by the International Monetary Fund (IMF, 2010), as a metric.

Table 6.2 Development factor.

GDP per capita (thousands of USD)	Classification, with respect to level of wealth	F_d
≥ 50	Very high	1.00
$[30 - 50)$	High	1.05
$[20 - 30)$	Medium	1.15
$[10 - 20)$	Moderate	1.30
< 10	Low	1.50

The development factor, F_d, does not vary linearly with GDP per capita. The differences observed, with respect to land use practices, between regions of medium and very high levels of wealth is usually much smaller than the differences observed between regions of low and medium levels of wealth. As a country's GDP per capita decreases, the likelihood of it neglecting to follow geotechnical regulations generally increases at a faster rate. Poor countries simply cannot afford to take all necessary precautions against environmental damage and often lack professional expertise, therefore, their land use practices tend to degrade soil significantly more than wealthier regions.

c) Maintenance factor

The type of incoming population, with respect to skills and professional expertise, significantly influences the degree to which population increase affects regional slope stability levels. After all, it is important to realize that not all human activity adversely affects slope stability. Once natural landscapes have been altered, it is often necessary to safeguard against erosion, maintain drainage

systems, etc., which requires human interference. Thus, a maintenance factor is introduced as part of a 'human influence' multiplicative indicator (described earlier in this section). The ranking system for the maintenance factor is shown in Table [6.3]

Table 6.3 Maintenance factor.

Characteristics of population	m
increase in population; no specific geotechnical focus	0.10
increase in population; includes a notable increase in geotechnical researchers	0.35
increase in population; introduction of more extensive slope stability mitigation techniques	0.50
increase in population; introduction of more extensive slope stability mitigation techniques and new geotechnical guidelines	0.75

Relationship between landslide hazard level and population increase

Since regional landslide hazard levels measure the probability of slope failure (i.e. landsliding), the expected change in hazard level, as a result of population increase, is dependent upon the effect of population increase on human-induced landslide frequency, f. This change in frequency can be estimated based on the variables introduced earlier in this section.

$$\Delta f = F_d \cdot F_{pd} \cdot a_L \cdot \Delta p \cdot (1 - m) \tag{6.3}$$

where a_L represents the fraction of past landslides induced by humans (see eq. [6.2]), F_d, F_{pd} and m are the model factors (described earlier in this section), and Δp represents the expected increase in population, as a fraction of the existing population.

If the hazard level, p_f, is broken down into its anthropogenic and natural components, such that

$$p_f = p_f \cdot a_L + p_f \cdot (1 - a_L) \tag{6.4}$$

then the future hazard level, p_{f_2}, expected for a region with an increased population, can be evaluated, using equations [6.3] and [6.4], as

$$p_{f_2} = p_f \cdot a_L(1 + \Delta f) + p_f \cdot (1 - a_L)$$

$$= p_f \cdot (1 + a_L \Delta f) \tag{6.5}$$

where p_f is defined in eq. [3.42], a_L is defined in eq. [6.2] and Δf is defined in eq. [6.3].

6.2.2 The Effect of Population Increase on Landslide Vulnerability Levels

The effect of population increase on vulnerability levels is much harder to predict than the effect on landslide hazard levels, therefore, several assumptions must be made. For instance, it is impossible to know what age the new inhabitants will be, so the most practical assumption is that there are a wide range of ages, thus the *percentage* of people in the vulnerable age categories (see Section 5.1) remains constant, as does the 'age' indicator ranking. Similarly, the most likely scenario is that the education level, integration level, income, agricultural dependence and housing constructs will vary across the board for the new arrivals. Furthermore, the remaining (recovery and administration type) indicators rely mostly on governmental and/or institutional control and thus, should not be overly influenced by urbanization or other common forms of population increase. The only indicator that is definitely affected by population increase is 1b, 'urban population' (see Chapter 5), which is has a weight of 1 and describes the population density of the region.

Therefore, the expected future vulnerability level, v_f, based on an expected increased population, is only a slight modification of the original vulnerability equation ([5.2]).

$$\begin{aligned} v_f &= \frac{v_{1b} \cdot (1 + \Delta p) + \sum_{i=1}^{12} [v_i \cdot w_i]}{3(5 \cdot 3) + 6(5 \cdot 2) + 3(5 \cdot 1) + 1[5 \cdot 1 \cdot (1 + \Delta p)]} \\ &= \frac{v_{1b} \cdot (1 + \Delta p) + \sum_{i=1}^{12} [v_i \cdot w_i]}{120 + 5 \cdot (1 + \Delta p)} \end{aligned} \tag{6.6}$$

where the indicator, $1b$ (urban population), is multiplied by the expected change in population, $(1 + \Delta p)$, before it is included in the summation of the twelve remaining weighted indicators.

6.3 Future Risk Levels

Equation [6.1] evaluates regional landslide risk, R, based on the existing hazard level, vulnerability level and population. The expected landslide risk associated with a region at a future point in time, R_f, when the population has increased by some fraction Δp, is computed, based on equations [6.5] and [6.6], as

$$\begin{aligned} R_f &= p_{f_2} \cdot v_f \cdot [n_p \cdot (1 + \Delta p)] \\ &= \left[p_f \cdot (1 + a_L \Delta f)\right] \left[\frac{v_{1b} \cdot (1 + \Delta p) + \sum_{i=1}^{12} [v_i \cdot w_i]}{120 + 5 \cdot (1 + \Delta p)}\right] \left[n_p \cdot (1 + \Delta p)\right] \end{aligned} \tag{6.7}$$

CHAPTER 7

Application of the Landslide Vulnerability & Future Hazard Assessment Models

7.1 Application of the Landslide Vulnerability Model, Literature Review

As mentioned in Chapter 5, the landslide vulnerability model was developed by the author along with U. Eidsvig at the International Centre for Geohazards (ICG) in Oslo, Norway. However, during the author's time at ICG, the vulnerability model was only developed theoretically. Therefore, this section, which applies the model to two regions in Norway, is a brief summary of the work completed by Eidsvig (2010).

The landslide vulnerability model developed in Chapter 5 has been applied to two regions in Norway: 1) Skien, a city of approximately 50,000 people along the southern coast, and 2) Stranda, a municipality of approximately 4,700 people in the western region of Norway. Skien is highly susceptible to sliding because of quick clay deposits and Stranda is a special case, which has been monitored since 2005, as it contains the Åknes rock slope, located over a fjord. If a rockslide were to occur at Åknes, there is potential for a tsunami, which could cause a significant amount of damage to the Stranda.

The indicators have been ranked for each of the regions, as shown in Figures [7.1] and [7.2]. The data used to evaluate the vulnerability indicators, and rank them accordingly, was obtained from either census data, interviews with local experts and/or subjective judgment of Eidsvig (due to budget limitations).

Result of analysis for Skien		
Indicator	**Description/reasoning for choice of indicator score**	**Indicator Score**
Age distribution	The ranking of the vulnerability was performed by looking into census data: • Children 0-5 and age over 65 : About 9700 • 51700 inhabitants Fraction of population less than 5 years and above 65 years: 19% Vulnerability 1	**1**
Housing type	A majority of the buildings in the area are wooden houses with reinforces concrete foundation walls, which would be classified as medium resistance houses.	**3**
Rural population	Preliminary vulnerability score (by judgment)	**2**
Urban population	Preliminary vulnerability score (by judgment)	**1**
Personal wealth	Gross Domestic Product (GDP) for Skien = 87000$ (From census data)	**1**
Vulnerable groups	Immigrant from other cultures: 7.8%. (From census data)	**1**
Education level	22% have attended a post-secondary institution. (From census data)	**2**
Hazard evaluation	Basic hazard maps available.	**2**
Regulation control	Consistent approach to the regulation of construction and land use on the basis of exposure to landslides.	**2**
Emergency response	Clear definition of roles and responsibilities at local level; proportional allocation of resources	**2**
Early warning system	No early warning system	**5**
Insurance and disaster funds	Extensive coverage for private and public buildings, existence of government-sponsored landslide funds	**1**
Quality of medical services	In census data not given number of hospital beds but number of medical doctors. Judgemental ranking.	**2**

Figure 7.1 Ranked vulnerability indicators for Skien, Norway.

Result of analysis for Stranda		
Indicator	**Description/reasoning for choice of indicator score**	**Indicator score**
Age distribution	The ranking of the vulnerability was performed by looking into census data: • About 1000 inhabitants younger than 5 years or older than 65 years. • 4745 in total Fraction of population less than 5 years and above 65 years: 21% Vulnerability 2	**2**
Housing type	A majority of the buildings in the area are wooden houses with reinforces concrete foundation walls, which would be classified as medium resistance houses.	**3**
Rural population	Preliminary vulnerability score (by judgment)	**3**
Urban population	Preliminary vulnerability score (by judgment)	**1**
Personal wealth	Gross Domestic Product (GDP) for Stranda = 96000$ (From census data)	**1**
Vulnerable groups	Immigrant from other cultures: 4.7 %. (From census data)	**1**
Education level	15% have attended a post-secondary institution. (From census data)	**3**
Hazard evaluation	Basic hazard map available	**2**
Regulation control	Fairly effective regulations for new developments however, potential problems with older constructions	**3**
Emergency response	Permanent coordination between responders in communities; specialized equipment and well-trained rescue services available throughout the country	**1**
Early warning system	Advances early warning system used in coordination with emergency response procedures	**1**
Insurance and disaster funds	Extensive coverage for private and public buildings, existence of government-sponsored landslide funds	**1**
Quality of medical services	In census data not given number of hospital beds but number of medical doctors. Judgmental ranking.	**2**

Figure 7.2 Ranked vulnerability indicators for Stranda, Norway.

In Figures [7.1] and [7.2], the 'housing type' indicator is equivalent to the 'building type' indicator in the model presented in this thesis. Similarly, the 'vulnerable groups' indicator is equivalent to this model's 'level of integration' indicator and the 'personal wealth' indicator is very similar to this model's 'GDP per capita' indicator.

Using the indicator weights as defined in Section 4.1, the total vulnerability, v_t, and normalized total vulnerability, v, can be calculated for each region using equations [5.1] and [5.2]:

Skien, Norway

$$v_t = \frac{\sum_{i=1}^{n} [v_i \cdot w_i]}{\sum_{i=1}^{n} w_i} = \frac{51}{25} = 2.04 \qquad (7.1a)$$

$$v = \frac{\left(\frac{\sum_{i=1}^{13}[v_i \cdot w_i]}{25}\right)}{\left(\frac{[3(5\cdot3)+6(5\cdot2)+4(5\cdot1)]}{25}\right)} = \frac{\sum_{i=1}^{13}[v_i \cdot w_i]}{125} = \frac{51}{125} = 0.408 \qquad (7.1b)$$

Stranda, Norway

$$v_t = \frac{49}{25} = 1.96 \qquad (7.2a)$$

$$v = \frac{49}{125} = 0.392 \qquad (7.2b)$$

The resulting levels of vulnerability to landslides are very similar in each of the regions tested. This is as expected since the majority of both the societal and physical indicators are similar throughout the whole of Norway. Although the smaller community of Stranda has a slightly older, more rural and less educated population than the larger city of Skien, its vulnerability level is balanced due to the fact that Standa is being monitored for potential tsunami-inducing rockslides. As a result, Stranda has improved early warning systems and emergency response procedures. This type of balance, improved administrative indicators for more hazardous regions, is typical of highly developed regions such as Norway.

The overall landslide vulnerability scores are relatively moderate, each representing approximately 40% vulnerability. Although the two regions have similar vulnerabilities, they do not necessarily have similar risk levels. Risk is also dependent upon the landslide hazard level and number of exposed persons. If Skien and Stranda are found to have similar regional probabilities of slope failure, approximately the same percentage of each of their populations will be exposed to considerable levels of landslide risk. However, once the number of exposed persons is considered, i.e. risk, taken as the number of people exposed to potential landslide damage, Skien will have a much higher risk level as its population is over ten times larger than that of Stranda.

On a final note, since the landslide vulnerability model evaluates the vulnerability of regions on a relative scale, it would be prudent to test other regions outside of, and different from, Norway (perhaps a region assumed to have a notably high level of vulnerability) to compare the final scores assigned to each (discussed further in the ‘Model Validation‘ portion of Section 8.2).

7.2 Application of the Future Landslide Hazard Assessment Model

As described in Chapter 6, a noticeable increase in the population of a region affects the level of landslide risk experienced by the communities within that region. The most important part involved in estimating the expected change in landslide risk, as a result of population increase, is to understand the effect of population increase on the frequency of *human*-induced landslides. The population of a region does not directly affect the frequency of naturally-induced landslides and the vulnerability level does not change significantly with increasing populations. The expected future vulnerability level (eq. [6.6]) is calculated using the same equation as the current vulnerability level (eq. [5.2]), except with an updated value for the 'urban population' vulnerability indicator.

In this section, data, obtained from the Norwegian Geotechnical Institute (NGI, 2010), for Norway is used to estimate the expected change in landslide hazard levels in Norway if its population were to increase by 50%, at some point in the future. This case study applies the methodology outlined in Section 6.2.1.

Regional soil lithology and landslide triggers

According to the Geological Survey of Norway (NGU, 2008) database 380 clay and 950 earth slides (1330 total) dating back to the 12^{th} Century have been reported in Norway by Astor Furseth (Nadim et al., 2010). When possible, the cause of the slides have been deduced according to the descriptions of the events, otherwise they were labeled as 'unknown'; 603 of the 1330 slides were categorized as 'unknown', i.e. over 45% of the slides. Therefore, in an effort to determine the total fraction of human-induced slides, it is preferable to consult regional experts than to use the historical data.

As part of the SafeLand project (Nadim et al., 2010) questionaries concerning human-induced landslides were created and sent out to leading geoscientists and geotechnical engineers across Norway. The questionnaires defined slide-inducing human intervention as:

1) cut-and-fills along railways, highways and secondary roads;

2) engineered slopes and embankments; and

3) large portions of natural terrain altered by human activity (e.g. forested areas removed for new developments).

The combined and averaged results indicated that approximately 73% of the clay (including quick clay) slides that occur in Norway are thought to be triggered by these human activities, as well as 16% of earth slides, 11% of debris slides and 8% of rock slides (Nadim et al., 2010). Thus, a_c = 0.73, a_e = 0.16, a_d = 0.11, and a_r = 0.08. From NGU's data, the fraction of slides categorized as clay can easily be computed as 380 over 1330, i.e. c_l = 0.29, similarly e = 950/1330 = 0.71, d = 0 and r = 0. Therefore, using eq. [6.2], the fraction of past landslides induced by human activity is approximately

$$\begin{aligned} a_L &= c_l \cdot a_c + e \cdot a_e + d \cdot a_d + r \cdot a_r \\ &= 0.29(0.73) + 0.71(0.16) \\ &= 0.33 \end{aligned} \tag{7.3}$$

Furthermore, the experts questioned estimated that a 50% increase (Δp = 05) in the exposed Norwegian population, with no major changes in geotechnical regulations, would increase the frequency of human-induced landslides by 18% (Δf = 0.18). Although this prediction will not be entered into the model, the results will be compared with it.

Degree of human influence on regional slope stability levels

Norway has a population of approximately 4,635,000 spread over an area of 324,220 km^2, thus its population density is just over 14 people/km^2 (Jaedicke et al., 2010) and the resulting value of F_{pd} is 1.10. Its GDP per capita is approximately 79 000 USD (IMF, 2010), hence F_d = 1.00.

Relationship between landslide hazard level and population increase

If, over the next x years, the population of Norway is expected to increase by 50%, the frequency of human-induced landslides is also expected to increase, by some value Δf. Assuming that the

population increases uniformly, a 50% increase in the total population also implies a 50% increase in the exposed population. If the incoming population does not include a substantial number of geotechnical researchers, so that m = 0.10, this situation would result in the following increase in human-induced landslide frequency:

$$\begin{aligned}\Delta f &= F_d \cdot F_{pd} \cdot a_L \cdot \Delta p \cdot (1 - m) \\ &= 1.00 \cdot 1.10 \cdot 0.33 \cdot 0.5 \cdot (1 - 0.1) \\ &= 0.16\end{aligned} \tag{7.4}$$

However, if the incoming population does include a notable number of geotechnical researchers, so that m = 0.35, the increase in landslide frequency would be reduced to:

$$\begin{aligned}\Delta f &= 1.00 \cdot 1.10 \cdot 0.33 \cdot 0.5 \cdot (1 - 0.35) \\ &= 0.12\end{aligned} \tag{7.5}$$

This model estimates that the landslide frequency will increase by between 12% and 16% if the exposed Norwegian population increases by 50%, again with no major changes in geotechnical regulations. This corresponds very well to the Norwegian expert predictions of 18% (see prediction made earlier in this section).

The future hazard level, p_{f_2}, based on the expected increase in population, can be estimated with eq. [6.5]. Assuming that the incoming population does not include a substantial number of geotechnical researchers, the future hazard level is estimated as,

$$\begin{aligned}p_{f_2} &= p_f \cdot (1 + a_L \Delta f) \\ &= p_f(1 + 0.3253 \cdot 0.16) \\ &= 1.052 p_f\end{aligned} \tag{7.6}$$

The expected future landslide hazard level, $p_{f_2} = 1.052 p_f$, implies that the probability of slope failure in Norway would increase by just over 5% if the population were to increase by 50% (but all other conditions remained the same). This change in slope failure probability refers to all types of slope failures, i.e. both natural and anthropogenic.

CHAPTER 8

Summary and Conclusions

8.1 Landslide Risk Assessment

Risk, as it is most commonly defined, is a product of hazard, vulnerability and exposed population. This thesis addresses the issue of landslide risk assessment through the development of three separate methodologies: 1) landslide hazard assessment using DEMs, 2) landslide vulnerability assessment using an indicator based vulnerability model, and 3) assessment of the effects of population increase on landslide risk levels. When these three methodologies are combined, they provide a complete framework for regional landslide risk assessment.

The first model developed in this thesis, landslide hazard analysis, defines the regional hazard level as the probability of at least one slope failure throughout the region. This probability is estimated as a function of the distribution of maximum slope angles and the conditional probabilities of local slope failures. The second model, landslide vulnerability analysis, measures the physical and socioeconomic fragilities within a region using thirteen different vulnerability indicators. Each indicator is weighted according to its degree of relevance to the model, and ranked from 1 (lowest degree of vulnerability) to 5 (highest degree of vulnerability). The third and final model, future landslide risk assessment, addresses the impact of population increase on landslide risk. A model is formulated to describe how an increase in population, e.g., due to urbanization, alters the regional frequency of human-induced landslides, and furthermore, how this increased landslide probability affects the overall landslide risk level.

These three models have been described in detail in Chapters 3, 5 and 6 respectively, and tested in several regions throughout Europe in Chapters 4 and 7. The accuracy of the models is discussed

in depth in Section 8.1.1 below, and recommendations for future work, including model validation techniques, are outlined in Section 8.2.

8.1.1 Accuracy of the Landslide Hazard Assessment Model

The distribution of maximum slope angles, as estimated using digital elevation models (DEMs), is required in order to assess landslide hazard levels and in order to describe this distribution, the variance of the slope angles must be estimated. Since the elevations measured by each cell, within a DEM, are necessary for the maximum slope angle variance calculations, the accuracy of the elevation measurements is crucial. The size of each cell of a given DEM is directly related to the accuracy of the elevation measurement; since there is only one elevation recorded for each cell, the larger the cell, the more local averaging required over that cell. Local averaging smooths out variation in terrain and reduces the amount of detail observed by the DEM. As a result, less variance is observed in low resolution elevation data, which leads to less variance observed in the maximum slope angles (computed as the derivative of the elevation data). Typically, steep slopes that are small in spatial extent are overlooked by low resolution DEMs as a result of local averaging. Unfortunately, many of these small, steep slopes often present high probabilities of failure, and if they are not considered by a DEM, the regional hazard level (i.e. regional probability of slope failure) is underestimated. This can create serious issues for landslide preparedness planning. For example, important precautions, such as emergency response procedures and construction regulations, may be neglected if the landslide hazard level is considerably underestimated, which would increase the community's level of risk to loss in the event of a landslide.

Furthermore, the degree of local averaging experienced by a DEM is also dependent upon the type of terrain within the domain (see eq. [3.38]), in addition to the cell size. As the amount of variation in the elevation profile increases, the effect of local averaging becomes more pronounced. Therefore, in a region with a fairly homogeneous elevation profile, there will be less difference between the slope angles (and correspondingly, the hazard levels) computed by a DEM of relatively high resolution and one of a lower resolution than in a region with a very erratic elevation profile.

For example, consider the two case studies presented in this thesis. Case study one, located in the Alps, computed the relationship between the slope angles perceived by the 3-arc second resolution model (T_1) versus the 30-arc second resolution model (T_2) to be $s_{T_1} = \left(\frac{0.178}{0.311}\right) \cdot s_{T_2} \rightarrow s_{T_2} = 1.748 \cdot s_{T_1}$ (see eq. [4.10]). Whereas case study two, located in the southwest of Norway, calculated $s_{T_1} = \left(\frac{0.066}{0.930}\right) \cdot s_{T_2} \rightarrow s_{T_2} = 14.09 \cdot s_{T_1}$ (see eq. [4.26]). These results reveal a much larger discrepancy between the slope angles perceived by the two DEMs in the southwest of Norway than between the slope angles perceived by the same two DEMs in the Alps. Thus, it can be concluded from this comparison ($s_{T_2} = 1.748 \cdot s_{T_1}$ versus $s_{T_2} = 14.098 \cdot s_{T_1}$) that the effects of local averaging are more pronounced in the test region in Norway than in the Alps, which is indeed the case (under the assumption that the water surfaces are all at zero elevation). The correlation length in the Alps is over 4 km (4260 m), while only 840 m in Norway, which is less than than one-fifth of that of the Alps. As defined in Section 3.3.2, the correlation length describes the degree of linear dependence between data points, therefore, the smaller the correlation length, the more erratic the profile.

In order to reduce the inaccuracies resulting from the effects of local averaging on a DEM, the hazard level can be estimated at a critical scale. The critical scale refers to the minimum scale at which a landslide would be deemed hazardous, i.e. the critical cell size corresponds to the minimum size landslide which could cause a noteworthy amount of damage to the surroundings. The regional probability of slope failure is estimated at the critical scale using local averaging theory with data provided by two DEMs. This landslide hazard model uses the Rayleigh distribution to model the distribution of maximum slope angles throughout the region. Therefore, as it currently stands, this model only provides accurate hazard estimations for regions with an approximately normally distributed elevation profile.

In addition to error resulting from local averaging, there is a second type of error inherently associated with DEMs: vertical measurement error. Vertical error refers to the discrepancy between the true and observed elevations at points measured by a DEM. The vertical error directly affects the estimation of the elevation variance, and this error is carried through, to some degree, to the slope

variance and regional probability of slope failure. First of all, the following equation illustrates the difference between the observed and true elevations,

$$Z_T^o(i) = Z_T(i) + \epsilon_i \tag{8.1}$$

where $Z_T^o(i)$ represents the elevation observed by a DEM in the ith cell, $Z_T(i)$ represents the true average cell elevation, and ϵ_i represents the vertical error associated with the DEM measurement. Thus, the variance of the observed DEM elevation is

$$\text{Var}\left[Z_T^o(i)\right] = \text{Var}\left[Z_T(i)\right] + \text{Var}\left[\epsilon_i\right] \tag{8.2}$$

The amount of vertical error associated with a DEM is dependent upon the specific DEM under consideration. For example, the Shuttle Radar Topography Mission (SRTM) DEM, used in both case studies presented in Chapter 4, was launched in 2000 and was the first to provide global high quality elevation data at 1 and 3-arc second resolutions (Rabus et al., 2003). The SRTM elevation data was acquired using synthetic aperture radar (SAR) interferometry and has a vertical accuracy requirement of $\pm$16 m for 90% of the data across the entire mission, which covered all land masses from 60 $^\circ$ N to 57 $^\circ$ South (Rabus et al., 2003). In each of Rabus et al.'s test sites (in Australia, Scotland and Switzerland) as well as in Bhang et al.'s (2007) study of SRTM vertical accuracy in Otter Trail, MN, the vertical accuracy requirement was met. The point on the standard normal distribution having area above it equal to 0.05 is 1.645 (i.e. if 90% lies inside the confidence interval, then 5% lies above it and 5% lies below it). Therefore, the standard deviation of the error is:

$$\sigma_\epsilon = \frac{16}{1.645} = 9.73 \text{ m} \tag{8.3}$$

To illustrate the degree of influence of the vertical error on the elevation variance, the SRTM data from the Alps case study, in Chapter 4, will be used. In this example, the variance of the elevation, as observed by the SRTM DEM, was found to be $\text{Var}\left[Z_T(i)\right] = (702.57 \text{ m})^2 \simeq 493,605$ m^2. The true DEM variance of the elevation data can now be calculated by substituting this value of σ_ϵ into eq. [8.2] as shown below,

$$\text{Var}\left[Z_T(i)\right] = 702.57^2 - 9.73^2$$

$$\simeq 493,510\,\mathrm{m}^2 \tag{8.4}$$

The maximum expected difference between the true and observed DEM variances of the elevation data, as a percentage, is calculated as the difference between the observed and true variances, divided by the true variance,

$$\frac{493,605 - 493,510}{493,510} = 0.00019 \tag{8.5}$$

The difference between the true and observed elevation variances is approximately 0.02%. While in other regions the vertical error may be larger than 0.02%, it will still likely be much less influential than the error resulting from local averaging. Furthermore, if the analysis of vertical error is continued to consider the variance of the slope angles, which is the parameter that is actually required for the regional hazard analysis, it will be found that, in most cases, the error impact is even less than the 0.02% effect on the elevation variance. The slope angles, in the horizontal and vertical directions, are computed with eq. [3.23] as the derivative of the elevation data. Therefore, the true slope, S_T, at point i, can be evaluated as shown in both of the equations below

$$S_T(i) = \frac{Z_T(i-1) - Z_T(i+1)}{\Delta T} \tag{8.6a}$$

$$S_T(i) = \frac{[Z_T^o(i-1) + \epsilon_{i-1}] - [Z_T^o(i+1) + \epsilon_{i+1}]}{\Delta T} \tag{8.6b}$$

Using equations [8.6a] and [8.6b], the following relationship can be developed to describe the difference between the observed and true slopes,

$$Z_T^o(i-1) - Z_T^o(i+1) = [Z_T(i-1) + \epsilon_{i-1}] - [Z_T(i+1) + \epsilon_{i+1}] \tag{8.7}$$

The vertical error measured at cells close to one another will likely be very similar in magnitude. If the vertical errors are equal, $\epsilon_{i-1} = \epsilon_{i+1}$, then the variances are equal

$$\mathrm{Var}\left[Z_T^o(i-1) - Z_T^o(i+1)\right] = \mathrm{Var}\left[Z_T(i-1) - Z_T(i+1)\right] \tag{8.8}$$

Although the vertical error in neighbouring cells will probably not be exactly equal to one another, they will probably be similar. In which case, the difference between the observed and true variances will be negligible. Therefore, the landslide hazard model presented in this thesis need not consider vertical error in its calculation.

8.1.2 Accuracy of the Landslide Vulnerability Assessment Model

One of the hardest tasks associated with a landslide vulnerability analysis is that of data acquisition. The methods used to acquire the data required for the model presented in Chapter 5 will vary depending on the region under analysis. Some regions keep accurate and up to date census data, which contains a significant portion of the required information, while others may not have any reliable data available. The size of the region is also important. It is much easier to collect data via surveys in small villages than in large cities. Due to these large variations, there is no consistent approach to collecting the data. Pre-existing data should obviously be reviewed first, and then the remaining information acquired using sampling methods such as surveys, distributed to randomly selected households and/or governmental bodies throughout the region. The percentage of the population sampled will vary depending on the size of the region and the amount of resources available. Thus, the overall accuracy of the landslide vulnerability model is highly dependent upon the data acquired to rank the vulnerability indicators.

8.2 Recommendations for Future Work

While the landslide risk assessment model developed in this thesis addresses the factors that affect risk, by considering its hazard and vulnerability components individually, this is a first attempt. If work is continued on this model, its performance could be improved and its applications expanded. Future work in the following areas of research are recommended:

1) Model validation:

   a) *Landslide hazard model* (Chapter 3): If the landslide hazard model were used to create hazard maps in a region that has been well-documented (for landslides) in the past, the hazard maps could be compared with the historical records to see how well it predicted highly hazardous regions. Furthermore, by performing this test in several areas, each with different types of terrain, the accuracy could be evaluated as a function of terrain type.

b) *Landslide vulnerability model* (Chapter 5): This model evaluates the total vulnerability level of a region on a relative scale. That is to say, for example, that a regional vulnerability score of 0.6 does not necessarily imply that 60% of the population are vulnerable to loss from landslides, but it does imply that the population is much more vulnerable than another region which was found to have a vulnerability score of 0.2. Therefore, by applying the vulnerability model to multiple regions that have already experienced landslides, the results from the model can be compared with the actual amount of loss experienced in the regions after the landslides occured. If the results do not match very well, the ranking systems can be adjusted as necessary. For example, it may be found that a vulnerability indicator currently assigned a weight of 3 (i.e. of highest relevance) causes regions that were actually quite invulnerable to loss to be given too high a vulnerability score. Thus, it may be deemed appropriate to change this indicator weight to a lower value in this case.

b) *Future landslide hazard model* (Section 6.2.1): As it currently stands, this model also uses a relative scale since the evaluation techniques (i.e. population density, development and maintenance factors) require some calibration. The ranking systems defined for the model factors can be improved by applying the model to regions that have, in the past, experienced significant levels of population growth. By analyzing the region, based on its conditions prior to population growth, with the future landslide hazard model, the predicted change in human-induced landslide frequency can be compared with the actual change in frequency. If there is a discrepancy in the results, the ranking systems can be modified, and the region can be retested to see if the predicted frequency is closer to the actual outcome. Once the necessary modifications have been made, several other regions should be tested. If the results of these tests are all relatively accurate, the model can be used with confidence in its predictions.

2) Magnitude of slope failure: By comparing the probability of slope failure at different resolutions, it is possible to break the failure probability down by landslide size. For example, there may be an overall 50% probability of slope failure at the critical scale, but only a 30%

probability that the slide will be over 100 m $\times$ 100 m in size and only a 2% probability that it will be over 1000 m $\times$ 1000 m in size. Consideration of these results would allow for a more detailed landslide analysis that considers frequency vs. consequence of slides of different sizes, in addition to the overall regional hazard analysis.

3) Alternative elevation datasets: The accuracy of the landslide hazard assessment model can potentially be improved by obtaining elevation data from other types of geographic information systems (GIS) that have higher resolutions than digital elevation models. For instance, lidar imaging can be used to measure surface elevations with centimeter-scale resolutions. However, it is important to note that these extremely high resolution models generally cover less surface area than DEMs, so there are benefits and drawbacks to each type of GIS model. Depending on the size of the region under analysis, the required level of accuracy, and the amount of resources available, the most appropriate model can be selected for the analysis.

4) Multiple slope failures: The current landslide hazard assessment model defines the regional hazard level as the probability that one or more slopes within the region fail. By assuming independence between the slopes, and constant conditional probability of failure, the probability of one or more slope failures is evaluated as one minus the probability of non-failure (binomial distribution). However, if the analysis were able to consider the probability that two or more slopes fail, or ten or more slopes fail, etc., the model would be more useful, especially for large regions such as those considered in the two case studies presented in Chapter 4.

5) Avalanche risk assessment: With a few modifications, the framework presented in this model could be applied to evaluate avalanche risk levels, in addition to landslide risk levels. The only subcomponent of the risk framework presented in this thesis that would need to be adjusted is the hazard level. The regional hazard level computation requires the regional conditional probability of slope failure and the distribution of maximum slope angles. The methodology developed to evaluate the conditional failure probability would be very similar for both avalanches and landslides. In fact, the ground strength parameters required for Rslope2d would be easier to obtain for avalanche analyses as there is generally less variability

in the ground strength parameters for snow and ice than for soil. While the methodology used to estimate the regional distribution of maximum slope angles for landslides is also applicable avalanches, an additional factor must be considered in order to maintain accuracy: changing snow and ice levels. By analyzing long-term weather data for the region under analysis, it is possible to predict how the distribution of maximum slope angles are expected to change throughout the year (i.e. by determining the average monthly, weekly, and/or daily precipitation levels).

REFERENCES

Aysen, A., *Soil Mechanics: Basic Concepts and Engineering Applications*, Taylor & Francis Group, London, UK, 2005.

Bhang, K.J., Schwartz, F.W. and Braun, A., Verification of the Vertical Error in C-Band SRTM DEM Using ICESat and Landsat-7, Otter Tail County, MN, *IEEE Transactions on Geoscience and Remote Sensing*, **45**(1), 2007, 36–44.

Center for International Earth Science Information Network (CIESIN), Gridded Population of the World. Available: http://sedac.ciesin.columbia.edu/gpw/, 2007.

Chang, K. and Tsai, B., The Effect of DEM Resolution on Slope and Aspect Mapping, *Cartography and Geographic Information Science*, **18**(1), 1991, 69–77.

Chow, T.E. and Hodgson, M.E., Effects of Lidar Post-Spacing and DEM Resolution to Mean Slope Estimation, *International Journal of Geographical Information Science*, **23**(10), 2009, 1277–1295.

Claessens, L., Heuvelink, G.B.M. and Veldkamp, A., DEM Resolution Effects on Shallow Landslide Hazard and Soil Redistribution Modelling, *Earth Surface Processes and Landforms*, **30**(4), 2005, 461–477.

Cutter, S.L., Boruff, B.J. and Shirley, L.W., Social Vulnerability to Environmental Hazards, *Social Science Quarterly*, **84**(2), 2003, 242–261.

Deng, Y., Wilson, J.P. and Bauer, B.O., DEM Resolution Dependencies of Terrain Attributes Across a Landscape, *International Journal of Geographical Information Science*, **21**(2), 2007, 187–213.

Eidsvig, U., McLean, A., Vangelsten, B.V. and Kalsnes, B., *Work Project 2.2: Vulnerability to Landslides*, Deliverable 2.6, SafeLand - Living with Landslide Risk in Europe, EU FP7 Research Project No 226479, 2010.

Eidsvig, U., *Work Project 2.2: Case Studies for Societal Vulnerability*, Deliverable 2.7, SafeLand - Living with Landslide Risk in Europe, EU FP7 Research Project No 226479, 2010.

Fenton, G.A. and Vanmarcke, E.H., Simulation of random fields via Local Average Subdivision, *ASCE Journal of Engineering Mechanics*, **116**(8), 1990, 1733–1749.

Fenton, G.A. and Griffiths, D.V., *Risk Assessment in Geotechnical Engineering*, John Wiley & Sons, New York, 2008.

Fleming, M.D. and Hoffer, R.M., *Machine Processing of Landsat MSS Data and DMA Topographic Data for Forest Cover Type Mapping*, Purdue University , Laboratory for Applications of Remote Sensing, LARS Technical Report 062879, West Lafayette, Indiana, USA, 1979.

Geological Survey of Norway (NGU), Skred (in Norwegian). Available: http://www.ngu.no/no/hm/Geofarer/Skred/, 2008.

Geotechnical Information, Career Development and Resources for Geotechnical Engineers. Available: http://www.geotechnicalinfo.com/youngs_modulus.html, 2007.

Griffiths, D.V. and Fenton, G.A., Probabilistic slope stability analysis by finite elements, *ASCE Journal of Geotechnical and Geoenvironmental Engineering*, **130**(5), 2004, 507–518.

Griffiths, D.V. and Fenton, G.A., Probabilistic settlement analysis by stochastic and random finite element methods, *ASCE Journal of Geotechnical and Geoenvironmental Engineering*, **135**(11), 2009, 1629–1637.

Heinimann, H.R., *Risikoanalyse bei gravitativen Naturgefahren (In German)*, Fallbeispiele und Daten, Umwelt-Materialen 107/I, Bern, Germany, 1999.

International Monetary Fund (IMF), World Economic Outlook Database-April 2010. Available: http://www.imf.org/external/pubs/ft/weo/2010/01/, 2010.

iTouchMap, Latitude and Longitude of a Point, *iTouchMap.com*. Available: http://itouchmap.com/latlong.html, 2010.

Jaedicke, C., Sverdrup-Thygeson, K., Vangelsten, B.V., Nadim, F. and Kalsnes, B., *Work Project 2.4: Identification of Landslide Hazard and Risk Hotspots in Europe*, Deliverable 2.10, SafeLand - Living with Landslide Risk in Europe, EU FP7 Research Project No 226479, 2010.

Jones, K.H., A Comparison of Algorithms used to Compute Hill Slope as a Property of the DEM, *Computers and Geosciences*, **24**(4), 1998, 315–323.

Lahidji, R., *Measuring the Capacity to Cope with Natural Disasters*, Contribution to the UN OCHA project 'Risk Assessment and Mitigation Measures for Natural and Conflict-related Hazards in Asia Pacific' Appendix G. Available: http://www.grid.unep.ch/product/publication/download/Naturalconflictrelatedhazard_Asia_Pacific.pdf, 2008.

Liu, L., Civil Engineering 3101 Lecture Notes: Soil Mechanics, *Dalhousie University*, 2009.

Manzari, M.T. and Nour, M.A., Significance of Soil Dilatancy in Slope Stability Analysis, *ASCE Journal of Geotechnical and Geoenvironmental Engineering*, **126**(1), 2000, 75–80.

Nadim, F., Kjekstad, O., Peduzzi, P., Herold, C. and Jaedicke, C., Global Landslide and Avalanche Hotspots, *Landslides*, **3**(2), 2006, 159–173.

Nadim, F., Haugland, H. and McLean, A., *Work Project 1.4: Landslides Triggered by Anthropogenic Factors*, Deliverable 1.6, SafeLand - Living with Landslide Risk in Europe, EU FP7 Research Project No 226479, 2010.

National Imagery and Mapping Agency (NIMA), *Department of Defense World Geodetic System 1984: Its Definition and Relationship with Local Geodetic Systems*. Available: http://earth-info.nga.mil/GandG/publications/tr8350.2/wgs84fin.pdf, St. Louis, Missouri, USA, 2000.

Natural Resources Canada (NRC), The Atlas of Canada - Landslides. Available: http://atlas.nrcan.gc.ca/site/english/maps/environment/naturalhazards/landslides/ , 2009.

Norwegian Geotechnical Institute (NGI), Natural Hazards Division, 2010.

Peitgen, H-O. and Saupe, D., eds., *The Science of Fractal Images*, Springer-Verlag, New York, NY, 1988.

Raaflaub, L.D. and Collins, M.J., The Effect of Error in Gridded Digital Elevation Models on the Estimation of Topographic Parameters, *Environmental Modelling and Software*, **21**(5), 2006, 710–732.

Rabus, B., Eineder, M., Roth, A. and Bamler, R., The Shuttle Radar Topography MIssion - A New Class od Digital Elevation Models Acquired by Spacebourne Radar, *ISPRS Journal of Photogrammetry and Remote Sensing*, **57**(4), 2003, 241–262.

Roberts, N.J., Nadim, F. and Kalsnes, B., Quantification of Vulnerability to Natural Hazards, *Georisk*, **3**(3), 2009, 164–173.

Rowe, R.K., *Geotechnical and Geoenvironmental Engineering Handbook*, Kluwer Academic Publishers, Norwell, Massachusetts, USA, 2001.

Smith, M.J., Goodchild, M.F. and Longley, P.A., *Geospatial Analysis: A Comprehensive*, Vol. Guide to Principles, Techniques and Software Tools, Matador, Leicester, UK, 2007.

Stark, T.D., Choi, H. and McCone, S., Drained Shear Strength Parameters for Analysis of Landslides, *ASCE Journal of Geotechnical and Geoenvironmental Engineering*, **131**(5), 2005, 575–588.

Stinführer, A., Marchi, B., Kuhlicke, C., Scolobig, A., Tapsell, S. and Tunstall, S., *Vulnerability, Resilience and Social Constructions of Flood Risk in Exposed Communities*, FLOODsite report T11-07-12. Available: http://www.floodsite.net/html/publications2.asp?ALLdocs=on&Submit=View, 2009.

Strang, G., *Calculus*, Vol. 1, Wellesley-Cambridge Press, Huddersfield, England, 1991.

Tapsell, S.M., Tunstall, S.M., Green, C. and Fernandez, A., *Social Indicator Set*, FLOODsite Report T11-07-01. Available: http://www.floodsite.net/html/publications2.asp?ALLdocs=on&Submit=View, 2005.

The World Bank, The World Bank Development Indicators - Hospital Beds (per 1,000 people). Available: http://data.worldbank.org/indicator/SH.MED.BEDS.ZS/countries/1W?display=default, 2010.

United Nations Disaster Relief Coordinator (UNDRO), Natural Disasters and Vulnerability Analysis, report of the expert meeting group, Geneva, 1979.

Zhang, X., Drake, N.A., Wainwright, J. and Mullian, M., Comparison of Slope Estimates from Low Resolution DEMs: Scaling Issues and a Fractal Method for their Solution, *Earth Surface Processes and Landforms*, **24**(9), 1999, 763–779.

APPENDIX A Rslope2d Program Structure and Inputs

Table [A.1] illustrates the manner in which the ground parameters must be entered into the random finite element method (RFEM) program, Rslope2d.

Table A.1 Stability of a 1:1 (i.e. 45 °) slope, clay strength parameters.

Echo input data to stats file?	t
Report progress to standard output	t
Dump debug data to stats file	t
Display one random field? [realization] [which]	t 1 c
Display displaced FEM mesh? [realization]	t
Number of x-elements to left of embankment	20
Number of x-elements to right of embankment	20
Number of y-elements in embankment	**12**
Number of y-elements in foundation	5
Gradient of slope (integer) (y/x)	**1**
Element size, X [X Y] dimensions	2.5 2.5
Iteration convergence tolerance	0.00 01
Maximum number of iterations	500
Cohesion: mean, SD, and distribution	0. 0. deterministic
Friction angle: mean, SD, and distribution*	26.0 5.0 bounded 21.0 31.0 0.0 2.0
Dilation angle: mean, SD, and distribution	0. 0. deterministic
Unit weight: mean, SD, and distribution**	13.0 1.5 lognormal
Elastic modulus: mean, SD, and distribution***	2.0E+04 1.5E+04 lognormal
Poisson's ratio: mean, SD, and distribution	0.3 0. deterministic
Deterministic strength reduction factors	1.0 1.1 1.2 1.3 1.4 1.5 2.0 2.5 3.0
Number of realizations	1000
Generator seed (0 for random seed)	0
Scale of fluctuation (x and y directions)	13.0 13.0
Variance function name	dlavx2
Material Property Correlation Matrix Data	(no input)
Show element boundaries	t
Show random field as background [log?] [prop?]	t t phi
Width of displaced mesh output plot in inches	4

The only changes made for varying soil types corresponds to the starred fields shown in Table [A.1].

Table A.2 Stability of a 1:1 (i.e. 45°) slope, gravely sand strength parameters.

* Friction angle	40.0	5.0	bounded	35.0	45.0	0.0	2.0
** Unit weight	18.0	1.0	lognormal				
*** Elastic modulus	1.25E+05	7.5E+04	lognormal				

The only changes made for the varying slope angles corresponds to the bolded fields shown in Table [A.1].

Table A.3 Stability of a 2:1 (i.e. 26.57°) slope.

Number of y-elements in embankment	6
Gradient of slope (integer) (y/x)	2

Table A.4 Stability of a 3:1 (i.e. 18.43°) slope.

Number of y-elements in embankment	4
Gradient of slope (integer) (y/x)	3

For a full explanation of the Rslope2d parameters see Griffiths and Fenton (2004).